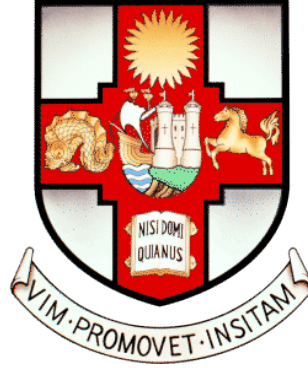


Connectivity and Centrality in Dense Random Geometric Graphs

Alexander P. Kartun-Giles



UNIVERSITY OF BRISTOL
EPSRC CENTER FOR DOCTORAL TRAINING IN COMMUNICATIONS

*A dissertation submitted to the University of Bristol in accordance with the
requirements for the degree of Doctor of Philosophy in the Faculty of Engineering*

March 2017.

i

†

i

Abstract

Due to shorter range communication becoming more prevalent with the development of multiple-input, multiple-output antennas (MIMO) and millimeter wave communications, multi-hop, intra-cell communication is anticipated to play a major role in 5G. This is developed in this thesis. Our analysis involves a stochastic spatial network model called a *random geometric graph*, which we use to model a network of interconnected devices communicating wirelessly without any separate, pre-established infrastructure.

Extending recent work on the *random connection model* by relaxing the convexity restriction on the bounding geometry \mathcal{V} , we study the asymptotic connectivity of a model of randomly distributed, randomly linked vertices embedded within an annulus. Vertices, resembling communicating devices, are linked according to a Rayleigh fading model of signal attenuation in built-up urban environments. We notice that vertices near obstructions in the domain have an exceptionally high betweenness centrality, and highlight the need to quantify this sort of measure analytically. Following up on this, in a theoretical *continuum limit*, where vertex density goes to infinity and the connection range goes to zero compared with the size of the domain, we approximate betweenness centrality in a random network with a known special function called the elliptic integral of the second kind. This provides analytic support to various delay tolerant networking protocols currently used in 5G scenarios, wireless sensor networks, and intelligent vehicle networks, which avoid what are often intractably complex algorithmic computations, even when distributed over many mobile processors.

Due to the obvious break with our model at lower densities, we then relax the continuum limit, and investigate the expected number of shortest paths which run between two spatially separated vertices in a unit disk graph in order to develop an understanding of betweenness centrality at finite density, which is based on counting shortest paths in networks. It also develops so called range-free localisation beyond estimating distances to location-aware anchors via hop counts, instead using the more sensitive *number* of geodesic paths. We

conclude with the difficulties of combinatorial enumeration in spatial networks, and highlight the need to develop probabilistic techniques to deal with the deep issues of spatial dependence.

†

Acknowledgements

I acknowledge with great thanks and gratitude the help and support of Professor Carl P. Dettmann, Dr Orestis Georgiou of Toshiba Research Europe, and Professor Justin P. Coon of the Oxford University Communications Research Group, all of whom have provided the supervision of this thesis. Also, thanks to everyone at the CDT, including Bagots, Brett, Dave, Leo, Suzanne, Mark, Simon, and everyone else, and finally, thanks to all those at 26 Cadogan Square.

v

†

v

Author's Declaration

I declare that the work in this dissertation was carried out in accordance with the requirements of the University's Regulations and Code of Practice for Taught Programmes and that it has not been submitted for any other academic award. Except where indicated by specific reference in the text, this work is my own work. Work done in collaboration with, or with the assistance of others, is indicated as such. I have identified all material in this dissertation which is not my own work through appropriate referencing and acknowledgement. Where I have quoted or otherwise incorporated material which is the work of others, I have included the source in the references. Any views expressed in the dissertation, other than referenced material, are those of the author.

Alexander Paul Kartun-Giles
4th of March 2017

†

Contents

1	Introduction	1
1.1	Current state of the art	5
1.2	What is done in this thesis	7
1.3	Contribution to the field	9
1.4	Thesis structure	11
2	Concepts	12
2.1	Connectivity	12
2.1.1	Isolated vertices	13
2.1.2	The connection probability	15
2.1.3	Boundary effects and non-convex domains	16
2.2	Betweenness centrality	17
2.2.1	Computation	17
2.2.2	Shortest paths	19
2.3	Extended Concepts	20
2.3.1	Binomial point processes	20
2.3.2	Markov point processes	20
2.3.3	Geometric preferential attachment	22
2.3.4	Hyperbolic random geometric graphs	23
2.3.5	Current flow betweenness	24
3	Connectivity	26
3.1	Introduction	26
3.2	Rayleigh fading	28
3.3	The annulus domain \mathcal{A}	30

3.3.1	No obstacles	31
3.3.2	Small obstacles	33
3.3.3	Large obstacles	35
3.4	The spherical shell \mathcal{S}	36
3.4.1	Small spherical obstacles	36
3.4.2	Large spherical obstacles	38
3.5	Discussion	41
3.5.1	Numerical simulation	41
3.5.2	Multiple obstacles	41
3.5.3	Surfaces without boundary	42
3.5.4	Quasi-one-dimensional regime	42
3.5.5	Betweenness centrality near obstacles	42
4	Betweenness centrality	43
4.1	Introduction	43
4.2	The model	45
4.3	The δ function	48
4.4	Discussion	50
4.4.1	Numerical simulation	50
4.4.2	Applications	51
4.4.3	The advantages of betweenness	53
4.4.4	Convergence	55
5	Geodesic Paths	56
5.1	Introduction	56
5.2	A recursive formula for $\sigma_{r_{xy}}$	59
5.3	Geodesics in d -dimensions	62
5.4	Numerical simulation	67
6	Discussion	70
6.1	Applications in communication networks	70
6.1.1	Understanding skeletons	70
6.1.2	Topology-based geolocalisation	71
6.1.3	Future vehicular ad hoc networks	72

6.2	Mathematical directions	73
6.2.1	The distribution of the number of geodesics	73
6.2.2	Non-optimal geodesics	75
6.3	Final words	77
	Appendices	78
	A Percolation	79
	B Proof of the isolated vertices theorem	83

List of Figures

1.1	An example random geometric graph. These combinatorial objects can be used to model networks of millimeter wave-connected 5G base stations in ultra-dense urban deployment [1]. It has been formed from a Poisson point process by adding an edge between vertices whenever they fall within a Euclidean distance of 0.25 of each other. All six shortest paths from vertex 1 to 10 have been highlighted in red as a structure of intersecting paths.	3
2.1	Betweenness centrality in a unit disk graph of 30 vertices drawn inside the unit square, with $r_0 = 0.3$. The size of the vertices is proportional to their betweenness.	18
2.2	Two vertices at center separation 2.5 in a unit disk graph, taking $r_0 = 1$. The connection ranges, and an extra range (large disks), are drawn. The degrees of the three coloured vertices are dependent random variables. In this example, the green vertex has degree zero, the blue vertex has degree two and the yellow vertex also has degree two. This spatial dependence of vertex degrees in random geometric graphs such as the unit disk graph depicted here is ignored in various independence assumptions, as discussed in the text.	19

2.3	The Strauss process. A binomial point process of $n = 250$ vertices (taking $\Omega = 0.07$ and $r_0 = 0.08$) is updated in a step by step fashion by the Metropolis-Hastings algorithm. It creates a pattern of repelling points. From Irons et al 2011, referenced in the text.	21
2.4	A current of $1A$ flows into the left most vertex of a network of unit resistors. It is then extracted from the right most vertex. Two different current conserving flows are shown on the same simple network. The values on the edges are the currents flowing along those edges. Flow B minimises the total dissipated energy, and so satisfies the Kirchhoff laws.	24
3.1	A soft random geometric graph, first defined at the beginning of Chapter 1, inside the annulus (large obstacle case), and inside a square with two circular obstacles. Vertices with low degree are highlighted in purple. We derive the graph connection probability in these simple obstructed domains.	27
3.2	A depiction of the integration regions used for the annulus domain \mathcal{A} with small obstruction (middle panel) and large obstruction (right panel), with the integration regions highlighted. The small, cone-like region in the middle domain \mathcal{A} is highlighted in purple.	31
3.3	A depiction of the integration regions used for the disk domain \mathcal{D} . The small, cone-like region in the middle domain \mathcal{A} is highlighted in purple.	33
3.4	We numerically estimate the connection probability of soft random geometric graphs drawn inside the annuli \mathcal{A} and spherical shell \mathcal{S} . Every curve is compared with our analytic predictions given by Eqs. 3.3.6, 3.3.8, 3.3.11 and 3.4.8, where indicated. The discrepancy at low density is expected due to the fact we calculate only the probability of a single isolated vertex, and use its complement as an approximation to the connection probability in a typical dense network scenario.	39

-
- 3.5 A soft random geometric graph inside a Sinai domain, and in a domain with multiple obstructions. The betweenness centrality is plotted in light tones (low) to darker tones eventually becoming red (high), showing the skeleton form around the obstacles. . . 40
- 4.1 Four realisations of soft random geometric graphs and their betweenness centrality bounded within various domains, including the disk \mathcal{D} , square, right-angled triangle and square domain containing two circular obstacles: in both the left and upper right figures the darker colour represents low centrality, whereas the lighter colour high centrality, whereas in the obstructed square domain (lower right) the least central nodes are faded to grey and the most central are highlighted in red. Note that the boundaries of the domains are locations where betweenness is at a minimum. The link colours are based on the average betweenness of the two connected nodes. 46
- 4.2 The disk domain \mathcal{D} , and the three vertices i, j and k . We are trying to obtain a dense network approximation to the betweenness centrality of a vertex placed at k . The scalar k_{\perp} represents the smallest Euclidean distance from k to any point on the straight line joining i and j . The axis are centred on k , while the circle is centred at $(-\epsilon, 0)$. The angles ϕ_i and ϕ_j and the distances r_i and r_j are also shown. 47
- 4.3 Numerical evaluation of our continuum approximation Eq. 4.3.6. Increasing the density of the point process, we ensure it contains a point z at distance ϵ from the centre of \mathcal{D} . A soft random geometric graph with a Rayleigh fading connection function of vanishing range $\beta \gg 1$, as in Chapter 3, is then formed, and the betweenness centrality of z is calculated numerically. The thicker line at the top is Eq. 4.3.6. The finite density simulations never converge to this approximation, but the error is small. . 52

5.1	Vertices 4 and 8 are separated by Euclidean distance 2.4 in a unit disk graph, with the connection range $r_0 = 1$. They are joined by ten geodesic paths, each of four hops. We evaluate the expectation of this quantity in terms of the mutual Euclidean separation of vertices.	57
5.2	Points x and y separated by $\lambda \in [1, 2)$ create an area highlighted in blue, which is A_λ . Vertices falling within this blue region lie on one of potentially many (what will necessarily be) shortest paths which run between these two vertices, each of two hops.	58
5.3	Some node (red) lying a distance λ from j (green) will connect directly to all nodes within r_0 of its position (the red circle). All of those vertices which simultaneously lie within a distance r_0 of j , denoted by the yellow area, will form two hop paths, and thus each three hop paths $i \leftrightarrow j$	60
5.4	The smooth decaying blue lines are Monte Carlo data for <i>optimal geodesic cardinality</i> , with our approximation Eq. 5.3.20 with $d = 2$. The green stars are the actual shortest path counts. The blue pluses and green stars are numerical results, while the smooth curves are our analytic results.	68
5.5	The expected number of two-hop paths and our approximation Eq. 5.3.20, for $\rho = 15, 17, 20$ and $d = 2$	69
5.6	Eq. 5.3.20 plotted for three increasing densities $\rho = 20, 40, 100$ over a long range of displacements. The expected number of paths rises and falls as r_{xy} increases.	69
6.1	A one-dimensional unit disk graph. The colours are used to help distinguish paths. The geodesic length between the end points is three hops. This can be used to model an ad hoc communication network of vehicles queuing in traffic.	72

6.2	Top: The small boxes are Monte Carlo approximations to the probability $P(\sigma_{r_{xy}} = k)$ with $r_{xy} = 1.6$. In this distance interval the distribution of geodesic paths is Poisson, as described by the green line Eq. 6.2.2. Bottom: The blue line is the curve $\text{Po}(\mathbb{E}(\sigma_{r_{xy}=2.7}))$, and the boxes Monte Carlo data for this larger displacement. The number of geodesic paths is therefore not Poisson.	74
6.3	The graph shows 96 geodesics, each of 13-hops, from vertex 63 to vertex 70. Since the Euclidean distance between the endpoints is 9.8, these geodesics are not optimal. As r_{xy} increases, the probability there existing at least one 'optimal' alignment of vertices, which is an alignment of points of \mathcal{Y} that induces a path of $\lceil r_{xy} \rceil$ hops from x to y , vanishes. The chain of links is more likely to break as it grows longer. This explains the rising and falling effect in Fig. 5.6.	76
A.1	50×50 bond percolation with p increasing from 0.3 to 0.8 in steps of 0.1. Criticality occurs at $p = 0.5$. The largest connected component is highlighted in sky blue throughout.	80
B.1	The component H is bounded by its convex hull $\Phi(H)$, itself encased in the upright rectangle R . In this case, the exclusion area is non-empty, and the vertex combination fails to satisfy the conditions of the component H in Lemma B.0.4.	87

List of Tables

5.1	The minimum number of hops required for two vertices to communicate in a unit disk graph, which is always the ceiling of the Euclidean distance separating the vertices.	59
5.2	Solutions to the recursion relation 5.2.9.	62
5.3	Solutions to the recursion relation 5.2.9 with $d = 3$	64
5.4	Solutions to the recursion relation 5.2.9 for general dimension d	67

†

Chapter 1

Introduction

Ultra-dense spatial deployment of cellular base stations is among the most promising ways in which the data capacity of large scale wireless networks is to be enhanced [1]. The density of this deployment is highly anticipated, as of 2016, to be around 40-50 base stations per km^2 . New technology introduced into these units will result in their communication range falling by an order of magnitude compared to the 4G base stations which are currently deployed in an ad hoc fashion around our cities. This is partly due to the appearance of multiple-input multiple-output (MIMO) antennas, which offer faster data rates (Gbit/s), but utilise over a hundred antennas simultaneously, each at reduced power [2]. Compounding this, the anticipated high-frequency millimeter wave technologies in the 30-300 Ghz range will attenuate very quickly, allowing only short range communication between devices [3]. Therefore, in order to increase the range of special gateway-enabled cells, networks will have to employ a form of multi-hop, cell-to-cell communication. According to this much anticipated theory, 5G is therefore likely to consist, at least in part, of densely deployed, millimeter wave connected ‘small’ cells routing data from mobile devices between themselves in a sort of daisy chain toward gateway cells, and then finally into the backhaul network, enabling much higher throughput networks [4].

Now, these small cells will form a spatially embedded network. Combinatorial analysis of this sort of system has long since been a topic of great

research interest. In this thesis, we contribute to this growing field by analysing a combinatorial object called a *random geometric graph*, an example of which is shown in Fig. 1.1, in order to perform statistical network analysis developing future intra-cell communications. We will focus on two models:

- **Soft random geometric graph**, also known as the **Random Connection Model** when embedded in the entire real plane rather than a bounding geometry such as a disk, is a type of random network formed by distributing vertices in a region $\mathcal{V} \subseteq \mathbb{R}^d$ according to a Poisson point process \mathcal{Y} of density ρ , and then adding an edge between points $\{x, y\} \in \mathcal{Y}$ with probability $H(\|x - y\|)$, where $H : \mathbb{R}^+ \rightarrow [0, 1]$ is the connection function, and $\|x - y\|$ is the distance between vertices given by some metric [5]. We often use the Rayleigh fading connection function $H(\|x - y\|) = \exp(-\beta\|x - y\|^2)$ defined in Section 3.2. This is parametrised by $\beta \in \mathbb{R}^+$, and we then write $r_0 = 1/\sqrt{\beta}$ to denote the typical distances over which vertices connect, when the context is clear.
- The **Unit disk model** is the limit of this model where the connection function $H(\|x - y\|) \rightarrow \mathbf{1}\{\|x - y\| < r_0\}$, with $r_0 \in \mathbb{R}^+$ the critical range over which vertices connect [6].

These random graphs have been used to model the following two types of wireless network:

- **Ad hoc wireless networks**, where devices communicate, as discussed, between themselves without utilising separate, pre-established infrastructure. This is achieved by routing data in a ‘multi-hop¹’ fashion between users. Apart from in future 5G urban networks, they are seen in deployed in disaster zones since they can offer a larger range than simple point-to-point radio communication. There are whole journals related to this topic, but see e.g. [7] for a good discussion.
- **Wireless sensor networks**, which are densely deployed networks of low-power sensors. They are used for many different sensing tasks. Wirelessly

¹A hop is an edge in a graph. One *hops* between vertices, hence the commonly used term.

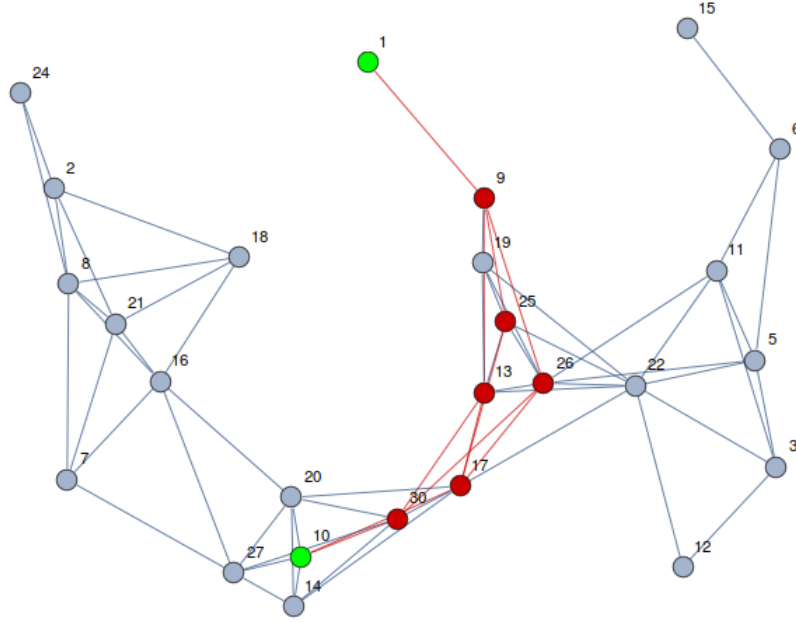


Figure 1.1: An example random geometric graph. These combinatorial objects can be used to model networks of millimeter wave-connected 5G base stations in ultra-dense urban deployment [1]. It has been formed from a Poisson point process by adding an edge between vertices whenever they fall within a Euclidean distance of 0.25 of each other. All six shortest paths from vertex 1 to 10 have been highlighted in red as a structure of intersecting paths.

communicating with each other, sensors with limited battery resources and limited computational performance collect data from an environment and route it in a multi-hop fashion toward an elected *sink* sensor. The sink then sends the collected information toward a cloud or distant base station. For further discussion, see e.g. [8].

The major result which has lead to such great interest in random networks around the world was published surrounding a 1957 conference on Monte Carlo techniques in the UK. Broadbent and Hammersley showed that a non-trivial, first order phase transition of ‘sudden connectivity’ occurred when an array of vertices is adorned at random with links between neighbouring pairs with a

critically high probability p [9]. This is called *percolation*². Interestingly, with an infinite array of vertices, the phase transition is ‘sharp’ [10]. Mathematical study of this simple model has lead to many important results in modern science, with Fields medals awarded recently for proving certain results concerning a conformal invariance property of extremely fine lattices exactly at the moment of percolation, called *criticality* [11]. Similarly, both the unit disk and random connection model mentioned above display a percolation phenomenon³.

Now, these graphs are excellent models of randomly constructed wireless networks of radio transmitters dispersed over a large geographic region [13]. One can therefore investigate analogous results to percolation, but in a wireless network setting [14]. Indeed, this is the most common application of the theory today. Results, generally, concern theoretical methods for the optimal use of what are now very expensive communication resources.

The field is broad:

1. “(There) is a sense of missing unification and a lack of general methods that apply to large families of different models.” [7, 15].
2. The task of then applying mathematical results such as performance bounds to actual networks and the way they run is not straightforward, nor is it commonly performed in industry. This has lead to a lack of focus.
3. The probabilistic analysis of spatial communication networks, sometimes involving dynamical processes, is often very difficult. Well developed techniques from random graph theory can rarely be applied effectively [16].

Despite these difficulties, there are well cited results over the last two decades which constitute a research frontier, either concerning mathematical features of commonly applied random graph models, or the specific use of random graphs in communication problems.

²We introduce this model with greater detail in Appendix A.

³More formally, taking $H(\|x - y\|) = \mathbf{1}\{\|x - y\| < r_0\}$, in a unit disk graph of expected n vertices distributed over a square of side \sqrt{n} there exist supercritical connection ranges $r_0(n) > r_c(n)$ for which a giant cluster exists asymptotically almost surely (i.e. with probability 1 in the limit $n \rightarrow \infty$). There exists a similar asymptotic connection rule in the random connection model [6, 12].

1.1 Current state of the art

As a broad introduction to a rich field, we first introduce some of the recent trends in the developing theory of random networks. Then, in Chapter 2, we focus on topics which provide the background to the contribution of this thesis, focusing on the areas of connectivity and centrality in communication networks.

1. **Mobility models:** Networks with moving vertices are used as models for *mobile* ad hoc networks (MANETs). For example, consider the *random walk model*: vertices are distributed uniformly at random on the surface of a flat torus, but move, at each time step, to a new location a distance d (a parameter of the model) and angle θ (selected uniformly at random for each time step) away from where they currently are [17]. One can then ask certain questions related to the communication theory of mobile networks, such as to what extent a static graph can be used as an approximate model of a mobile systems, amongst related topics.

Mobility studies, for example, is particularly important in the case of *delay tolerant networking* [18]. Here, mobile users offload and collect their data from a network of intermediate (and also mobile) devices, which store, carry and forward data as the relay opportunity arises. The specific mobility model on which the dynamic network is based will significantly alter the analysis of performance. State of the art research concerns the more realistic models of human mobility, such as the Levy Walk model (LW) [19], and *Self-Similar Least Action Human Walk* (SLAW) [20], both of which capture, for example, the self-similarity of human walks, and the distribution of inter-meeting times within which message relays can occur.

Also, the use of betweenness centrality [21], is already established within this field. Numerical calculation of these network centrality indices can assist certain delay tolerant networking protocols by encouraging mobile vertices to relay data toward exceptionally central mobile vertices whenever possible [18].

2. **Symmetric motifs:** A symmetric motif is a potentially disconnected

subset of vertices with the property that any permutation of indices preserves adjacency [22]. They can be identified in the graph Laplacian by identifying the integer eigenvalues and reading off the non-zero components of corresponding eigenvectors. The induced subgraph⁴ of these components is the corresponding symmetric motif [23].

They occur more frequently in spatial networks due to the geometric factor. Their characteristic nature, mixed with a simple connection to the graph's Laplacian spectrum, make them a fascinating and much undervalued research approach to processes running on dense communication networks.

3. **The Rado graph:** Infinite random geometric graphs concern networks which have an infinite number of vertices, rather than specifically taking the *thermodynamic* or high-density *continuum limit*. As an example, the unit disk graph has a version of this, taking the vertex set V to be a countably infinite subset of the Euclidean metric space, and $\|V\| \rightarrow \infty$. Graphs formed this way are not necessarily isomorphic, contrasting a similar theory concerning non-spatial random graphs (the Erdős-Rényi or *random graph* [11]) presented in one of the earliest works on the subject, by Erdős and Rényi [24], where all infinite random graphs are of a unique isomorphism type denoted the *Rado graph*. For the geometric case, this infinite limit can help reveal large-scale structure and long term behaviour [25].
4. **Non-Homogeneous point processes:** The simple Poisson point process model can be extended to address more realistic situations where the distribution of points is not uniform in space. The most common variant is the *Strauss process*, which is a point process defined by a Markov chain Monte Carlo algorithm involving repelling points; densely deployed stations are randomly dispersed, but never right next to each other, which is the main lack of realism encountered in the Poisson point process model. See Sec 2.3.1, 2.3.2 and 2.3.3.

⁴The graph consisting of those vertices, and edges whose end points form a subset of those vertices.

5. **Measures of centrality:** This involves introducing centrality analysis into communication networks [26]. Example applications include boundary detection, and as part of routing protocols which assign centrality indices to vertices in order to assess a sort of ‘routing potential’. Also, techniques which networks can employ to determine the centrality of their constituent vertices are of current interest [27].
6. **Aerial networks:** One may consider employing aerial base stations, such as drones. This can provide spontaneously adaptive coverage. Exactly whether or not this solution can outperform ground station-reliant networks can be assessed using analysis of random geometric networks [28].
7. **Localisation:** Wireless devices often demand essential location information. Indoor localisation cannot use GPS, given a line-of-sight requirement with multiple satellites. Underground, aerial and secret military localisation techniques are currently being developed. In a random network, one can *multilaterate* by first measuring hop-counts to location-aware anchor vertices (such as access points), and then converting hop-counts to Euclidean distances via a conditional distribution parameterised by Euclidean distance. [29].
8. **Secure communication:** The use of random secrecy graphs, which consist of a superimposed point process of eavesdroppers and users on which a geometric graph is formed, can provide useful limits on the ability of wireless networks to communicate in secure environments [30].

1.2 What is done in this thesis

In this thesis, we focus on two key, developing areas:

- 1) *Connectivity in non-convex domains:* Since many real world domains are not convex subsets of \mathbb{R}^2 , we extend the analysis of high-density random network connectivity into the more realistic scenario of a domain containing randomly arranged circular obstacles. As with other work concerning non-convexity [31, 32], the obstructions in the domain introduce specific

features to the enclosed graph. Specifically, obstacles act like internal perimeters, encouraging isolated vertices. We describe this effect in detail in chapter 3, showing how small obstacles⁵ encourage isolated vertices according to a factor proportional to their area $\frac{\pi^{d/2}}{\Gamma(\frac{d}{2}+1)}(r_{\text{obstacle}}/r_0)^d$, while large obstacles attract isolated vertices according to a factor proportional to their perimeter $\frac{\pi^{d+1/2}}{\Gamma(\frac{d+1}{2})}(r_{\text{obstacle}}/r_0)^{d-1}$. This implies small obstacles have a negligible effect on connectivity, since one sees a power of the ratio r_{obstacle}/r_0 , and hence the contribution vanishes for small obstacles $r_{\text{obstacle}} \ll r_0$. Also, we show the compound effect of obstacles is a linear combination of separate contributions, given they are not too close.

We then observe that vertex isolation near an inner boundary can be more likely than other parts of the domain, and more likely than the outer boundary when the obstacles are numerous. This is because vertices on the inner perimeter have an exceptionally high betweenness centrality, acting as popular bridging vertices between distant parts of the domain. [21].

Noticing the importance of this sort of structural concept to communication processes running on dense urban networks, we begin to analyse it directly.

- 2) In Chapter 4, we consider analytically quantifying betweenness centrality in a random geometric graph. In a limiting density scenario, which we describe as a *continuum limit*, shortest paths between vertices are approximated by the convex hulls of their endpoints i.e. by straight line segments. Based on the assumption that only a single geodesic path will join any two vertices, by simply counting the number of convex hulls which 1) can be formed by any pair of points in $x, y \in \mathcal{V}$ and 2) run through k we can then count the number of geodesic paths which intersect $k \in \mathcal{V}$.

Using delta functions, we then show how the (expected⁶, normalised) betweenness centrality $g^*(k)$ of some polar point $k = (\epsilon, \theta)$ in a disk

⁵Small and large here mean on a length scale significantly lesser or greater than the typical distance r_0 over which vertices connect.

⁶Note in our continuum limit, betweenness and expected betweenness are equal.

domain metric space is, in fact, a known integral:

$$g^*(k) = \frac{2}{\pi}(1 - \epsilon^2) \int_0^{\pi/2} \sqrt{1 - \epsilon^2 \sin^2(\theta)} d\theta \quad (1.2.1)$$

i.e. the elliptic integral of the second kind scaled by a quadratic function of displacement from the disk's center. We then discuss numerical convergence of expected betweenness to this integral as the point process density goes to infinity, showing how centrality is well approximated, but never exactly equal to, our convex hull based continuum approximation.

Given the importance of centrality, we then develop the analysis at lower densities:

- 3) In Chapter 5, in light of the above, we evaluate the expected number of geodesic paths $\sigma_{r_{ij}}$ which run between two vertices at displacement $r_{xy} = \|x - y\|$ in a unit disk graph. These are the *pair dependencies* which are summed in the evaluation of betweenness, see section 2.2.1. Taking the point process density $\lambda < \infty$ in a domain of arbitrary dimension d , this is approximately equal to a polynomial in $\lceil r_{xy} \rceil - r_{xy}$ of order $\frac{1}{2} \lfloor r_{xy} \rfloor (d + 1)$

$$\mathbb{E}(\sigma_{r_{xy}}) \approx \frac{\rho^{\lfloor r_{xy} \rfloor} (2\pi)^{\frac{1}{2} \lfloor r_{xy} \rfloor (d-1)} \lceil r_{xy} \rceil^{\frac{1}{2} (1-d)}}{\Gamma\left(\frac{\lceil r_{xy} \rceil + 1}{2} + \frac{\lfloor r_{xy} \rfloor d}{2}\right)} (\lceil r_{xy} \rceil - r_{xy})^{\frac{1}{2} \lfloor r_{xy} \rfloor (d+1)}$$

We highlight the difficulties in providing a better approximation. We also numerically corroborate our formulas, and discuss some interesting features which appear when non-geodesic paths are incorporated.

- 4) Finally, in Chapter 6, we discuss potential applications of this research, and make the relationship between theory and practice clearer.

1.3 Contribution to the field

The statistical analysis of centrality metrics on random communication networks can provide useful insights into performance. What is already known is how

betweenness can be algorithmically determined, either by a central computer, or by the constituent vertices in a centralised way. What is advanced is how this can ultimately be done analytically. This avoids an infamously expensive computation (see Section 2.2.1).

We now list our key contributions:

- a) In ultra-dense networks, we show how non-convex features of bounded domains can be highlighted by centrality indices.
- b) $(d - 1)$ -dimensional subgraphs meandering around urban obstructions can become critical to optimal performance.
- c) Isolated vertices do not determine connection in quasi-one-dimensional random geometric graphs.
- d) A simple approximation to network-theoretic betweenness centrality can be used by various high-layer wireless network routing protocols in order to omit the expensive and often impossible computation which would normally occur during operation. We also discuss interesting applications of analytic formulas.
- e) An approximation to the expected number of geodesic paths joining two distant vertices will lead to a more complete understanding of the value of these sorts of statistics in straightforward interference management techniques applied to 5G small cell deployments. Also, the expected number of geodesics can be used by ad hoc vertices as part of estimating the distance to an underground point, where GPS is unavailable. This may develop into overground localisation where appropriate.

We finally highlight the need to develop the field of spatial probabilistic combinatorics with a greater focus on applications, in, for example, communication theory, particularly concerning issues such as the spatial dependence of network observables.

1.4 Thesis structure

The rest of this thesis is structured as follows:

In Chapter Two we introduce a number of concepts in communication theory and random geometric graphs which are relevant to the arguments in this thesis.

In Chapter Three we study the effect of non-convexity on the random connection model.

In Chapter Four we introduce *betweenness centrality* in asymptotically dense random geometric graphs.

In Chapter Five the continuum limit is relaxed, and we approach betweenness centrality at finite density, finding the expected number of geodesic paths between two vertices in a unit disk graph (of general dimension d).

In Chapter Six we discuss the applications of this research to dense networks, and conclude.

Also, **Appendix A** reviews the basic results of percolation, and **Appendix B** details a proof related to the isolated vertices theorem discussed in [Section 2.1](#).

Chapter 2

Concepts

In this chapter, we introduce a number of concepts that will prove important for the work that follows in this thesis. In particular, we introduce the rich field of random networks and their current relation to communication theory. This provides a background and historical context for the our contribution. We first discuss connectivity, isolated vertices and non-convexity in random geometric graphs, and then discuss more recent developments in communication networks which have emerged in network science, specifically centrality indices, which for example measure the structural importance of networked communication nodes. We then briefly discuss current trends in the area.

2.1 Connectivity

One of the early graph-theoretic communication problems was a derivation of the probability that a random geometric graph was connected in the *thermodynamic limit*, where both the number of vertices and the domain volume $n, V \rightarrow \infty$ in such a way that the vertex density is constant [33]. The result goes as follows: take a simple Poisson point process \mathcal{Y} of expected n vertices inside a square of side \sqrt{n} , and form a graph by linking pairs of this process whenever they are within Euclidean distance r_0 of each other. Call this graph $\mathcal{G}(n, \pi r_0^2)$. According to Penrose [34], and later Gupta and Kumar [33], the asymptotic connection probability of the model with *logarithmic* growth of the connection

disks, i.e. $\mathcal{G}(n, \log n + c(n))$, is given by

$$\mathbb{P}(\mathcal{G}(n, \log n + c(n)) \text{ is connected}) \rightarrow e^{-e^{-c(n)}} \quad (2.1.1)$$

as $n \rightarrow \infty$. Therefore, if $c(n)$ goes to infinity with n , the graph will connect asymptotically almost surely.

To see this, consider a disk of area πr_0^2 centred at some vertex $x \in \mathcal{V}$: this contains no other points of \mathcal{V} with probability $\exp(-\pi r_0^2)$. For large n , these empty disks, which are isolated vertices, occur independently in the limit. Therefore the number of isolated vertices n_0 is distributed as a binomial random variable $\text{bin}(n, \exp(-\pi r_0^2))$. A simple Poisson process $\mathcal{Y}_{n_0} \subset \mathcal{V}$ of isolated vertices will therefore be observed in the limit. This process is empty with probability:

$$\begin{aligned} \mathbb{P}(n_0 = k) \Big|_{k=0} &= \frac{1}{k!} e^{-ne^{-\pi r_0^2}} \left(ne^{-\pi r_0^2} \right)^k \Big|_{k=0} \\ &= \frac{1}{k!} e^{-ne^{-(\log n + c(n))}} \left(ne^{-(\log n + c(n))} \right)^k \Big|_{k=0} \\ &= \frac{1}{k!} e^{-e^{-c(n)}} \left(e^{-c(n)} \right)^k \Big|_{k=0} \\ &= e^{-e^{-c(n)}} \end{aligned} \quad (2.1.2)$$

The question is, does this lack of isolated vertices imply the graph is connected?

2.1.1 Isolated vertices

Consider the following two lemmas [34]:

Lemma 2.1.1 (No two components are large). *Assuming $c > 0$, there exists a C such that asymptotically almost surely the random graph $G(n, c \log n)$ does not consist of two or more connected components each with Euclidean diameter¹ at least $C\sqrt{\log n}$.*

This means that two large enough components will merge asymptotically almost surely (a.a.s.). But how large?

¹This is the largest Euclidean distance which can be found between any two vertices in a component.

Lemma 2.1.2 (All small components consist of a single vertex.). *The graph $G(n, \log n - \frac{1}{2} \log \log n)$ contains no components H of more than one vertex and Euclidean diameter strictly less than $C\sqrt{\log n}$.*

These two lemmas imply that there exists a specific phase of the sub-logarithmic growth of r_0 where a single giant component forms surrounded by isolated vertices². We have just shown that these isolated vertices form a Poisson point process of their own. This means that one can effectively approximate the connection probability P_{fc} as

$$P_{fc} \sim 1 - \mathbb{P}(n_0 = 0) \quad (2.1.3)$$

To see the first of these lemmas, tile the square domain with tiles of side $r_0/\sqrt{20}$. This ensures that any two vertices found in any two adjacent squares are no more than $r_0/2$ apart. Then argue that

1. A component U of Euclidean diameter at least $C\sqrt{\log n}$ covers many tiles as $n \rightarrow \infty$.
2. Since the tiles have side $r_0/\sqrt{20}$, all tiles adjacent to U must be empty while the component exists.
3. There are many empty boundary tiles, given the size of U .
4. As $n \rightarrow \infty$, they cannot all be empty.

Thus any component of diameter at least $C\sqrt{\log n}$ will merge with another component, leaving only small components. We do not explicitly prove parts 1-3, but refer directly to Walter's review [35]; it essentially suffices to count the tiles.

Now, the second part is based on the same sort of argument: that an empty area must be maintained around a small component in order to keep it small, and that this area is, asymptotically, filled, unless it is a single vertex. Thus all large components join together, all small components are isolated vertices, and $P_{fc} \sim \mathbb{P}(n_0 = 0)$.

²Though we provide a summary of the proof in this section, we provide its detail in Appendix B.

2.1.2 The connection probability

Given this relation between isolated vertices and connectivity, it suffices to evaluate the probability that a single isolated vertex exists in the random connection model, then suggest that as the density $\rho \rightarrow \infty$,

$$P_{fc} \sim 1 - \mathbb{P}(n_0 = 1) \quad (2.1.4)$$

We now evaluate this. Consider a vertex at some fixed $x \in \mathcal{V}$. Its degree $k(x)$ can be determined by looking at a *marked* Poisson point process \mathcal{Y}^* , where the marks are $U[0, 1]$ random variables

$$\mathcal{Y}^* = \{\zeta, u : \zeta \in \mathcal{V}, u \sim U[0, 1]\} \quad (2.1.5)$$

which is of intensity ρdx on $\mathcal{V} \times U[0, 1]$, and dx is Lebesgue measure on \mathbb{R}^{d+1} . The degree is given by a sum over this marked point process:

$$k(x) = \sum_{(y,u) \in \mathcal{V} \times U[0,1]} \mathbf{1}\{u < \chi(x, y) H(\|x - y\|)\} \quad (2.1.6)$$

According to Campbell's theorem, one of the elementary theorems about point processes [36], we have that $k(x)$ is Poisson with expectation

$$\mathbb{E}k(x) = \rho \int_{\mathcal{V}} \chi(x, y) H(r_{xy}) dy \quad (2.1.7)$$

and therefore

$$\mathbb{P}(k(x) = 0) = \exp\left(-\rho \int_{\mathcal{V}} \chi(x, y) H(r_{xy}) dy\right) \quad (2.1.8)$$

which gives the probability that a vertex find itself isolated.

Now, given the conjecture discussed in 2.1 (that isolated vertices occur as a simple Poisson point process), it is natural in light of Eq. 2.1.8 to conjecture that as $\rho \rightarrow \infty$, the total number of isolated vertices is well approximated by a Poisson distribution with mean

$$\rho \int_{\mathcal{V}} \exp\left(-\rho \int_{\mathcal{V}} \chi(x, y) H(r_{xy}) dy\right) dx \quad (2.1.9)$$

In this limit, as discussed, the obstacle to connectivity is the presence of isolated vertices, and so, as $\rho \rightarrow \infty$,

$$P_{fc} \sim \exp \left(-\rho \int_{\mathcal{V}} e^{-\rho} \int_{\mathcal{V}} \chi(x,y) H(r_{xy}) dy dx \right)$$

which is approximately

$$1 - \rho \int_{\mathcal{V}} e^{-\rho} \int_{\mathcal{V}} \chi(x,y) H(r_{xy}) dy dx$$

for large ρ . One can therefore evaluate the connection probability of the random connection model with an integral.

2.1.3 Boundary effects and non-convex domains

We now discuss the introduction of non-convexity. This occurs when at least one straight line segment with endpoints in the domain intersects the domain's complement. We use this function in order to highlight this:

$$\chi(x, y) = \begin{cases} 1 & \text{if } x + \lambda(y - x) \in \mathcal{V} \text{ for all } \lambda \in [0, 1] \\ 0 & \text{otherwise} \end{cases} \quad (2.1.10)$$

The perimeter itself, which may be the outside of a building, arena or city, plays a significant role in connectivity. In [14], the connectivity of the random connection model was shown to be influenced by the meandering boundary's ability to block the viewing angle vertices, decreasing it from the usual 2π radians. In fact, pressed right up on the boundary of a disk, vertices see less than π radians. The extent to which this results in vertices becoming isolated is quantified by the expected degree of a point x , which is

$$\mathbb{E}k(x) = \int_{\mathcal{V}(x)} H(\|x - y\|) dy \quad (2.1.11)$$

where $\mathcal{V}(x)$ is the region of the domain visible to x , itself a domain³. This is often called the *connectivity mass* of a point $x \in \mathcal{V}$.

³This is often centred at x , to make the integral more tractable.

Thought of as a functional, Eq. 2.1.11 is minimised in the domain's sharpest corner [14,31]. In non-convex domains, the internal perimeter, part of which may be the boundary of an obstacle, provides another point where the connectivity mass is lower than the bulk. We investigate this in chapter 3.

2.2 Betweenness centrality

Shortest path betweenness counts all *shortest* paths between all pairs of vertices in a graph. Taking $\Sigma_{r_{xy}}$ as the set of all paths between two vertices i, j (at Euclidean displacement r_{xy}), and $\Sigma^* \subseteq \Sigma_{r_{xy}}$ as that proportion of paths of length, in hops, shorter than or equal to any other path in $\Sigma_{r_{xy}}$, then

$$\sigma_{r_{xy}} := \|\Sigma^*\| \quad (2.2.1)$$

where the norm here means the cardinality of the set. In analogy with differential geometry, we call these paths *geodesic*.

Some of these geodesics will potentially run through some specific vertex $z \in \mathcal{V}$. This is counted as $\sigma_{r_{xy}}(z)$. For example, if all geodesic paths from x to y pass through z , then the ratio $\sigma_{r_{xy}}(z)/\sigma_{r_{xy}}$ will equal unity. Otherwise, it will be a real number between zero and one. To quantify the extent to which a vertex lies on many geodesic paths, this ratio is summed over all vertex pairs in \mathcal{G} to produce the *shortest path node betweenness centrality* of z

$$\sum_{i \neq j, j \neq k, k \neq i} \frac{\sigma_{r_{xy}}(z)}{\sigma_{r_{xy}}} \quad (2.2.2)$$

The terms in this sum are called *pair dependencies* [37].

2.2.1 Computation

In order to exploit the sparsity of geodesics, a traversal algorithm is used to evaluate betweenness, due to Brandes [37]. Two steps are required. The first, just discussed, is:

- 1) Calculate σ_{xy} for all $x, y \in \mathcal{V}$.

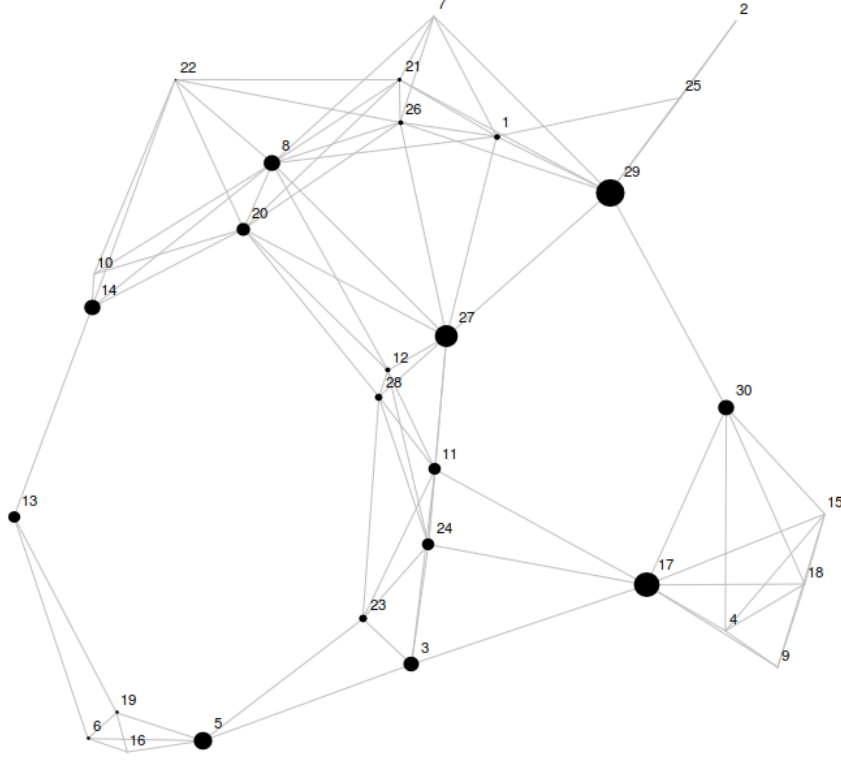


Figure 2.1: Betweenness centrality in a unit disk graph of 30 vertices drawn inside the unit square, with $r_0 = 0.3$. The size of the vertices is proportional to their betweenness.

The second involves the evaluation of the pair dependencies in Eq. 2.2.2:

- 2) Calculate $\sigma_{xy}(z)$ for all $x, y \in \mathcal{V}$, and sum to find $\sum_{i \neq j \neq k} \frac{\sigma_{rxy}(z)}{\sigma_{rxy}}$.

For a single pair, the first step is at worst $\mathcal{O}(|E|)$. A modified version of the Floyd-Warshall algorithm is used. Brandes incorporates the second step into the first by recursively updating the pair dependencies during the various evaluations of σ_{xy} . A vector of betweenness can then be obtained in at worst $\mathcal{O}(|V||E|)$.

As networks become large, this computation is notoriously intensive. It also relies on co-operation between all networked devices, which may prove impossible in practice. Though, interesting random sampling methods are known to speed up computation, see e.g. [38].

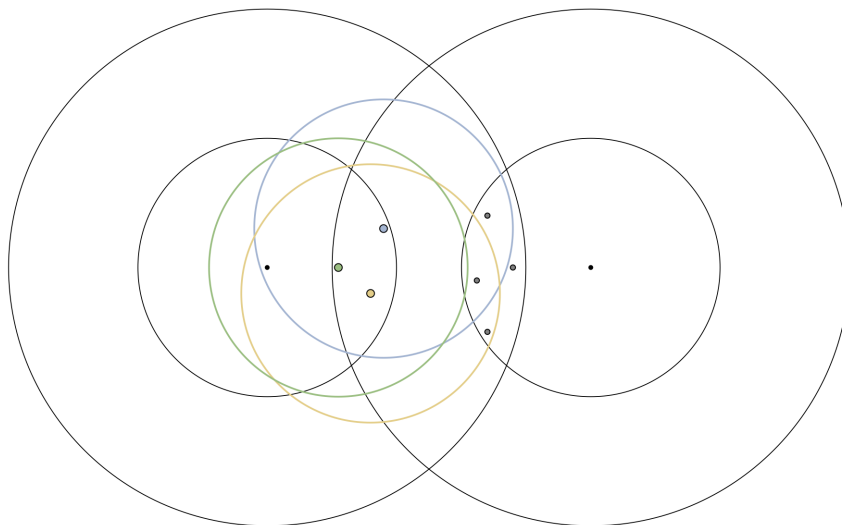


Figure 2.2: Two vertices at center separation 2.5 in a unit disk graph, taking $r_0 = 1$. The connection ranges, and an extra range (large disks), are drawn. The degrees of the three coloured vertices are dependent random variables. In this example, the green vertex has degree zero, the blue vertex has degree two and the yellow vertex also has degree two. This spatial dependence of vertex degrees in random geometric graphs such as the unit disk graph depicted here is ignored in various independence assumptions, as discussed in the text.

2.2.2 Shortest paths

Part of the problem of analytically evaluating betweenness centrality involves the difficulty of enumerating the number of geodesic paths which run between two vertices in a random geometric graph. In the Erdős-Rényi case⁴ [24], where the connection probability is just some constant function, this is relatively simple: one recursively calculates the probability that some vertex is one hop to its destination, which is p , two hops, which is the probability two vertices form a link to the same vertex and don't connect directly, which is $(1-p)(n-2)p^2$, and so on. When the connection function is not constant, however, nearby vertices have positively correlated vertex degrees. This complex spatial dependence is characteristic of combinatorial problems with a geometric element.

⁴Take n vertices and link them independently with probability p .

Now, in order to avoid this, one can make the so called *independence assumption* [39, 40]. This has been used to produce approximations to the distribution of the length of paths between vertices in the unit disk model [41], the random connection model [39], and the log-normal fading model [42]. The issue is depicted in Fig. 2.2.

The *number* of geodesics is an alternative statistic, related, as discussed, to betweenness centrality. This random *number* of geodesics is currently used by two important delay tolerant networking algorithms, BubbleRap and COAR, which algorithmically count geodesics in order to assess possible routing strategies [18].

2.3 Extended Concepts

We now discuss some extended topics related to point processes, alternative metrics, and centrality variants.

2.3.1 Binomial point processes

If we simply fix the number of vertices in a Poisson point process, we have a binomial point process. This can be a more realistic model of wireless networks, since the device numbers cannot vary so much over time (in fact, they don't vary at all).

However, the Poisson point process is used with good reason: with exactly N vertices, the modelling can become intractable, since the distance between points in a (BPP) formed within a domain $\mathcal{V} \subset \mathbb{R}^d$ is given by the beta distribution, which is only expressible in terms of a special function. Even worse, sequences of inter-point distances are no longer independent.

In [43], potential use of the binomial point process as a model of device distribution in wireless networks is discussed in detail.

2.3.2 Markov point processes

Consider a Markov chain \mathcal{M} on the space of unit disk graphs. A simple example

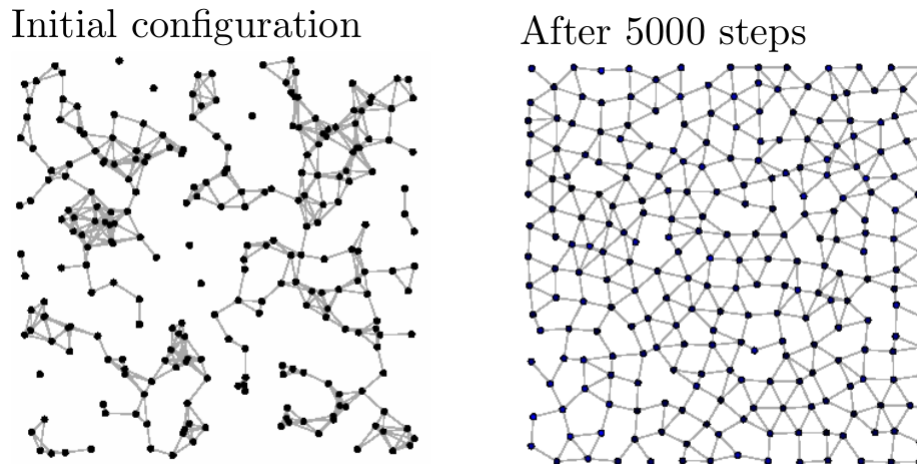


Figure 2.3: The Strauss process. A binomial point process of $n = 250$ vertices (taking $\Omega = 0.07$ and $r_0 = 0.08$) is updated in a step by step fashion by the Metropolis-Hastings algorithm. It creates a pattern of repelling points. From Irons et al 2011, referenced in the text.

is the Strauss process. Pairs of points $\{\zeta, \eta\} \subset \mathcal{Y}$ ‘interact’ with a geometric potential ϕ , given by their Euclidean separation

$$\log \phi(\{\zeta, \eta\}) \propto \frac{1}{\|\zeta - \eta\|} \quad (2.3.1)$$

The probability of a configuration, $\mathbb{P}(x_1, x_2, \dots, x_N)$, is then given by a sum over the set \mathcal{C} of all 2-vertex cliques in the respective unit disk graph formed on the configuration

$$\log \mathbb{P}(x_1, x_2, \dots, x_N) \propto \sum_{\{\zeta, \eta\} \in \mathcal{C}} \log \phi(\{\zeta, \eta\}) \quad (2.3.2)$$

which is associated with a state of \mathcal{M} .

One can generate these configurations with the Metropolis-Hastings algorithm [44]. The algorithm goes as follows:

1. Distribute N points over a domain $\mathcal{V} \subseteq \mathbb{R}^d$.

2. Pick a vertex (call its position v), and, picking an angle uniformly, randomly displace it a distance given by the Beta distribution⁵, rejecting moves which put the vertex outside the square. Call this new location μ .
3. Calculate two quantities, first

$$n_v = \sum_{i \neq v} I_{\{\|i-v\| < \Omega\}} \frac{\Omega}{\|i-v\|} \quad (2.3.3)$$

with Ω a parameter of the process with units of distance, and then

$$n_\mu = \sum_{i \neq \mu} I_{\{\|i-\mu\| < \Omega\}} \frac{\Omega}{\|i-\mu\|} \quad (2.3.4)$$

The move is then accepted with probability $\min(1, \omega^{n_\mu - n_v})$, where $\omega \in [0, 1]$ is some parameter of the model quantifying the amount of inter-point repulsion.

The fact that the potential of the whole configuration can be written as a product of all two vertex cliques in the graph implies that the density $\mathbb{P}(x_1, x_2, \dots, x_N)$ is a Gibbs ensemble:

$$\mathbb{P}(x_1, x_2, \dots, x_N) \propto \prod_{\{\zeta, \eta\} \in \mathcal{C}} \phi(\{\zeta, \eta\}) \quad (2.3.5)$$

which is a factorisation over cliques.

This sort of repelling points model helps combat the most unrealistic assumption of the Poisson process model, that there will sometimes be nearby base stations. Determinantal point processes, which are processes whose spatial distributions are related to the determinant of a matrix, are an interesting avenue of further research.

2.3.3 Geometric preferential attachment

Considers a binomial point process \mathcal{Y} of n points x_1, x_2, \dots, x_n on the surface of a torus \mathbb{T} . Allowing multiple edges, each point is selected in turn such that,

⁵Which gives the distance between points of a binomial point process [43].

at time $t \in \{1, 2, \dots, n\}$, vertex $x_t \in \Phi$ forms m randomly selected connections to those vertices within Euclidean distance r_0 ; for each $i \in \{1, 2, \dots, m\}$, the probability vertex v is selected is

$$P(v \text{ is selected}) = \frac{\deg_t v}{\max \left(\sum_{\|x_t - v\| \leq r_0} \deg_t v, \gamma \right)} \quad (2.3.6)$$

with

$$P(x_t \text{ connects to itself}) = 1 - \frac{\sum_{\|x_t - v\| \leq r_0} \deg_t v}{\max \left(\sum_{\|x_t - v\| \leq r_0} \deg_t v, \gamma \right)} \quad (2.3.7)$$

The factor $\gamma = \alpha m \pi r_0^2 t$ tunes the probability of loop formation (i.e. self connection). This propensity for loop formation increases with time, the number of edges m we intend to add, and the connection radius r_0 .

This model is an extension of the *online nearest neighbour graph* (see e.g. [45], or the earlier⁶ paper of Berger, Bollobás, Borgs, Chayes and Riordan [46]), which is a simple growing spatial network: vertices are placed one by one in some domain, and each time joined to their nearest neighbour [6].

2.3.4 Hyperbolic random geometric graphs

Apart from altering the nature of the point process as in subsection 2.3, one can transform the underlying metric space in which the graphs are embedded. An interesting example of this is the *hyperbolic random geometric graph* [47], where a simple Poisson point process is formed on the hyperbolic plane with points retained inside a bounded region. Pairs of points are then joined according to the unit disk rule, but now considering the distance g between two points (x_1, y_1) and (x_2, y_2) to be

$$g((x_1, y_1), (x_2, y_2)) = \operatorname{arcosh}(\cosh(y_1) \cosh(x_2 - x_1) \cosh(y_2) - \sinh(y_1) \sinh(y_2))$$

where the Cartesian axis are embedded in the hyperbolic plane, and the two arguments of g read off accordingly.

⁶This was published in 2007, a year before [45].

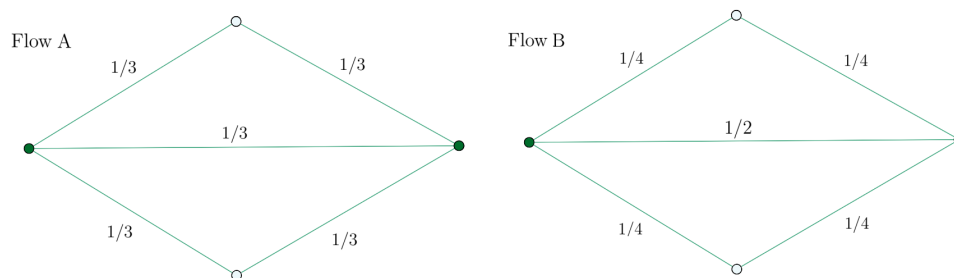


Figure 2.4: A current of $1A$ flows into the left most vertex of a network of unit resistors. It is then extracted from the right most vertex. Two different current conserving flows are shown on the same simple network. The values on the edges are the currents flowing along those edges. Flow B minimises the total dissipated energy, and so satisfies the Kirchhoff laws.

As a current application area, these non-standard RGG's are used to study theories concerning *complex systems* [48, 49].

2.3.5 Current flow betweenness

Two alternative forms of betweenness, the first introduced by Freeman [50] called *flow betweenness*, and the second by Newman [51] called *current flow betweenness*, aim to quantify the effect of non-geodesic paths on the centrality of vertices:

1. Flow betweenness considers a function $f : V \rightarrow \mathbb{R}$ quantifying the current passing through some vertex $v \in V$ while the flow through the network is maximal. The capacity of all edges must be defined, and one sums of all possible source-destination pairs.
2. Current flow betweenness considers the unique ‘unit flow’, which is a current of $1A$ (one Ampere), passing through the network while satisfying the Kirchhoff laws. Note there is only one flow which minimises the dissipated energy, and hence only one flow which satisfies Kirchhoff's laws [11]. Again, one sums this over all source-destination pairs.

Note, dissipated energy is the product of current and voltage. Equivalently

$$E = \sum_{e \in E} I_e^2 R_e \quad (2.3.8)$$

where I_e is the current flowing over edge e , and R_e is the resistance of edge e . Minimising this using Lagrange multipliers with the Kirchhoff current law as a constraint [52], see for example Fig. 2.4, provides currents flowing through each vertex with respect to two other vertices $v_i, v_j \in V$, the sum of which, over all i, j , or ‘source sets’, is the current flow betweenness.

For example, in Fig. 2.4, the dissipated energy for flow A is $5/9$, while for flow B , it is $1/2$. Therefore, given we consider a unit flow, flow B is the unique solution to the Kirchhoff laws. This would contribute to the vector of current flow betweenness centralities as one of the many source-sink pair contributions.

Also, note that current flow betweenness is equivalent to random walk betweenness [51]. Where data is flooded through a network of small cells, or through a vehicle network, this current flow betweenness can be useful in estimating the routing load on set of vertices when betweenness is shown to be uncharacteristic i.e. when data is often diverted from shortest paths. It is difficult to analyse analytically, and may be more appropriately obtained algorithmically in realistic settings [27].

Chapter 3

Connectivity

3.1 Introduction

Soft random geometric graphs consist of a set of vertices placed according to a point process in some domain $\mathcal{V} \subseteq \mathbb{R}^d$ which are coupled with a probability dependent on their Euclidean separation. The more common deterministic connection is generalised to probabilistic connection [5, 12, 14] in order, in our case, to model signal fading. Commonly known as the *random connection model*, we now have a connection function $H(\|x - y\|)$ giving the probability that links will form between nodes $x, y \in \mathcal{V}$ of a certain Euclidean displacement $\|x - y\|$. In a band-limited world of wireless communications continuously pressed for the theoretical advances that can enable 5G cellular performance, this is an important new flexibility in the model.

Connectivity has been shown the initial interest [12, 14, 31]. For example, in [14], using a cluster expansion technique from statistical physics, at high vertex density ρ the connection probability of a soft random geometric graph formed within a bounded domain \mathcal{V} is approximated as (the complement of) the probability that exactly one isolated vertex appears in an otherwise connected graph. This is justified by a conjecture of Penrose [5], asserting that the number of isolated vertices follows a Poisson distribution whose mean quickly decays as $\rho \rightarrow \infty$, thus highlighting the impact of the domain's enclosing boundary [12, 14, 26] where isolation is most common.

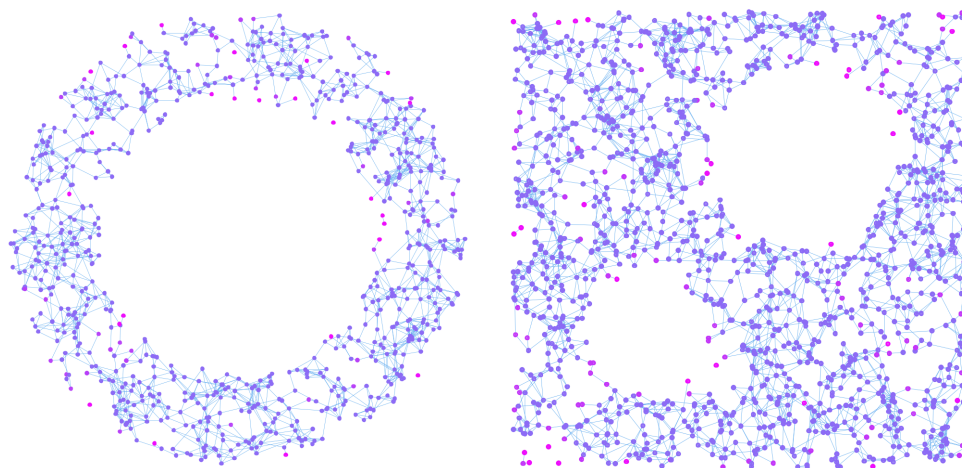


Figure 3.1: A soft random geometric graph, first defined at the beginning of Chapter 1, inside the annulus (large obstacle case), and inside a square with two circular obstacles. Vertices with low degree are highlighted in purple. We derive the graph connection probability in these simple obstructed domains.

Internal boundaries, such as obstacles, cause similar problems. In this chapter, we focus our efforts on how this particular aspect of the domain effects the graph behaviour. We therefore extend recent work on connectivity within non-convex domains, such as those incorporating internal walls [31] or a complex, fractal boundary [53], deriving analytic formulas for the connection probability P_{fc} of soft random geometric graphs formed within the annulus and spherical shell geometries, quantifying how simple convex obstacles affect connectivity. Specifically, we consider the situation where nodes connect with a probability decaying *exponentially* with their mutual Euclidean separation. This models the *Rayleigh fading* commonly observed in mobile communications.¹

The advantage of soft graphs is this ability to incorporate a fading model. In built up urban environments where signals scatter repeatedly off walls, and

¹Most of this chapter has been accepted with minor revisions for publication at *The Journal of Statistical Physics* [54]. The work in this chapter remains solely that of the author of this thesis unless otherwise indicated, given collaboration with supervisors in the appropriate fashion.

offering no direct line of sight between transmitter and receiver, the relevant fading statistics are, as mentioned, those of the Rayleigh distribution, implying the connection function

$$H(\|x - y\|) = \exp\left(-\beta\|x - y\|^2\right) \quad (3.1.1)$$

is to be implemented. We now discuss how this comes about.

3.2 Rayleigh fading

In Rayleigh fading, the channel *impulse response* [55] is modelled as a *complex Gaussian process* ξ , a sequence of complex-valued random variables

$$\xi =: \{z_n | n \in \mathbb{N}\}, \quad z_n = U_n(t) + iV_n(t) \quad (3.2.1)$$

with $U_n(t)$ and $V_n(t)$ Gaussian for all n , independent of both each other, and the remaining elements of ξ , for all n . One can think of this as a sequence of vectors, each real component of which is the randomly attenuated amplitude of the quadrature and in-phase components of a frequency modulated radio signal.

The amplitudes of the impulse response are therefore given by a Pythagorean relation between these Gaussianly distributed quadrature and in-phase amplitudes:

$$r = \sqrt{\|U\|^2 + \|V\|^2} \quad (3.2.2)$$

i.e. the radial component of the sum of two independent Gaussian variables. The amplitudes r are thus *Rayleigh distributed*. To see this, integrate the joint density of U and V along the perimeter of a disk of radius λ

$$\begin{aligned} P(r = \lambda) &= \frac{1}{2\pi\sigma^2} \int_{-\infty}^{\infty} du \int_{-\infty}^{\infty} dv f_U(u) f_V(v) \delta(\lambda - \sqrt{u^2 + v^2}) \\ &= \frac{1}{2\pi\sigma^2} \int_{-\infty}^{\infty} du \int_{-\infty}^{\infty} dv e^{-u^2/2\sigma^2} e^{-v^2/2\sigma^2} \delta(\lambda - \sqrt{u^2 + v^2}) \\ &= \frac{\lambda}{\sigma^2} e^{-\lambda^2/2\sigma^2} \end{aligned} \quad (3.2.3)$$

which is the density of the Rayleigh distribution.

Now, consider the so called outage probability P_{out} , which is the proportion of time the information-theoretic decoding error at the receiver falls below a critical rate Υ :

$$P_{\text{out}} = P \left[\log_2 \left(1 + \frac{P}{N_0} \|h\|^2 \right) < \Upsilon \right] \quad (3.2.4)$$

We are thus interested in the random channel gain $\|h\|^2$, and the signal power P . These power gains are proportional to the *square* of the impulse response's Rayleigh distributed amplitudes, so are exponentially distributed:

$$P(\|h\|^2 = \lambda) = \frac{1}{2\sigma^2} \exp\left(\frac{-\lambda}{2\sigma^2}\right) \quad (3.2.5)$$

Also, the signal suffers from a propagation decay. Writing the signal power as P , and the noise power as N_0 , the signal-to-noise ratio decays as a power η of the transmitter-receiver propagation distance $\|x - y\|$

$$\frac{P}{N_0} = c \|x - y\|^{-\eta} \quad (3.2.6)$$

This is the path loss exponent, with $\eta = 2$ related to free-space propagation. Rearranging 3.2.4 gives the source-destination connection probability as the complement of the outage probability

$$H(\|x - y\|) = 1 - P \left[\|h\|^2 < \frac{N_0 (2^\Upsilon - 1)}{P} \right] \quad (3.2.7)$$

Finally, extracting the constant β :

$$\begin{aligned} \frac{N_0 (2^\Upsilon - 1)}{P} &= \frac{N_0 \|x - y\|^\eta}{c} (2^\Upsilon - 1) \\ &= \left(\frac{N_0}{c} (2^\Upsilon - 1) \right) \|x - y\|^\eta \\ &= \beta \|x - y\|^\eta \end{aligned}$$

This implies the Rayleigh fading connection function is given by

$$\begin{aligned} H(r_{xy}) &= 1 - P \left[\|h\|^2 < \beta \|x - y\|^\eta \right] \\ &= \exp(-\beta \|x - y\|^\eta) \end{aligned} \quad (3.2.8)$$

since $\|h\|^2$ is exponentially distributed, as discussed.

To clarify notation, we sometimes refer to the constant

$$r_0 = \beta^{-1/\eta} \quad (3.2.9)$$

to signify the length scale over which nodes typically connect, since the exponent $\beta \|x - y\|^\eta > 1$ whenever $\|x - y\| > r_0$, and so the connection probability is low.

3.3 The annulus domain \mathcal{A}

Take our domain to be the annulus \mathcal{A} of inner radius r and outer radius R , two examples of which are depicted in Fig. 3.2. Consider the outer radius of this annulus to be large compared to the typical connection range. We are interested in evaluating

$$\mathbb{P}(n_0 = 0) \approx 1 - \rho \int_{\mathcal{V}} e^{-\rho \int_{\mathcal{V}} \chi^{(x,y)} H(r_{xy}) dy} dx \quad (3.3.1)$$

as discussed in Section 2.1.2. There, we defined the connectivity mass at a point $x \in \mathcal{A}$, and its analogue over the region visible to x

$$\mathcal{M}(x) = \int_{\mathcal{A}(x)} H(\|x - y\|) dy \quad (3.3.2)$$

This mass is approximated within two obstacle-size regimes, the first where $r \ll r_0$, and the second where $r \gg r_0$. In each regime we can make some assumptions about the geometry of the region $\mathcal{A}(x)$ visible to x , which yields tractable formulas for the connectivity mass in terms of powers of the distance ϵ from the obstacle's perimeter. We then have P_{fc} in the annulus \mathcal{A} . This

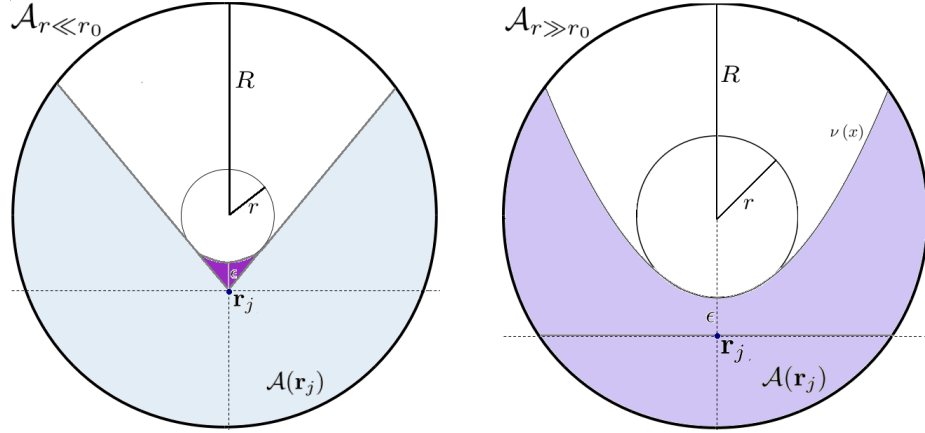


Figure 3.2: A depiction of the integration regions used for the annulus domain \mathcal{A} with small obstruction (middle panel) and large obstruction (right panel), with the integration regions highlighted. The small, cone-like region in the middle domain \mathcal{A} is highlighted in purple.

complements the result of the disk domain, presented first in [14].

3.3.1 No obstacles

We first take the case where $r = 0$ depicted in Fig 3.2. This is the disk \mathcal{D} . We first derive an approximation to P_{fc} in this limiting domain.

Firstly, the connectivity mass a distance ϵ from the disk's centre is

$$\begin{aligned} \mathcal{M}(\epsilon) &= \frac{\pi}{2\beta} + 2 \left(\int_{\mathcal{D}_1} e^{-\beta(x^2+y^2)} dy dx - \int_{\mathcal{D}_2} e^{-\beta(x^2+y^2)} dy dx \right) \\ &= \frac{\pi}{2\beta} - 2 \int_0^R \int_0^{\epsilon - \sqrt{R^2 - x^2}} e^{-\beta(x^2+y^2)} dy dx \end{aligned} \quad (3.3.3)$$

since the integral over \mathcal{D}_1 cancels. Now, consider two regimes for the distance ϵ : in the first, where $\epsilon \approx R$ (close to the boundary), we can make the approximation $\exp(-\beta y^2) \approx 1$, since the distances y from the horizontal to the lower semi-circle in Fig. 3.3 will be small, so we can approximate the integral in Eq.

3.3.3

$$\begin{aligned} \int_0^R \int_0^{\epsilon - \sqrt{R^2 - x^2}} e^{-\beta(x^2 + y^2)} dy dx &\approx \int_0^R \int_0^{\epsilon - \sqrt{R^2 - x^2}} e^{-\beta x^2} dy dx \\ &= \frac{\sqrt{\pi}}{2\sqrt{\beta}} \epsilon - \int_0^R e^{-\beta x^2} \sqrt{R^2 - x^2} dx \end{aligned}$$

such that

$$\mathcal{M}(\epsilon \approx R) = \frac{\pi}{2\beta} - \frac{1}{R\sqrt{\beta}} \left(\frac{\sqrt{\pi}}{4\beta} \right) + (R - \epsilon) \sqrt{\frac{\pi}{\beta}} + \mathcal{O}((R - \epsilon)^2) \quad (3.3.4)$$

after Taylor expanding Eq. 3.3.4 for $\epsilon \approx R$, since the mass is smallest on the boundary, dominating Eq. 3.3.1

For the other regime where $\epsilon \ll R$:

$$\begin{aligned} \mathcal{M}(\epsilon \ll R) &\approx \int_0^{2\pi} \int_0^\infty r' e^{-\beta r'^2} dr' d\theta \\ &= \pi/\beta \end{aligned} \quad (3.3.5)$$

due to the exponential decay of the connectivity function, and so we have the probability of connection P_{fc} in the disk domain:

$$\begin{aligned} P_{fc} &\approx 1 - \rho \int_{\mathcal{V}} e^{-\rho} \chi(x, y) H(r_{xy}) dy dx \\ &= 1 - \rho \int_0^{2\pi} \int_0^{L^+} \epsilon \exp\left(-\frac{\rho\pi}{\beta}\right) d\epsilon d\theta \\ &\quad - \rho \int_{L^+}^R \exp\left(-\rho \left(\left(\frac{\pi}{2\beta} - \frac{1}{R\sqrt{\beta}} \left(\frac{\sqrt{\pi}}{4\beta} \right) \right) + (R - \epsilon) \sqrt{\frac{\pi}{\beta}} \right)\right) \epsilon d\epsilon d\theta \\ &\approx 1 - \pi R^2 \rho e^{-\frac{\rho\pi}{\beta}} - 2\pi R \sqrt{\frac{\beta}{\pi}} e^{-\frac{\rho}{\beta} \left(\frac{\pi}{2} - \frac{1}{R\sqrt{\beta}} \left(\frac{\sqrt{\pi}}{4} \right) \right)} \end{aligned} \quad (3.3.6)$$

where L^+ is the point where the two mass approximations equate. This approaches equation Eq. 38 of reference [14] as $R\sqrt{\beta} \rightarrow \infty$. The correction $\frac{\pi}{2} - \frac{1}{R\sqrt{\beta}} \left(\frac{\sqrt{\pi}}{4} \right)$ in the exponential is a curvature correction to the previous result, since before the boundary mass is expanded in a Taylor series truncated to its first term, equivalent to ignoring the curvature of the boundary.

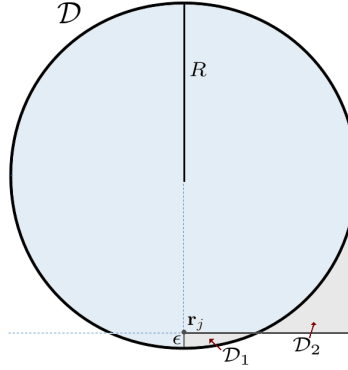


Figure 3.3: A depiction of the integration regions used for the disk domain \mathcal{D} . The small, cone-like region in the middle domain \mathcal{A} is highlighted in purple.

Monte-Carlo simulations, where graphs are drawn algorithmically and enumerated if they connect, are presented in Fig. 3.4 alongside our approximation in Eq. 3.3.6, corroborating our approximation. The simulations show an improvement on previous result in [14]. The discrepancy at low density is expected since we only consider the probability of a single isolated vertex. We also highlight the interesting composition 3.3.6. There is a bulk term (whose coefficient is proportional to the area of \mathcal{D}) and a boundary term (proportional to the circumference of \mathcal{D}). This is discussed in greater detail in e.g. [14], though we again emphasise the dominance of the boundary term as $\rho \rightarrow \infty$.

3.3.2 Small obstacles

Consider the case where $r \ll r_0$. We make the approximation that the small cone-like domain \mathcal{A}_c making up a portion of the region visible to x , denoted $\mathcal{A}(x)$, and shown in the middle panel of Fig. 3.2, is only significantly contributing to the connectivity mass at small displacements ϵ from the obstacle, since at larger displacements it thins and the wedge-like region $\mathcal{A}(x) \setminus \mathcal{A}_c$ dominates. Practically, it is \mathcal{A}_c that presents the main integration difficulties, so we approximate $H(\|x - y\|)$ over this region where the radial coordinate

$r' \ll 1$, using $\exp - (\beta r'^2) \approx 1$

$$\begin{aligned}
 \mathcal{M}(\epsilon \ll r_0) &\approx \int_{-\pi + \arcsin(\frac{r}{r+\epsilon})}^{\pi - \arcsin(\frac{r}{r+\epsilon})} \int_0^\infty e^{-\beta r'^2} r' dr' d\theta \\
 &+ 2 \int_0^{\arcsin(\frac{r}{r+\epsilon})} \int_0^{(r+\epsilon) \cos(\theta) - \sqrt{r^2 - (r+\epsilon)^2 \sin^2(\theta)}} r' dr' d\theta \\
 &= \frac{1}{\beta} \left(\pi - \arcsin\left(\frac{r}{r+\epsilon}\right) \right) \\
 &+ \int_0^{\arcsin(\frac{r}{r+\epsilon})} \left((r+\epsilon) \cos(\theta) - \sqrt{r^2 - (r+\epsilon)^2 \sin^2(\theta)} \right)^2 d\theta \\
 &= \frac{\pi}{\beta} + \left(r^2 - \frac{1}{\beta} \right) \arcsin\left(\frac{r}{r+\epsilon}\right) + r \sqrt{2r\epsilon + \epsilon^2} - \frac{\pi}{2} r^2
 \end{aligned}$$

and then expand, giving

$$\mathcal{M}(\epsilon \ll r_0) = \frac{\pi}{2\beta} + \frac{\sqrt{2}}{\beta\sqrt{r}} \epsilon^{1/2} + \frac{8\beta r^2 - 5}{6\beta\sqrt{2}r^{3/2}} \epsilon^{3/2} + \mathcal{O}(\epsilon^2) \quad (3.3.7)$$

leaving us to integrate over the annulus

$$\begin{aligned}
 P_{fc} &\approx 1 - \rho \int_{\mathcal{A}} e^{-\rho \mathcal{M}(x)} dx \\
 &\approx 1 \\
 &- \rho \int_0^{2\pi} \int_0^{L^-} (r+\epsilon) \exp \left(-\rho \left(\frac{\pi}{2\beta} + \frac{\sqrt{2}}{\beta\sqrt{r}} \epsilon^{1/2} + \frac{8\beta r^2 - 5}{6\beta\sqrt{2}r^{3/2}} \epsilon^{3/2} \right) \right) d\epsilon d\theta \\
 &\quad - \pi R^2 \rho e^{-\frac{\rho\pi}{\beta}} - 2\pi R \sqrt{\frac{\beta}{\pi}} e^{-\frac{\rho}{\beta} \left(\frac{\pi}{2} - \frac{1}{R\sqrt{\beta}} \left(\frac{\sqrt{\pi}}{4} \right) \right)} \\
 &\approx 1 \\
 &- 2\pi \rho \int_0^{L^-} (r+\epsilon) e^{-\frac{\rho\pi}{2\beta}} e^{-\rho \frac{\sqrt{2}}{\beta\sqrt{r}} \epsilon^{1/2}} \left(1 - \rho \frac{8\beta r^2 - 5}{6\beta\sqrt{2}r^{3/2}} \epsilon^{3/2} \right) d\epsilon - \pi R^2 \rho e^{-\frac{\rho\pi}{\beta}} \\
 &- 2\pi R \sqrt{\frac{\beta}{\pi}} e^{-\frac{\rho}{\beta} \left(\frac{\pi}{2} - \frac{1}{R\sqrt{\beta}} \left(\frac{\sqrt{\pi}}{4} \right) \right)} \\
 &\approx 1 - \pi r^2 \frac{2\beta^2}{\rho} e^{-\frac{\rho\pi}{2\beta}} - \pi R^2 \rho e^{-\frac{\rho\pi}{\beta}} - 2\pi R \sqrt{\frac{\beta}{\pi}} e^{-\frac{\rho}{\beta} \left(\frac{\pi}{2} - \frac{1}{R\sqrt{\beta}} \left(\frac{\sqrt{\pi}}{4} \right) \right)} \quad (3.3.8)
 \end{aligned}$$

where L^- is the point where the connectivity mass in the bulk meets our approximation $\mathcal{M}(\epsilon \ll r_0)$ near the obstacle. We numerically corroborate Eq. 3.3.8 in Fig. 3.4 using Monte Carlo simulations.

Note that this obstacle term is extremely small compared to the other contributions in Eq. 3.3.8, given its coefficient decays linearly with ρ and the factor of $(r\sqrt{\beta})^2 \ll 1$. We conclude that a small internal perimeter of radius r in any convex domain \mathcal{V} results in a negligible effect on connectivity.

3.3.3 Large obstacles

For the large obstacle case $r \gg r_0$, the relevant mass is

$$\begin{aligned} \mathcal{M}(\epsilon \ll r_0) &\approx 2 \int_0^\infty \int_0^\infty e^{-\beta(x^2+y^2)} dx dy + \int_{-\infty}^\infty \int_0^{\epsilon + \frac{1}{2r}x^2} e^{-\beta(x^2+y^2)} dy dx \\ &= \frac{\pi}{2\beta} + \frac{\sqrt{\pi}}{2\sqrt{\beta}} \int_{-\infty}^\infty e^{-\beta x^2} \operatorname{erf} \left[\left(\epsilon + \frac{1}{2r}x^2 \right) \sqrt{\beta} \right] dx \end{aligned} \quad (3.3.9)$$

yielding a power series in ϵ

$$\begin{aligned} \mathcal{M}(\epsilon \ll r_0) &\approx \frac{\pi}{2\beta} + \frac{\pi}{2\beta} \operatorname{erf} \left[\sqrt{\beta} \epsilon \right] + \frac{1}{r\sqrt{\beta}} \left(\frac{\sqrt{\pi}}{4\beta} e^{-\beta \epsilon^2} \right) \\ &= \frac{\pi}{2\beta} + \frac{1}{r\sqrt{\beta}} \left(\frac{\sqrt{\pi}}{4\beta} \right) + \frac{\sqrt{\pi}}{\sqrt{\beta}} \epsilon + \mathcal{O}(\epsilon^{3/2}) \end{aligned} \quad (3.3.10)$$

This implies the connectivity mass is scaling in the same way as for the outer boundary, but where the curvature correction is of opposite sign. We therefore have

$$P_{fc} \approx 1 - 2\pi r \sqrt{\frac{\beta}{\pi}} e^{-\frac{\rho}{\beta} \left(\frac{\pi}{2} + \frac{1}{r\sqrt{\beta}} \left(\frac{\sqrt{\pi}}{4} \right) \right)} - \pi R^2 \rho e^{-\frac{\rho\pi}{\beta}} - 2\pi R \sqrt{\frac{\beta}{\pi}} e^{-\frac{\rho}{\beta} \left(\frac{\pi}{2} - \frac{1}{R\sqrt{\beta}} \left(\frac{\sqrt{\pi}}{4} \right) \right)} \quad (3.3.11)$$

which is corroborated numerically in Fig. 3.4.

This implies that large obstacles behave like separate, internal perimeters. In the large-domain limit (where the node numbers go to infinity and the connection range is tiny compared to the large domain geometry), we can thus

use

$$P_{fc} \approx 1 - 2\pi(R+r) \sqrt{\frac{\beta}{\pi}} e^{-\frac{\rho\pi}{2\beta}} - \pi(R^2 - r^2) \rho e^{-\frac{\rho\pi}{\beta}} \quad (3.3.12)$$

3.4 The spherical shell \mathcal{S}

Consider now the spherical shell domain \mathcal{S} of inner radius r and outer radius R , which is the three-dimensional analogue of the annulus.

3.4.1 Small spherical obstacles

The region visible to the node at x is again decomposed into two parts, the three-dimensional version of \mathcal{A}_c , called \mathcal{S}_c , and the rest of the region visible to x , denoted $\mathcal{S}(x) \setminus \mathcal{S}_c$. As in the annulus with the small obstacle, we approximate $H(\|x - y\|)$ over this region where the radial coordinate $r' \ll 1$, remembering the axis of integration is centered at x :

$$\begin{aligned} \mathcal{M}_{\mathcal{S}_c}(\epsilon) &= \int_{\mathcal{S}_c} r'^2 e^{-\beta r'^2} \sin \theta dr' d\theta d\varphi \\ &\approx \int_{\mathcal{S}_c} r'^2 \sin \theta dr' d\theta d\varphi \end{aligned} \quad (3.4.1)$$

Eq. 3.4.1 is then evaluated by breaking up \mathcal{S}_c into the area of a cone of radius λ , height h and apex angle $2\theta_c$

$$\begin{aligned} \lambda &= \frac{r}{r + \epsilon} \sqrt{2r\epsilon + \epsilon^2} \\ h &= \frac{2r\epsilon + \epsilon^2}{r + \epsilon} \\ \theta_c &= \arcsin\left(\frac{r}{r + \epsilon}\right) \end{aligned}$$

Note that the apex is at a distance ϵ from the obstacle. The volume of the cone like region is given by

$$\begin{aligned}
\mathcal{M}_{\mathcal{S}_c}(\epsilon) &= \frac{1}{3}\pi\lambda^2 h - \frac{1}{6}\pi(r + \epsilon - h)(3\lambda^2 + (r + \epsilon - h)^2) \\
&= \frac{\epsilon^2\pi r^2(\epsilon + 2r)^2}{3(\epsilon + r)^3} - \frac{\epsilon^2\pi r^3(2\epsilon + 3r)}{3(\epsilon + r)^3} \\
&= \frac{\epsilon^2\pi r^2}{3(\epsilon + r)}
\end{aligned} \tag{3.4.2}$$

Adding the mass over $\mathcal{S}(x) \setminus \mathcal{S}_c$, we use the fact that the full solid angle available to a bulk node is 4π , and that the angle $\omega \leq \Omega$ available to the node at x is

$$\begin{aligned}
\omega &= \frac{1}{4\pi} \int_0^{2\pi} \int_0^{\theta_c} \sin(\theta) d\theta d\varphi \\
&= \frac{1}{2} \left(1 - \cos \left(\arcsin \left(\frac{r}{r + \epsilon} \right) \right) \right) \\
&= \frac{1}{2} \left(1 - \sqrt{1 - \left(\frac{r}{r + \epsilon} \right)^2} \right)
\end{aligned} \tag{3.4.3}$$

such that

$$\int_{\mathcal{S}(x) \setminus \mathcal{S}_c} r'^2 e^{-\beta r'^2} \sin \theta dr' d\theta d\varphi = \frac{\pi\sqrt{\pi}}{\beta\sqrt{\beta}} \left(1 - \frac{1 - \sqrt{1 - \left(\frac{r}{r + \epsilon} \right)^2}}{2} \right)$$

We then have $\mathcal{M}(\epsilon \ll r_0)$

$$\begin{aligned}
\mathcal{M}(\epsilon \ll r_0) &\approx \frac{\epsilon^2\pi r^2}{3(\epsilon + r)} + \frac{\pi\sqrt{\pi}}{\beta\sqrt{\beta}} \left(1 - \frac{1 - \sqrt{1 - \left(\frac{r}{r + \epsilon} \right)^2}}{2} \right) \\
&= \frac{\pi\sqrt{\pi}}{2\beta\sqrt{\beta}} + \frac{\pi\sqrt{\pi}}{\beta\sqrt{\beta}} \frac{1}{\sqrt{2}r} \epsilon^{1/2} + \frac{3\pi^{3/2}}{4\sqrt{2}(r\beta)^{3/2}} \epsilon^{3/2} + \mathcal{O}(\epsilon^2)
\end{aligned}$$

which implies that small spherical obstacles reduce the connection probability within the unobstructed sphere domain $\mathcal{S}_{r=0}$ to give a connection probability of

$$\begin{aligned}
 P_{fc}^{\mathcal{S}_{r \ll r_0}} &\approx P_{fc}^{\mathcal{S}_{r=0}} \\
 &- \rho e^{-\rho \left(\frac{\pi\sqrt{\pi}}{2\beta\sqrt{\beta}} \right)} \int_0^{2\pi} \int_0^\pi \int_0^{L_S^-} (r + \epsilon)^2 \sin(\theta) \\
 &\quad e^{-\rho \left(\frac{\pi\sqrt{\pi}}{2\beta\sqrt{\beta}} + \frac{\pi\sqrt{\pi}}{\beta\sqrt{\beta}} \frac{1}{\sqrt{2r}} \epsilon^{1/2} + \frac{3\pi^{3/2}}{4\sqrt{2}(r\beta)^{3/2}} \epsilon^{3/2} \right)} d\epsilon d\theta d\varphi \\
 &\approx P_{fc}^{\mathcal{S}_{r=0}} - \frac{4}{3} \pi r^3 \left(\frac{12\beta^3}{\rho\pi^3} \right) e^{-\rho \left(\frac{\pi\sqrt{\pi}}{2\beta\sqrt{\beta}} \right)} \quad (3.4.4)
 \end{aligned}$$

3.4.2 Large spherical obstacles

For large obstacles ($r \gg r_0$), we extend Eq. 3.3.9 into the third dimension. $\mathcal{M}(\epsilon \ll r_0)$ thus becomes

$$\begin{aligned}
 \mathcal{M}(\epsilon \ll r_0) &\approx 4 \int_0^\infty \int_0^\infty \int_0^\infty dx dy dz e^{-\beta(x^2+y^2+z^2)} \\
 &\quad + \int_{-\infty}^\infty \int_{-\infty}^\infty \int_0^{\nu(x,z)} dy dx dz e^{-\beta(x^2+y^2+z^2)} \quad (3.4.5)
 \end{aligned}$$

where $\nu(x, z) = \epsilon + \frac{1}{2r}(x^2 + z^2)$, yielding

$$\begin{aligned}
 \mathcal{M}(\epsilon \ll r_0) &\approx \frac{\pi\sqrt{\pi}}{2\beta\sqrt{\beta}} + \frac{\pi \left(r\sqrt{\beta\pi} \operatorname{erf}[\epsilon\sqrt{\beta}] + e^{-\beta\epsilon^2} \right)}{2r\beta^2} \\
 &= \frac{\pi\sqrt{\pi}}{2\beta\sqrt{\beta}} + \frac{\pi}{2\beta^2 r} + \frac{\pi}{\beta} \epsilon + \mathcal{O}(\epsilon^2) \quad (3.4.6)
 \end{aligned}$$

implying the connection probability is

$$\begin{aligned}
 P_{fc}^{\mathcal{S}_{r \gg r_0}} &\approx P_{fc}^{\mathcal{S}_{r=0}} - \rho e^{-\rho \left(\frac{\pi\sqrt{\pi}}{2\beta\sqrt{\beta}} + \frac{\pi}{2\beta^2 r} \right)} \int_0^{2\pi} \int_0^\pi \int_0^{L_S^-} (r + \epsilon)^2 \sin(\theta) d\epsilon d\theta d\varphi e^{-\rho \left(\frac{\pi}{\beta} \epsilon \right)} \\
 &\approx P_{fc}^{\mathcal{S}_{r=0}} - 4\pi r^2 \left(\frac{\beta}{\pi} \right) e^{-\rho \left(\frac{\pi\sqrt{\pi}}{2\beta\sqrt{\beta}} + \frac{1}{R\sqrt{\beta}} \left(\frac{\pi}{2\beta\sqrt{\beta}} \right) \right)} \quad (3.4.7)
 \end{aligned}$$

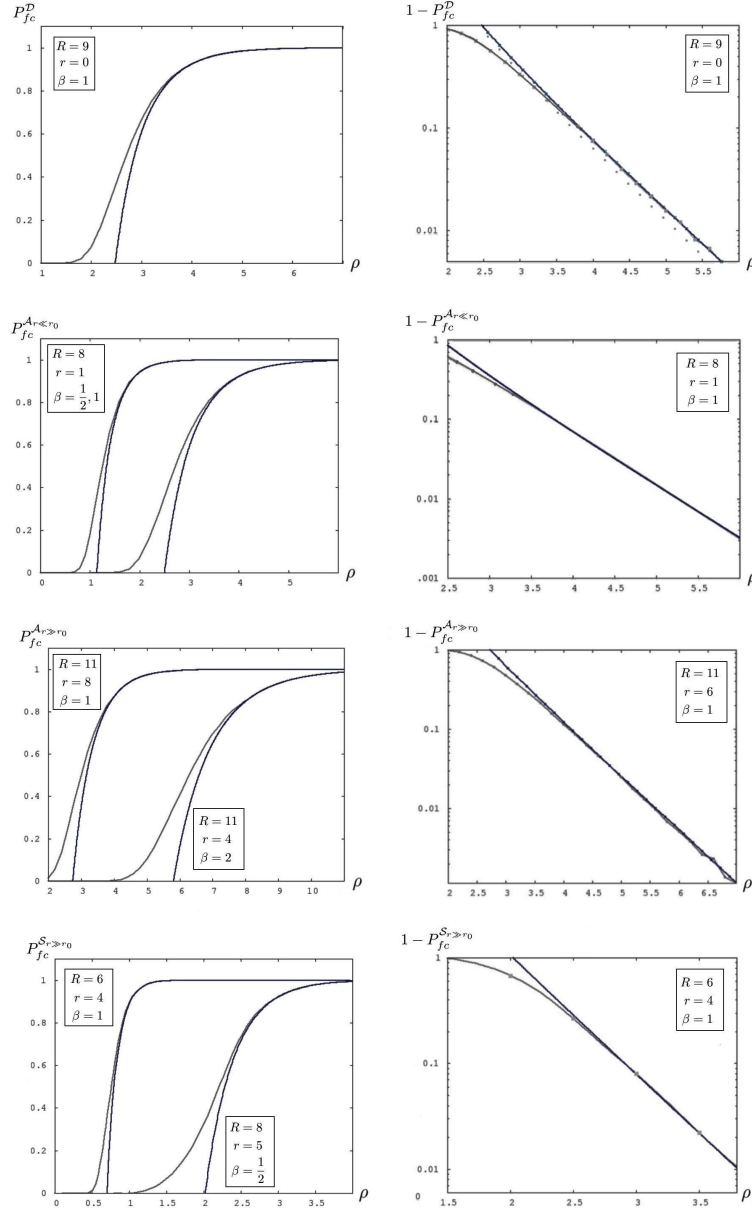


Figure 3.4: We numerically estimate the connection probability of soft random geometric graphs drawn inside the annuli \mathcal{A} and spherical shell \mathcal{S} . Every curve is compared with our analytic predictions given by Eqs. 3.3.6, 3.3.8, 3.3.11 and 3.4.8, where indicated. The discrepancy at low density is expected due to the fact we calculate only the probability of a single isolated vertex, and use its complement as an approximation to the connection probability in a typical dense network scenario.

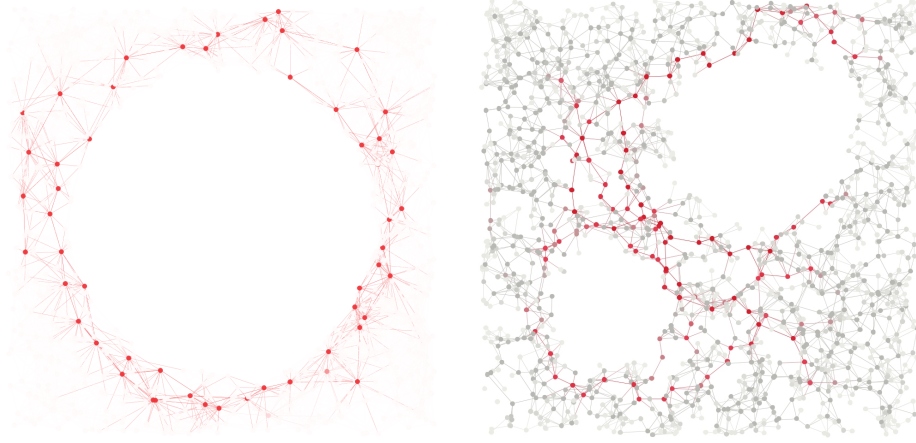


Figure 3.5: A soft random geometric graph inside a Sinai domain, and in a domain with multiple obstructions. The betweenness centrality is plotted in light tones (low) to darker tones eventually becoming red (high), showing the skeleton form around the obstacles.

where L^- is the point where our mass approximation in Eq. 3.4.6 is equal to the mass in the bulk of the sphere $(\pi/\beta)^{3/2}$.

We now have the connection probability in the spherical shell \mathcal{S}

$$P_{fc}^{\mathcal{S}} \approx 1 - \frac{4\pi}{3} (R^3 - r^3) \rho e^{-\rho \left(\frac{\pi\sqrt{\pi}}{\beta\sqrt{\beta}} \right)} - 4\pi R^2 \left(\frac{\beta}{\pi} \right) e^{-\rho \left(\frac{\pi\sqrt{\pi}}{2\beta\sqrt{\beta}} - \frac{1}{R\sqrt{\beta}} \left(\frac{\pi}{2\beta\sqrt{\beta}} \right) \right)}$$

$$- \begin{cases} \frac{4}{3}\pi r^3 \left(\frac{12\beta^3}{\rho\pi^3} \right) e^{-\rho \left(\frac{\pi\sqrt{\pi}}{2\beta\sqrt{\beta}} \right)} & \text{if } r \ll r_0 \\ 4\pi r^2 \left(\frac{\beta}{\pi} \right) e^{-\rho \left(\frac{\pi\sqrt{\pi}}{2\beta\sqrt{\beta}} - \frac{1}{R\sqrt{\beta}} \left(\frac{\pi}{2\beta\sqrt{\beta}} \right) \right)} & \text{if } r \gg r_0 \end{cases} \quad (3.4.8)$$

which is corroborated in Fig. 3.4 for the large obstacle case. Just as with the annulus, small spherical obstacles have little impact on connectivity, and large spherical obstacles behave like separate perimeters. This behaviour is likely the same for all dimensions $d > 3$, where the geometry is a hypersphere containing a convex d -dimensional obstacle.

3.5 Discussion

We have derived analytic formulas for the connection probability of soft random geometric graphs drawn inside various annuli and shells given the link formation probability between two vertices is an exponentially decaying function of their Euclidean separation. This models the Rayleigh fading of radio signal propagation within a wireless *ad hoc* network.

3.5.1 Numerical simulation

Monte Carlo corroboration of Eqs. 3.3.6, 3.3.8, 3.3.11 and 3.4.8 are presented in Fig. 3.4. We numerically construct random graphs and count how many connect. This provides a numerical estimate of the actual connection probability.

3.5.2 Multiple obstacles

We have thus extended the soft connection model into simple non-convex spaces based on circular or spherical obstacles (rather than fractal boundaries [53], internal walls [31] or fixed obstacles on a grid [32]). We highlight situations where obstacles are (and are not) important influences on connectivity:

1. Small obstacles have little impact on connectivity.
2. Large obstacles have a similar impact on connectivity as the enclosing perimeter, but their effects are dominated by the boundary as $\rho \rightarrow \infty$.

One may therefore be think that obstacles have little impact on dense network connectivity. This is not true when they occur in great numbers: given that obstacles are not too close, their effects add up in a linear fashion, potentially outweighing the effect of the boundary. To demonstrate this, take the Sinai-like domain in the right hand panel of Fig. 3.1. Without obstacles, we have

$$P_{fc} = 1 - L^2 \rho e^{-\frac{\pi}{\beta} \rho} - 4L \sqrt{\frac{\beta}{\pi}} e^{-\frac{\pi}{2\beta} \rho} - \frac{16\beta}{\rho\pi} e^{-\frac{\pi}{4\beta} \rho} \quad (3.5.1)$$

taken from [14]. This is composed of a bulk term, a boundary term and a corner term. As we have seen, introducing n circular obstacles of various radii

r_i will reduce this connection probability to:

$$1 - \sum_{i=1}^n \pi r_i^2 \left(\frac{2\beta^2}{\rho} \right) e^{-\frac{\rho\pi}{2\beta}} - \left(L^2 - \sum_{i=1}^n \pi r_i^2 \right) \rho e^{-\frac{\pi}{\beta}\rho} - 4L\sqrt{\frac{\beta}{\pi}} e^{-\frac{\pi}{2\beta}\rho} - \frac{16\beta}{\rho\pi} e^{-\frac{\pi}{4\beta}\rho}$$

which holds whenever the obstacles are separated from each other and the boundary by at least $2r_0$.

3.5.3 Surfaces without boundary

Boundary effects can be removed by working on surfaces without an enclosing perimeter. Examples include the flat torus, popular in rigorous studies but difficult to realise in wireless networks, and the sphere. Thus as $\rho \rightarrow \infty$ the obstacle effects are the dominant contribution to P_{fc} . This may be of interest to pure mathematicians studying random graphs for purposes outside communication theory [6]. Fractal obstacles may be of particular interest [53].

3.5.4 Quasi-one-dimensional regime

Note that as the width of the annulus goes to zero, the approximation that connectivity is the same as no isolated vertices breaks down. The graph now disconnects by forming two clusters separated from each other by two unpopulated strips of width usually greater than r_0 . Studying the asymptotic connectivity of these quasi-1D random geometric graphs will be topic of further study.

3.5.5 Betweenness centrality near obstacles

Vertex isolation near obstacles will have a significant effect on network functionality. This is because vertices near obstacles have exceptionally high betweenness centrality, depicted in Fig. 3.5. Routing in obstructed domains must take this effect into account, or vertices will become overloaded near obstacles as they take on an excessive number of routing tasks. Studying the connectivity properties of this ring of vertices meandering around obstacles is another topic of further study.

Chapter 4

Betweenness centrality

4.1 Introduction

Betweenness centrality is a graph theoretic measure of how often a vertex z is on a shortest path of links between any other pair of vertices in a graph [21]. It is defined according to this sum:

$$\gamma(z) = \sum_{i \neq j, j \neq k, k \neq i} \frac{\sigma_{r_{ij}}(z)}{\sigma_{r_{ij}}} \quad (4.1.1)$$

$\sigma_{r_{ij}}$ is the total number of shortest paths that join i and j , and $\sigma_{r_{ij}}(z)$ gives the number of those geodesics that pass through k . Intuitively, nodes with high betweenness can be thought of as decisive for the functionality of decentralized communication networks, since they typically route more data packets, based on the assumption that traffic tries to follow only the shortest available multi-hop paths. Though the relation at this point between structural measures like betweenness, and related measures of actual network performance which follow from the underlying structure, is not clear, the existence of an important relationship is not in doubt. We seek to clarify this as part of our contribution.

This notion of importance is in sharp contrast to methods which simply enumerate node degrees, since a bridging node which connects two large clusters is, for example, of crucial importance to the whole network, even though it may only have two neighbours. This sort of information is brought out by

betweenness centrality, but usually goes undetected.

In router-based communication networks, the router itself has a normalised betweenness of unity, since all nodes connect to it directly, while all other nodes have a centrality of zero. In ad hoc networks, and in sensor networks, betweenness is distributed randomly at each vertex according to a distribution which depends on the geometric location of vertices, implying a diverse betweenness profile. Now, in wireless networks, this diversity can be harnessed in at least three separate ways: in 2005 Gupta et al. [56] used betweenness as a criteria for electing *cluster heads* which communicate to base stations on behalf of all the cooperating machines. Later, in 2010, Ercsey-Ravasz et al. [57] demonstrated how betweenness can be used to delineate the network's *skeleton* or *vulnerability backbone*, see also the more recent paper [58], which is a percolating cluster of the most structurally important vertices. Finally, in 2006, Wang et al. [59] researched the use of betweenness for boundary detection, since at high vertex density the betweenness of devices exhibits a bi-modal behaviour near the domain boundary, and can therefore elucidate its location.

Given the insights from the last chapter concerning the structural importance of vertices near non-convex features of domains such as connectivity obstacles, in this chapter we develop an understanding of how the expected betweenness of a vertex at some domain location changes with the parameters of the model to which it takes part, evaluating analytic formulas for betweenness as a function of domain position.

We start our derivation with the disk domain \mathcal{D} of radius R (Fig. 4.1). We will consider a ‘continuum’ density of vertices, with vanishing connection range. This is for two reasons:

1. For the sake of tractability.
2. To model a dense network.

We then argue that betweenness, a computationally intensive operation with possibly high communication overheads, can be well approximated by our analytical closed form predictions, and can therefore prove useful in practice.

This chapter is structured as follows: in Section 4.2 we present our basic network model and state our main assumptions. In Section 4.3 we introduce

an analytic formula for $\mathbb{E}(\gamma(z))$ in the continuum limit (where the node density $\rho \rightarrow \infty$), which is our main result. In Section 4.4.1 we present Monte Carlo simulations which corroborate our predictions, in Section 4.4 we discuss amongst other issues the applicability of the derived betweenness centrality formula within multi-hop wireless networks.

4.2 The model

Consider a soft random geometric graph formed by distributing vertices in a bounded region $\mathcal{V} \subseteq \mathbb{R}^d$ according to a Poisson point process \mathcal{Y} of density ρ , and then adding an edge between points $\{x, y\} \in \mathcal{Y}$ with probability $H(\|x - y\|)$, where $H : \mathbb{R}^2 \rightarrow [0, 1]$ is the connection function taken to be $\exp(-\beta\|x - y\|^2)$, as in the previous chapter, and $\|x - y\|$ is the Euclidean distance between vertices. We consider only the *continuum limit*, which is a sort of double limit where $\rho \rightarrow \infty$ and the typical connection range goes to zero *in such a way that the graph remains connected*. In this limit we make the assumption that all vertices on any straight line between any two other vertices lie on the shortest path, measured in hops, that links those two endpoint vertices. We seek the continuum analogue of Eq. 4.1.1.

Consider the domain \mathcal{V} to have volume V according to the Lebesgue measure. The probability that some vertex is placed at position \mathbf{r}_i in \mathcal{V} is $V^{-1}d\mathbf{r}_i$. Thus, the probability that any vertex pair will simultaneously be placed at $\{\mathbf{r}_i, \mathbf{r}_j\}$ and construct between itself a shortest path which passes through z is $V^{-2}d\mathbf{r}_i d\mathbf{r}_j \chi_{ij}(z)$, where the characteristic function $\chi_{ij}(z)$ equates to unity whenever z lies on the path $i \rightarrow j$ given by the straight line segment \mathbf{r}_{ij} that joins \mathbf{r}_i and \mathbf{r}_j , and is zero otherwise. Summing this over all possible $\{\mathbf{r}_i, \mathbf{r}_j\}$ pair locations gives a continuum approximation to the expected betweenness centrality of z :

$$g(z) = \frac{1}{2V^2} \int_{\mathcal{V}} d\mathbf{r}_i \int_{\mathcal{V}} d\mathbf{r}_j \chi_{ij}(z) \quad (4.2.1)$$

We take \mathcal{V} to be the disk domain \mathcal{D} of radius R , so $V = \pi R^2$. Note also that due to the symmetry of the disk we can describe the position of the node k by its Euclidean distance ϵ from the disk's centre.

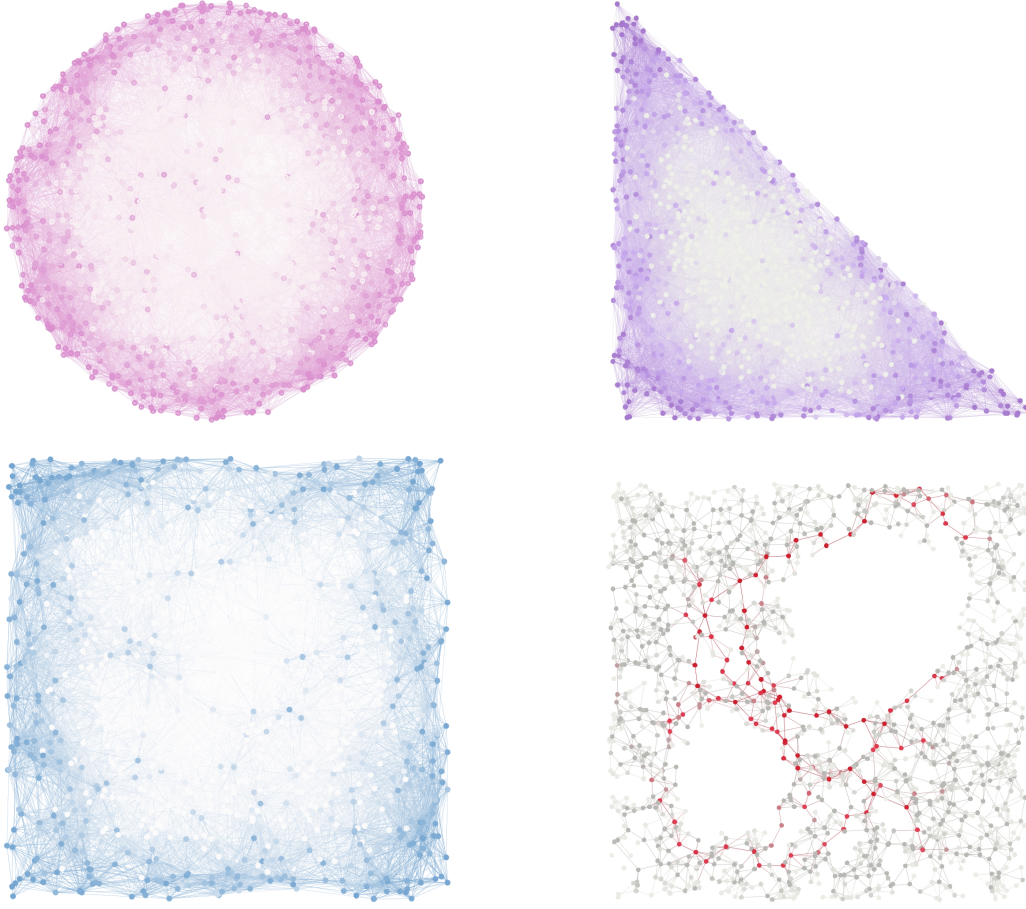


Figure 4.1: Four realisations of soft random geometric graphs and their betweenness centrality bounded within various domains, including the disk \mathcal{D} , square, right-angled triangle and square domain containing two circular obstacles: in both the left and upper right figures the darker colour represents low centrality, whereas the lighter colour high centrality, whereas in the obstructed square domain (lower right) the least central nodes are faded to grey and the most central are highlighted in red. Note that the boundaries of the domains are locations where betweenness is at a minimum. The link colours are based on the average betweenness of the two connected nodes.

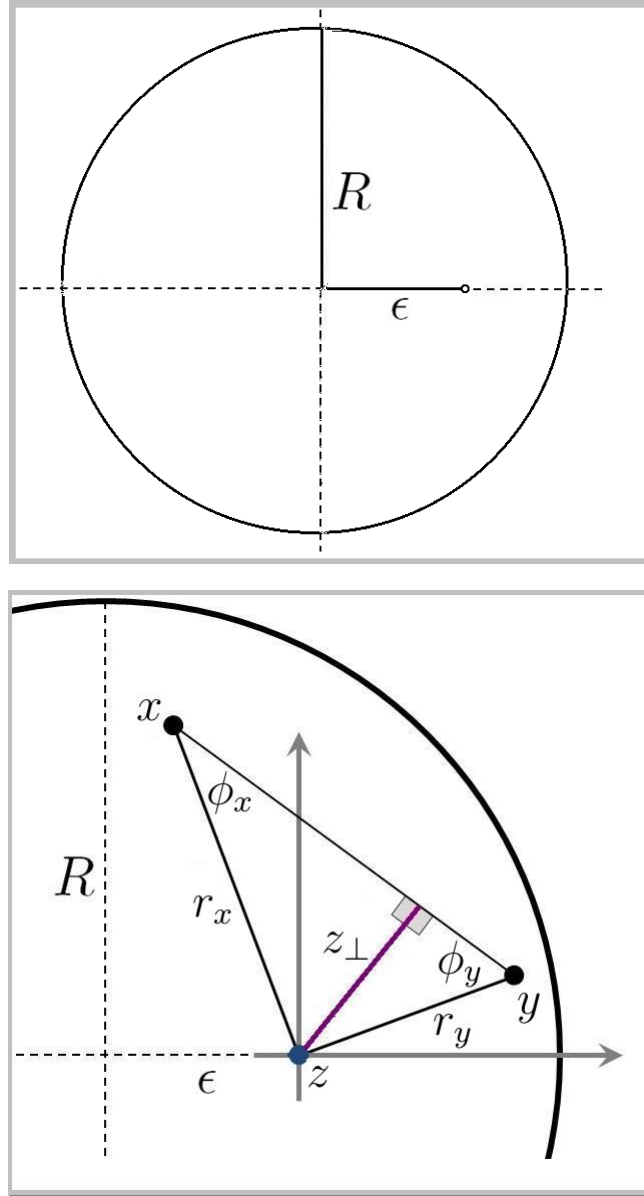


Figure 4.2: The disk domain \mathcal{D} , and the three vertices i, j and k . We are trying to obtain a dense network approximation to the betweenness centrality of a vertex placed at k . The scalar k_\perp represents the smallest Euclidean distance from k to any point on the straight line joining i and j . The axis are centred on k , while the circle is centred at $(-\epsilon, 0)$. The angles ϕ_i and ϕ_j and the distances r_i and r_j are also shown.

Consider Fig. 4.2. We define the scalar z_{\perp} as the distance of z from the straight line \mathbf{r}_{ij} . Defining the delta function $\delta(z_{\perp}(\mathbf{r}_i, \mathbf{r}_j))$, we then write the following:

$$\int_{\mathcal{D}} d\mathbf{r}_i \int_{\mathcal{D}} d\mathbf{r}_j \chi_{ij} = \int_{\mathcal{D}} d\mathbf{r}_i \int_{\mathcal{D}} d\mathbf{r}_j \delta(z_{\perp}) \quad (4.2.2)$$

The delta function will only contribute to the integral of Eq. 4.2.2 when its argument k_{\perp} is a zero of $\delta(k_{\perp})$. As such, if we then describe k_{\perp} such that it has a unique zero whenever k lies on the path $i \rightarrow j$, integrating $\delta(k_{\perp})$ over the space of all node pairs $\{\mathbf{r}_i, \mathbf{r}_j\}$ should return $g(k)$ as required.

4.3 The δ function

Fig. 4.2 shows z located a distance ϵ from the centre of \mathcal{D} , with the coordinate system centred on z and orientated such that the disk centre is at $(-\epsilon, 0)$. Considering nodes x and y at distances r_x and r_y from z respectively, we have that the internal angles ϕ_x , ϕ_y and $(\theta_x - \theta_y)$ sum to π . The perpendicular distance z_{\perp} from z to the line \mathbf{r}_{xy} then satisfies both

$$\frac{z_{\perp}}{r_x} = \sin(\phi_x)$$

and

$$\frac{z_{\perp}}{r_y} = \sin(\phi_y)$$

Adding the above and taking small angle approximations (since we are interested in the case where $z_{\perp} \ll 1$) we have that

$$\phi_x + \phi_y = \pi - \theta_y + \theta_x = z_{\perp} \left(\frac{1}{r_x} + \frac{1}{r_y} \right) \quad (4.3.1)$$

whenever $z_\perp \ll 1$. This approximation presents a unique zero of z_\perp whenever $\theta_x - \theta_y + \pi = 0$, allowing

$$\begin{aligned}\delta(z_\perp) &= \delta\left(\frac{\theta_x - \theta_y + \pi}{\frac{1}{r_x} + \frac{1}{r_y}}\right) \\ &= \delta(\theta_i - \theta_j + \pi) \left(\frac{1}{r_i} + \frac{1}{r_j}\right)\end{aligned}\quad (4.3.2)$$

due to the trivial scaling laws of the delta function. Eq. 4.2.2, a double volume integral, becomes a quadruple integral

$$\begin{aligned}g(\epsilon) &= \frac{1}{2V^2} \int_{\mathcal{D}} d\mathbf{r}_x \int_{\mathcal{D}} d\mathbf{r}_y \chi_{xy}(z) \\ &= \frac{1}{2V^2} \int_0^{2\pi} d\theta_x \int_0^{2\pi} d\theta_y \int_0^{r(\theta_x)} r_x dr_x \int_0^{r(\theta_y)} r_y dr_y \delta(z_\perp)\end{aligned}\quad (4.3.3)$$

Taking $r(\theta) = \sqrt{R^2 - \epsilon^2 \sin^2(\theta)} - \epsilon \cos(\theta)$, the polar equation of the circle bounding \mathcal{D} , Eq. 4.3.3 becomes

$$\frac{1}{2V^2} \int_0^{2\pi} d\theta_x \int_0^{2\pi} d\theta_y \delta(\theta_x - \theta_y + \pi) \int_0^{r(\theta_y)} r_y dr_y \int_0^{r(\theta_x)} \left(\frac{1}{r_x} + \frac{1}{r_y}\right) r_x dr_x$$

which is

$$\frac{1}{2V^2} \int_0^{2\pi} d\theta_x \int_0^{2\pi} d\theta_y \delta(\theta_x - \theta_y + \pi) \left(r(\theta_x) \frac{r^2(\theta_y)}{2} + r(\theta_y) \frac{r^2(\theta_x)}{2} \right)$$

then we integrate the delta function:

$$\begin{aligned}g(\epsilon) &= \frac{1}{4V^2} \int_0^{2\pi} d\theta_x r(\theta_x) r(\theta_x + \pi) (r(\theta_x) + r(\theta_x + \pi)) \\ &= \frac{1}{2V^2} \int_0^{2\pi} d\theta_x (R^2 - \epsilon^2) \sqrt{R^2 - \epsilon^2 \sin^2(\theta_x)}\end{aligned}$$

leaving

$$g(\epsilon) = \frac{2(R^2 - \epsilon^2)}{\pi^2 R^3} E\left(\frac{\epsilon}{R}\right)\quad (4.3.4)$$

where

$$E(k) = \int_0^{\pi/2} d\theta \sqrt{1 - k^2 \sin^2(\theta)} \quad (4.3.5)$$

is the complete elliptic integral of the second kind (which is related to the perimeter of an ellipse [60]). We normalise this to $g^*(\epsilon)$ by dividing Eq. 4.3.4 by its maximum value (which is at $\epsilon = 0$), to obtain our main result

$$g^*(\epsilon) = \frac{2}{\pi} (1 - \epsilon^2) E(\epsilon) \quad (4.3.6)$$

with ϵ in units of R (and with betweenness now an element of the unit interval).

Elliptic integrals cannot be easily visualised, so for clarification we can expand Eq. 4.3.6 near the origin (i.e. when $\epsilon \ll 1$) to obtain

$$g^*(\epsilon \ll 1) = 1 - \frac{5\epsilon^2}{R^2} + \frac{13\epsilon^4}{64R^4} + \mathcal{O}(\epsilon^6) \quad (4.3.7)$$

while near the boundary (i.e. when $\epsilon \approx R$)

$$g^*(\epsilon \approx R) = \frac{4(R - \epsilon)}{\pi R} + \mathcal{O}((R - \epsilon)^2) \quad (4.3.8)$$

which implies a quadratic scaling of betweenness near the centre, and a linear scaling near the periphery.

4.4 Discussion

In this section we discuss numerical corroboration, and potential applications of this centrality analysis.

4.4.1 Numerical simulation

Fig. 4.3 shows that the betweenness $\gamma(\kappa)$ of nodes situated in the bulk of \mathcal{D} is typically high. Binning the centrality in small increments of displacement from the domain centre and averaging over many network realizations, we can plot this computationally acquired sample mean of betweenness against location, and thus demonstrate how at finite densities this betweenness approaches the

continuum prediction of Eq. 4.3.6, which we do in this figure. We take β to be the largest value required for full network connectivity, and increase ρ from 10 to 500, each time evaluating betweenness numerically using the algorithm defined in the Mathematica 10 language.

The limit is never reached, only approached. At high density the discrepancy is small. We propose this is simply due to the geodesic path not approaching a straight line with density. There are also many geodesic paths in the limit. So it appears this evident discrepancy will not go away by simply increasing the density. Nevertheless, the betweenness does indeed appear to be proportional to this mass of convex hulls which intersect k and lie within \mathcal{D} , and so this simple approximation may prove useful in practice.

4.4.2 Applications

We now discuss some possible applications of Eq. 4.3.6. Betweenness centrality has been used for electing cluster heads (CH) [56]). These are special vertices which take on the task of routing collected data, often sensor data, to some distant point on behalf of the network. In sensor networks, they are often called *sinks*. A number of routing protocols are usually implemented. For example, the basic LEACH (Low Energy Adaptive Clustering Hierarchy [61]) protocol uses a random selection of cluster heads at each round (i.e. time-step), the vertices each taking turns in bearing the burden of cluster head status, or, alternatively, EECS (Energy Efficient Clustering Scheme [62]), which requires vertices to broadcast their remaining power to first-degree neighbours, asking machines that find themselves with the most battery power to then elect themselves to cluster head status.

However, in large networks using a vanishing transmitter range these protocols don't work: far too many cluster heads get elected due to the huge vertex numbers and the efficiency problem that this technique is trying to mitigate re-arises. Potentially increasing transmitter range could resolve the problem (since the usual techniques are based on one-hop access to the head vertex), though this introduces interference problems, so one searches for another solution.

Betweenness is a possible alternative election criteria, since it is proportional to power consumption, and to routing load, unlike most other centrality

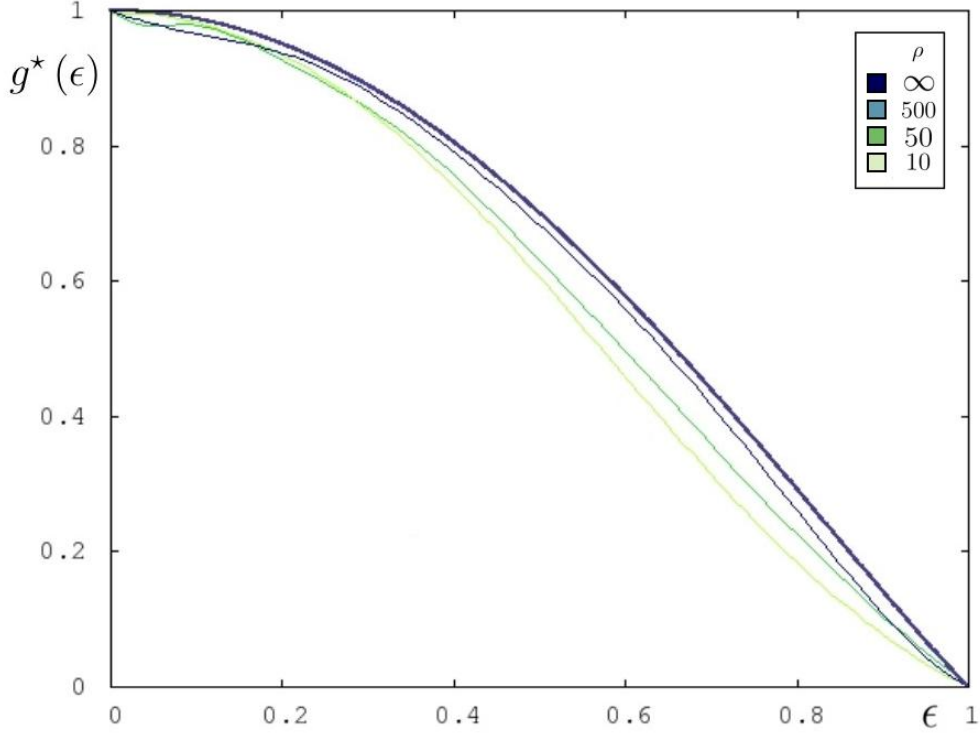


Figure 4.3: Numerical evaluation of our continuum approximation Eq. 4.3.6. Increasing the density of the point process, we ensure it contains a point z at distance ϵ from the centre of \mathcal{D} . A soft random geometric graph with a Rayleigh fading connection function of vanishing range $\beta \gg 1$, as in Chapter 3, is then formed, and the betweenness centrality of z is calculated numerically. The thicker line at the top is Eq. 4.3.6. The finite density simulations never converge to this approximation, but the error is small.

measures. This allows idle boundary vertices to act as cluster heads whenever power minimisation is preferred, or busy domain-center vertices whenever optimisation of vertex-to-vertex communication overheads is tasked. Knowledge of betweenness as a function of position helps in the selection of positions which, when occupied by vertices, results in CH election.

Note also that, based on the intuition that central vertices are easier to reach, communication-based resource consumption is minimised whenever high-betweenness vertices are, in general, used as cluster heads.

Boundary detection is another application. This is an important field, with various applications [59,63,64]. One potential use of betweenness as a boundary detector is for mitigating the so called boundary effect phenomenon [14], where high-density network connectivity is hampered through vertices becoming isolated near the domain boundaries. One potential mitigation technique is to increase the device transmit power at the domain boundary e.g. we can harness some spare power in the relatively idle boundary vertices, increasing machine transmit power appropriately with betweenness. This does not require the sharing of routing tables or other connectivity information, since betweenness is directly proportional to the devices current routing load. Finding the optimal function of the betweenness (or perhaps other centrality measures) is beyond the scope of this thesis, but we highlight that this is an interesting and important open problem.

Skeleton extraction is a third application of betweenness analysis in wireless networks. The skeleton [58] consists of the most central vertices, given by a rather arbitrary percentage (the top 5%, for example). Note the bottom right panel of Fig. 4.1, where betweenness is plotted over a square domain containing two circular obstacles (which restrict line-of-sight connections between vertices, e.g. [31]). The skeleton [58] forms around the circular obstacles. We discuss this further in Section 6.1.1.

4.4.3 The advantages of betweenness

The betweenness centrality of vertices stands alongside a variety of popular centrality variants, many of which originated in sociology. See e.g. [18] for a detailed discussion of those related to betweenness itself in the scope of delay

tolerant communication, defined in section 1.1. We now discuss the possible alternatives, though note that there are hundreds of existing variants that could be studied, e.g. analytically, with those briefly discussed in this section characteristic of the main themes. These themes include considering edges or nodes, flows, or analysis of matrices such as the Laplacian see e.g. [51].

1. **Edge betweenness centrality:** the number of shortest paths which involve a particular *edge* are considered [65].
2. **Flow betweenness centrality:** a flow of material through the network elucidates the importance of vertices [50].
3. **Node closeness centrality:** the sum of all geodesic distances to the remaining $N - 1$ vertices determines centrality, see e.g. [66].
4. **Node eigenvector centrality:** a sophisticated extension of degree centrality, a form of which is implemented in PageRank. Vertices are given centrality scores based on their proximity to other central vertices, which admits analysis using matrices [67].
5. **Node degree centrality:** vertices are ranked simply by the number of neighbours they have [68].

Edge betweenness highlights communication channels which may become over subscribed. This would be a good alternative investigation: it is just as difficult to compute on a sparse graph [65], and just as desirable in a closed, analytic form, for example near an obstacle. It can then be used as a complement to an algorithmic determination of edge betweenness centrality (for various reasons related to the prediction of e.g. channel characteristics). But as part of the current scope of centrality in wireless networks, it is perhaps less relevant. It cannot be used for boundary detection, for example, and it is sensitive to an exact specification of link efficiency, which is a difficult to characterise element of wireless performance.

Current flow betweenness is perhaps the better candidate for wireless network-theoretic development than edge betweenness, see e.g. [27]. It characterises the intuitive reason vertices, or edges, are central: they can't help

but be put under pressure during the operation of a flow. It is, however, too mathematically involved for an analysis of this sort. It may be more appropriate to algorithmically determine, as which is discussed in the aforementioned reference.

Closeness is also available as a topic of study in communication networks [69]. This is for the simple reason that short geodesic hop counts to all vertices characterise multi-hop routing in a straightforward way. But it does not capture the ‘bridging vertex’ issues picked up by betweenness.

Degree centrality, and sophisticated extensions such as PageRank [67], potentially suffer from the same sort of tractability issues as current flow betweenness if we intended to go beyond calculating expectations, and instead look for a distribution of a vector of degrees, since spatial dependence between nearby vertex degrees is difficult to deal with. Though the expected degree of a vertex is easier to calculate. The trade off between the characterisation of flows which betweenness can provide, the overall tractability of its first moment, and its established use in ad hoc networks, provides the motivation for an analytic study.

4.4.4 Convergence

Despite the disparity between betweenness centrality and our continuum approximation Eq. 4.3.6, Fig. 4.3 shows a remarkably good approximation, given we must take into account:

1. That there are many geodesic paths which join two vertices as $\rho \rightarrow \infty$.
2. That the paths are not straight, but appear to form geometric functions (see e.g. the discussion of Schramm–Loewner Evolutions in [11]).

Thus, the small discrepancy is a fair price to pay given the difficulty that a more accurate, finite density approximation appears to present.

Also, we have pointed out the quadratic scaling of betweenness as vertices moves away from the central region of the disk domain in Eq. 4.3.7. It is interesting to ask how sensitive this first order term is to details of the boundary.

Chapter 5

Geodesic Paths

5.1 Introduction

Minimising the total number of sequential transmissions required for two vertices to communicate is a common concern in multi-hop communication. This is due to:

1. The distortion caused by excessive amplify-and-forward activity,
2. The loss of SINR (signal-to-interference-plus noise ratio) caused by an overly intense spatio-temporal point process of relay transmissions.

Probabilistic modelling of the network's route statistics can prove important for the management of these issues, as well as surrounding concerns in multi-hop communication [39–41]. This motivates a number of problems concerning the statistics of paths, most prominently that of finding a function $g : \mathbb{Z} \rightarrow \{\Omega, \mathcal{F}, \mathbb{P}\}$ relating the minimum number of hops between two vertices x, y in a random geometric graph to a probability distribution on the set of Euclidean distances which could separate them in the metric space. The origins of this problem go back to Chandler's letter in the 1980's [70]. As an example application, this relationship can be used to provide location estimates to vertices possessing hop-counts to 'anchor' devices distributed around the domain. This is a particularly useful skill in wireless sensor networks where GPS is often unavailable, see e.g. [29].

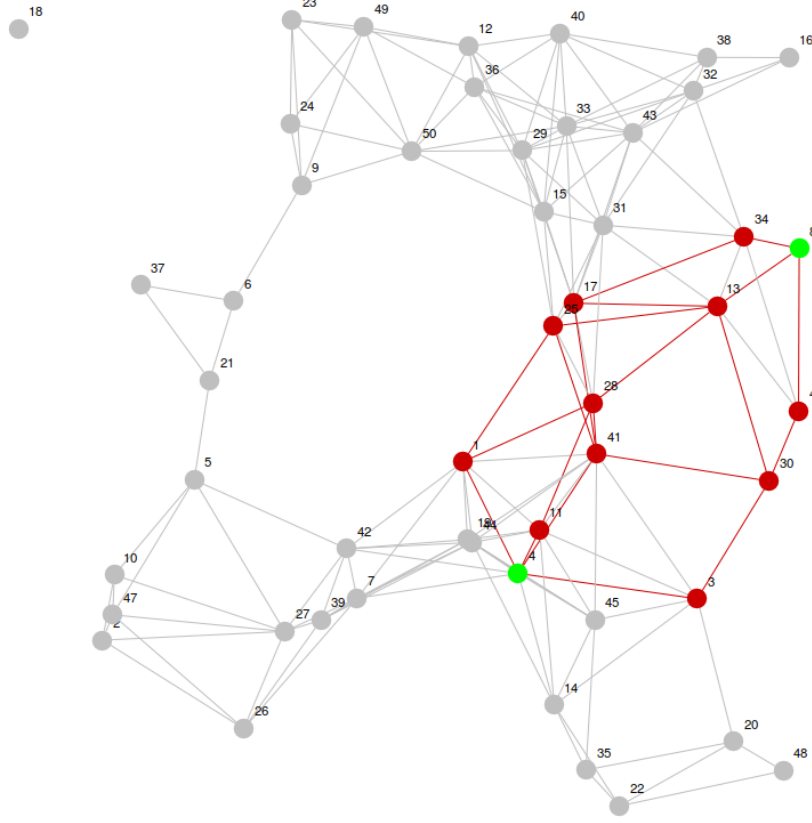


Figure 5.1: Vertices 4 and 8 are separated by Euclidean distance 2.4 in a unit disk graph, with the connection range $r_0 = 1$. They are joined by ten geodesic paths, each of four hops. We evaluate the expectation of this quantity in terms of the mutual Euclidean separation of vertices.

The *number* of geodesics is also potentially of interest. An example set of geodesics is depicted in Fig. 5.1. This is the more general statistic, since no k hops paths suggest paths are at least $k + 1$ hops. A distribution on the number of k hop paths can provide these probabilities. Therefore, let $\mathcal{V} \subseteq \mathbb{R}^d$ be a bounded region of volume V associated with both the Lebesgue measure dx and the Euclidean metric $r_{xy} = \|x - y\|$ for any $x, y \in \mathcal{V}$. Construct a *unit disk graph* $\mathcal{G}(n, \pi r_0^2)$ in \mathcal{V} by deterministically linking pairs of a Poisson point process $\mathcal{Y} \subseteq \mathcal{V}$ of density ρ whenever $\|x - y\| < r_0$.

Set $r_0 = 1$. Consider two nodes x and y in $\mathcal{G}(n, \pi)$, and call these *terminal*

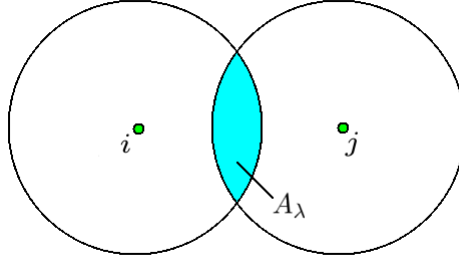


Figure 5.2: Points x and y separated by $\lambda \in [1, 2)$ create an area highlighted in blue, which is A_λ . Vertices falling within this blue region lie on one of potentially many (what will necessarily be) shortest paths which run between these two vertices, each of two hops.

nodes. In any graph realisation, these terminal nodes are either disconnected such that no path exists between them, or they are linked by a variety of different paths of various lengths. Consider now only the geodesic paths. Write $\sigma_{r_{xy}}$ for the number of paths of this geodesic length joining x and y , and separated by Euclidean distance r_{xy} . We name $\sigma_{r_{xy}}$ the *geodesic cardinality* of the distance r_{xy} , since it gives the cardinality or ‘number of elements’ $\sigma_{r_{xy}}$ in the set of geodesic paths joining x and y . Vertices lying mutually displaced by r_{xy} are expected to be linked by $\mathbb{E}(\sigma_{r_{xy}})$ geodesic paths. This is *expected geodesic cardinality*.

How long are these paths? They can be of potentially any number of hops *larger* than $\lceil r_{xy} \rceil$ (which is the smallest integer larger than or equal to r_{xy} known as its ‘ceiling’). To clarify this, we relate in Table 5.1 a range of Euclidean distances and the minimum number of hops required to join two vertices of that displacement r_{xy} . We now look for an analytic expression $\sigma_{r_{xy}}$ in terms of displacement r_{xy} , and density ρ . We only consider a density regime such that all vertices display at least one path to every other vertex in the graph which is of the *shortest possible length* $k = \lceil r_{xy} \rceil$ hops. This ensures the work is relevant to the ultra-dense 5G small cell scenario, and the associated communications problems, such as interference minimisation, discussed in the introduction.

Displacement r_{xy}	Minimum number of hops $i \rightarrow j$
$r_{xy} \in [0, 1)$	1 hop
$r_{xy} \in [1, 2)$	2 hops
$r_{xy} \in [2, 3)$	3 hops
$r_{xy} \in [3, 4)$	4 hops
$r_{xy} \in [4, 5)$	5 hops
\vdots	\vdots

Table 5.1: The minimum number of hops required for two vertices to communicate in a unit disk graph, which is always the ceiling of the Euclidean distance separating the vertices.

5.2 A recursive formula for $\sigma_{r_{xy}}$

We now work through the calculation for the expected number of $\lceil r_{xy} \rceil$ -hop paths in dimension $d = 2$, which is asymptotic to the number of geodesic paths as $\rho \rightarrow \infty$. Firstly,

$$\mathbb{E}(\sigma_{r_{xy} \in [0,1)}) = 1 \quad (5.2.1)$$

since nodes connect directly. For $r_{xy} \in [1, 2]$, notice that all nodes lying within the intersection of the two connection loci x and y , called ‘lenses’, will necessarily lie on a geodesic two-hop path. This is depicted in Fig 5.2. Therefore,

$$\begin{aligned} \mathbb{E}(\sigma_{r_{xy} \in [1,2)}) &= \rho A_{r_{xy}} \\ &= \rho \left(2 \arccos\left(\frac{\lambda}{2}\right) - \lambda \sqrt{1 - \frac{\lambda^2}{4}} \right) \end{aligned} \quad (5.2.2)$$

where $A_{r_{xy}}$ is the area of intersection of two unit circles at center separation λ .

For $r_{xy} \in [2, 3)$, things are significantly more involved. Fig. 5.3 shows the setup, which involves two lens, and we want the expected number of bridging links between them. In order to evaluate this expectation, construct a new area A_λ in the right-hand lens. Within this sub-region, vertices are Poissonly

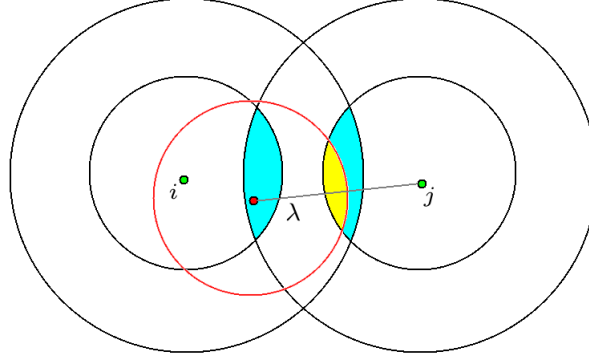


Figure 5.3: Some node (red) lying a distance λ from j (green) will connect directly to all nodes within r_0 of its position (the red circle). All of those vertices which simultaneously lie within a distance r_0 of j , denoted by the yellow area, will form two hop paths, and thus each three hop paths $i \leftrightarrow j$.

distributed with mean ρA_λ , and so:

$$\mathbb{E}(\sigma_{r_{xy} \in [2,3)}) = \int_{r_{xy}-1}^2 \rho A_\lambda \rho l_\lambda d\lambda \quad (5.2.3)$$

where

$$l_\lambda = 2\lambda \arccos\left(\frac{\lambda^2 + r_{xy}^2 - 1}{2r_{xy}\lambda}\right) \quad (5.2.4)$$

is a contour in the first lens at a distance λ from j , and

$$A_\lambda = 2 \arccos\left(\frac{\lambda}{2}\right) - \lambda \sqrt{1 - \frac{\lambda^2}{4}} \quad (5.2.5)$$

The expected number of three-hop paths is therefore given by an integral over all positions in the left lens:

$$\mathbb{E}(\sigma_{r_{xy} \in [2,3)}) = 4\rho^2 \int_{r_{xy}-1}^2 \lambda \arccos\left(\frac{\lambda^2 + r_{xy}^2 - 1}{2r_{xy}\lambda}\right) \left(\arccos\left(\frac{\lambda}{2}\right) - \frac{\lambda}{2} \sqrt{1 - \frac{\lambda^2}{4}} \right) d\lambda \quad (5.2.6)$$

Now, this integral has no closed form. Performing asymptotic analysis, Taylor

expand A_λ at $\lambda = \lceil r_{xy} \rceil$ and l_λ at $\lambda = r_{xy} - 1$. After dropping all but the first term, we should be able to extract the leading order behaviour

$$\mathbb{E}(\sigma_{r_{xy} \in [2,3]}) \approx 4\rho^2 \int_{r_{xy}-1}^2 \left(\sqrt{\frac{r_{xy}-1}{2r_{xy}}} (\lambda + 1 - r_{xy}) + \mathcal{O}((\lambda + 1 - r_{xy})^{3/2}) \right) \left(\frac{1}{3} (2 - \lambda)^{3/2} + \mathcal{O}((2 - \lambda)^{5/2}) \right) d\lambda$$

which evaluates to

$$\rho^2 \frac{\pi}{3\sqrt{3}} (3 - r_{xy})^3 + \mathcal{O}((3 - r_{xy})^4) \quad (5.2.7)$$

after finally expanding about $r_{xy} = \lceil r_{xy} \rceil$ and taking the first term. We can iterate this procedure to obtain an expression for $\mathbb{E}(\sigma_{r_{xy} \in [3,4]})$

$$\mathbb{E}(\sigma_{r_{xy} \in [3,4]}) = \rho^3 \int_{r_{xy}-1}^3 l_{\lambda_1} d\lambda_1 \int_{\lambda_1-1}^2 A_{\lambda_2} l_{\lambda_2} d\lambda_2$$

where

$$l_{\lambda_1} = 2\lambda_1 \arccos\left(\frac{\lambda_1^2 + r_{xy}^2 - 1}{2r_{xy}\lambda_1}\right)$$

$$l_{\lambda_2} = 2\lambda_2 \arccos\left(\frac{\lambda_2^2 + \lambda_1^2 - 1}{2\lambda_1\lambda_2}\right)$$

After expanding l_{λ_1} about $r_{xy} - 1$ and l_{λ_2} about $\lambda_1 - 1$ (as before), we have

$$\mathbb{E}(\sigma_{r_{xy} \in [3,4]}) = \rho^3 \frac{32\pi\sqrt{2}}{945} (4 - r_{xy})^{9/2} + \mathcal{O}((4 - r_{xy})^5) \quad (5.2.8)$$

after Taylor expanding Eq. 5.2.8 about $r_{xy} = \lceil r_{xy} \rceil$ and taking the leading term. Clearly we can go on and produce a recursive formula

$$\mathbb{E}(\sigma_{r_{xy}}) = \rho \int_{r_{xy}-1}^{\lceil r_{xy} \rceil} l_\lambda \mathbb{E}(\sigma_\lambda) d\lambda \quad (5.2.9)$$

We have already performed a few of these integrals. Table 5.2 lists them up to

Displacement r_{xy}	Expected geodesic cardinality $\sigma_{r_{xy}}$	Order of error
$r_{xy} \in [0, 1)$	1	(no error)
$r_{xy} \in [1, 2)$	$\frac{4\rho}{3} (2 - r_{xy})^{3/2}$	$\mathcal{O}\left((2 - r_{xy})^{5/2}\right)$
$r_{xy} \in [2, 3]$	$\frac{\pi\rho^2}{3\sqrt{3}} (3 - r_{xy})^3$	$\mathcal{O}\left((3 - r_{xy})^{8/2}\right)$
$r_{xy} \in [3, 4)$	$\frac{32\pi\rho^3\sqrt{2}}{945} (4 - r_{xy})^{9/2}$	$\mathcal{O}\left((4 - r_{xy})^{11/2}\right)$
$r_{xy} \in [4, 5)$	$\frac{\pi^2\rho^4}{180\sqrt{5}} (5 - r_{xy})^6$	$\mathcal{O}\left((5 - r_{xy})^{14/2}\right)$
$r_{xy} \in [5, 6)$	$\frac{1,024\pi^2\rho^5}{2,027,025\sqrt{3}} (6 - r_{xy})^{15/2}$	$\mathcal{O}\left((6 - r_{xy})^{17/2}\right)$

Table 5.2: Solutions to the recursion relation 5.2.9.

$r_{xy} \in [5, 6)$. A pattern is apparent in the coefficients. With $d = 2$, the pattern leads us directly to a general term:

$$\mathbb{E}(\sigma_{r_{xy}}) = \frac{\rho^{\lfloor r_{xy} \rfloor} (2\pi)^{\frac{1}{2}\lfloor r_{xy} \rfloor}}{\Gamma\left(\frac{3}{2}\lfloor r_{xy} \rfloor + 1\right) \sqrt{\lfloor r_{xy} \rfloor}} (\lceil r_{xy} \rceil - r_{xy})^{\frac{3}{2}\lfloor r_{xy} \rfloor} + \mathcal{O}\left((\lceil r_{xy} \rceil - r_{xy})^{\frac{1}{2}(3\lfloor r_{xy} \rfloor + 2)}\right) \quad (5.2.10)$$

The coefficient gives detailed information about how the number of paths scales over a unit interval.

5.3 Geodesics in d -dimensions

When the vertices are not constrained to lie in \mathbb{R}^2 , which is realistic since base stations are often also vertically dispersed around urban areas, we need a high dimensional analysis. The procedure above is therefore repeated for the three-dimensional case.

Starting again with $r_{xy} \in [0, 1)$, we immediately have

$$\mathbb{E}(\sigma_{r_{xy} \in [0, 1)}) = 1 \quad (5.3.1)$$

For the next interval, in place of $A_{r_{xy}}$ in Eq. 5.2.2, put the volume of intersection

$V_{r_{xy}}$ of two unit spheres separated by a distance r_{xy}

$$V_{r_{xy}} = \frac{\pi}{12} (4 + r_{xy}) (2 - r_{xy})^2 \quad (5.3.2)$$

leaving

$$\mathbb{E}(\sigma_{r_{xy} \in [1,2)}) = \frac{\pi \rho}{12} (4 + r_{xy}) (2 - r_{xy})^2 \quad (5.3.3)$$

in a similar manner to the case $d = 2$. Increasing the distance again, in place of A_λ in Eq. 5.2.3 put $V_\lambda = \frac{\pi}{12} (4 + \lambda) (2 - \lambda)^2$, and in place of l_λ we put the surface area S_λ of the spherical cap of a sphere-segment, which, omitting details, is

$$S_\lambda = 2\pi\lambda^2 \left(1 - \frac{r_{xy}^2 + \lambda^2 - 1}{2r_{xy}\lambda} \right) \quad (5.3.4)$$

The necessary integral is therefore

$$\begin{aligned} \rho^2 \int_{r_{xy}-1}^2 \left(\frac{\pi}{12} (4 + \lambda) (2 - \lambda)^2 \right) \left(2\pi\lambda^2 \left(1 - \frac{r_{xy}^2 + \lambda^2 - 1}{2r_{xy}\lambda} \right) \right) d\lambda \\ = \frac{\rho^2 \pi^2}{1260} \left((r_{xy} + 3) (r_{xy} + 9) - \frac{6}{r_{xy}} \right) (3 - r_{xy})^4 \end{aligned} \quad (5.3.5)$$

and this is exact, since the volume of intersection of two unit spheres is a polynomial in an integer power of the separation of their centres, and so can be integrated without the need for any expansions. The next term goes according to

$$\mathbb{E}(\sigma_{r_{xy} \in [3,4)}) = \rho^3 \int_{r_{xy}-1}^3 S_{\lambda_1} d\lambda_1 \int_{\lambda_1-1}^2 V_{\lambda_2} S_{\lambda_2} d\lambda_2 \quad (5.3.6)$$

which is

$$\frac{\rho^3 \pi^3}{453,600} \left((2 + r_{xy}) (8 + r_{xy}) (14 + r_{xy}) - \frac{144}{r_{xy}} \right) (4 - r_{xy})^6 \quad (5.3.7)$$

We then perform the same expansions as before. These expansions are listed

Displacement r_{xy}	Expected geodesic cardinality $\sigma_{r_{xy}}$	Order of error
$r_{xy} \in [0, 1)$	1	(no error)
$r_{xy} \in [1, 2)$	$\frac{\pi\rho}{2} (2 - r_{xy})^2$	$\mathcal{O}\left((2 - r_{xy})^3\right)$
$r_{xy} \in [2, 3)$	$\frac{\pi^2\rho^2}{18} (3 - r_{xy})^4$	$\mathcal{O}\left((3 - r_{xy})^5\right)$
$r_{xy} \in [3, 4)$	$\frac{\pi^3\rho^3}{360} (4 - r_{xy})^6$	$\mathcal{O}\left((4 - r_{xy})^7\right)$
$r_{xy} \in [4, 5)$	$\frac{\pi^4\rho^4}{12,600} (5 - r_{xy})^8$	$\mathcal{O}\left((5 - r_{xy})^9\right)$
$r_{xy} \in [5, 6)$	$\frac{\pi^5\rho^5}{680,400} (6 - r_{xy})^{10}$	$\mathcal{O}\left((6 - r_{xy})^{11}\right)$

 Table 5.3: Solutions to the recursion relation 5.2.9 with $d = 3$.

in Table 5.3.

In fact, at this point, we can evaluate the d -dimensional term directly. The necessary replacements of the lens area A_λ and arc length l_λ in d -dimensional hyperspace cannot be expressed in terms of elementary functions. We use the regularised incomplete beta function $I_x(a, b)$

$$I_x(a, b) \int_0^1 t^{a-1} (1-t)^{b-1} dt = \int_0^x t^{a-1} (1-t)^{b-1} dt \quad (5.3.8)$$

which is the ratio of the incomplete beta function and the complete beta function [71].

So, the $d - 1$ dimensional surface area of the hyperspherical cap of vertex angle $\phi \in [0, \pi]$ and radius λ is

$$A_\lambda = \frac{\pi^{d/2}}{\Gamma(d/2)} \lambda^{d-1} I_{\sin^2(\phi)}\left(\frac{d-1}{2}, \frac{1}{2}\right) \quad (5.3.9)$$

where

$$\phi = \arccos\left(\frac{\lambda^2 + r_{xy}^2 - 1}{2r_{xy}\lambda}\right) \quad (5.3.10)$$

is the colatitude at which the d -sphere is cut to produce the hyperspherical segment; cutting the hypersphere at $\phi = \pi/2$ would produce a hemisphere, for example, when $d = 3$. A_λ reduces to an arc length in Eq. 5.2.4 when $d = 2$, and the two-dimensional surface area of a spherical cap (Eq. 5.3.4) when $d = 3$ [71].

The volume of intersection of two unit hypersphere separated by r_{xy} is twice the *volume* of this hyperspherical cap (each are glued to the plane which cuts through the sphere-sphere intersection). Thus

$$V_\lambda = \frac{\pi^{d/2}}{\Gamma(d/2 + 1)} \lambda^d I_{\sin^2(\phi)} \left(\frac{d+1}{2}, \frac{1}{2} \right) \quad (5.3.11)$$

which reduces to the area of the lens when $d = 2$ (Eq. 5.2.5), and the volume of the sphere-sphere intersection when $d = 3$ (Eq. 5.3.13). As before, we have

$$\mathbb{E}(\sigma_{r_{xy} \in [2,3)}) = \int_{r_{xy}-1}^2 \rho V_\lambda \rho A_\lambda d\lambda \quad (5.3.12)$$

which is

$$\frac{\pi^d}{\Gamma(d/2) \Gamma(d/2 + 1)} \int_{r_{xy}-1}^2 \lambda^{2d-1} I_{\sin^2(\phi)} \left(\frac{d+1}{2}, \frac{1}{2} \right) I_{\sin^2(\phi)} \left(\frac{d-1}{2}, \frac{1}{2} \right) d\lambda$$

which is intractable, but we can extract the leading order term.

So, in place of $A_{r_{xy}}$ in Eq. 5.2.2, put the volume of intersection $V_{r_{xy}}$ of two unit hyperspheres separated by a distance r_{xy}

$$V_{r_{xy}} = \frac{\pi^{d/2}}{\Gamma(d/2 + 1)} r_{xy}^d I_{\sin^2(\phi)} \left(\frac{d+1}{2}, \frac{1}{2} \right) \quad (5.3.13)$$

leaving

$$\begin{aligned} \mathbb{E}(\sigma_{r_{xy} \in [1,2)}) &= \rho V_{r_{xy}} \\ &= \frac{\pi^{d/2} \rho}{\Gamma(d/2 + 1)} r_{xy}^d I_{\sin^2(\phi)} \left(\frac{d+1}{2}, \frac{1}{2} \right) \end{aligned} \quad (5.3.14)$$

in a similar manner to before. Increase the distance again, and in place of A_λ in Eq. 5.2.3, put V_λ

$$V_\lambda = \frac{\pi^{d/2}}{\Gamma(d/2 + 1)} \lambda^d I_{\sin^2(\phi)} \left(\frac{d+1}{2}, \frac{1}{2} \right) \quad (5.3.15)$$

and in place of l_λ put the surface area of the hyperspherical cap A_λ with

$$\phi = \arccos \left(\frac{\lambda^2 + r_{xy}^2 - 1}{2r_{xy}\lambda} \right) \quad (5.3.16)$$

as before. For reference this is

$$A_\lambda = \frac{\pi^{d/2}}{\Gamma(d/2)} \lambda^{d-1} I_{\sin^2(\phi)} \left(\frac{d-1}{2}, \frac{1}{2} \right) \quad (5.3.17)$$

so since (as before) we have

$$\mathbb{E} \left(\sigma_{r_{xy} \in [2,3]} \right) = \int_{r_{xy}-1}^2 \rho V_\lambda \rho A_\lambda d\lambda \quad (5.3.18)$$

then we need

$$\frac{\pi^d}{\Gamma(d/2) \Gamma(d/2 + 1)} \int_{r_{xy}-1}^2 \lambda^{2d-1} I_{\sin^2(\phi)} \left(\frac{d+1}{2}, \frac{1}{2} \right) I_{\sin^2(\phi)} \left(\frac{d-1}{2}, \frac{1}{2} \right) d\lambda$$

which was given explicitly in Eq. 5.3.18. Before (when this was intractable) we expanded A_λ at $\lambda = r_{xy} - 1$ and $V_{r_{xy}}$ (which is the previous term in the sequence) at $r_{xy} = \lceil r_{xy} \rceil = 2$ (and then replace r_{xy} with λ). Given

$$A_\lambda = \frac{(2\pi)^{\frac{d-1}{2}} r_{xy} (r_{xy} - 1)^d}{\Gamma\left(\frac{1}{2}(d+1)\right)} (1 - r_{xy} + \lambda)^{\frac{d-1}{2}} + \mathcal{O}\left((\lambda - (r_{xy} - 1))^{\frac{d+1}{2}}\right)$$

and

$$V_\lambda = \frac{\pi^{\frac{d-1}{2}} \rho}{\Gamma\left(\frac{1}{2}(d+3)\right)} (2 - \lambda)^{\frac{d+1}{2}} + \mathcal{O}\left((\lambda - 2)^{\frac{d+3}{2}}\right)$$

the integral in Eq. 5.3.18 evaluates to

$$\mathbb{E} \left(\sigma_{r_{xy} \in [2,3]} \right) = \frac{(2\pi)^{d-1} 3^{\frac{1}{2}(1-d)}}{\Gamma(2+d)} (3 - \lambda)^{d+1} + \mathcal{O}\left((\lambda - 3)^{d+2}\right) \quad (5.3.19)$$

after expanding as usual. The rest of these integrals are displayed in Table 5.4. and, finally, by inspecting a pattern in the coefficients, we have the expected

Displacement r_{xy}	Expected geodesic cardinality $\sigma_{r_{xy}}$	Order of error
$r_{xy} \in [0, 1)$	1	(no error)
$r_{xy} \in [1, 2)$	$\frac{\rho(2\pi)^{\frac{1}{2}(d-1)} 2^{\frac{1}{2}(1-d)}}{\Gamma(\frac{3+d}{2})} (2 - r_{xy})^{\frac{1}{2}(d+1)}$	$\mathcal{O}\left((r_{xy} - 2)^{\frac{1}{2}(d+3)}\right)$
$r_{xy} \in [2, 3)$	$\frac{\rho^2(2\pi)^{d-1} 3^{\frac{1}{2}(1-d)}}{\Gamma(\frac{1}{2}(2+d))} (3 - r_{xy})^{d+1}$	$\mathcal{O}\left((r_{xy} - 3)^{d+2}\right)$
$r_{xy} \in [3, 4)$	$\frac{\rho^3(\pi)^{\frac{3}{2}(d-1)} 2^{\frac{1}{2}(d-1)}}{\Gamma(\frac{1}{2}(5+3d))} (4 - r_{xy})^{\frac{3}{2}(d+1)}$	$\mathcal{O}\left((r_{xy} - 4)^{\frac{3}{2}(d+3)}\right)$

Table 5.4: Solutions to the recursion relation 5.2.9 for general dimension d .

number of $\lceil r_{xy} \rceil$ paths in d -dimensions.

$$\mathbb{E}(\sigma_{r_{xy}}) = \frac{\rho^{\lfloor r_{xy} \rfloor} (2\pi)^{\frac{1}{2}\lfloor r_{xy} \rfloor (d-1)} \lceil r_{xy} \rceil^{\frac{1}{2}(1-d)}}{\Gamma\left(\frac{\lfloor r_{xy} \rfloor + 1}{2} + \frac{\lfloor r_{xy} \rfloor d}{2}\right)} (\lceil r_{xy} \rceil - r_{xy})^{\frac{1}{2}\lfloor r_{xy} \rfloor (d+1)} \quad (5.3.20)$$

with error $\mathcal{O}\left((\lceil r_{xy} \rceil - r_{xy})^{\frac{1}{2}\lfloor r_{xy} \rfloor (d+3)}\right)$.

5.4 Numerical simulation

Fig. 5.5 gives an idea of the error introduced by the Taylor expansions we perform. Performing these integrals exactly is topic of current research. Notice also Fig. 5.6, which shows how Eq. 5.3.20 demonstrates a rising-and-falling behaviour as r_{xy} increases. This occurs because there are two competing forces which ‘create and destroy’ geodesic cardinality. The creation force involves increasing r_{xy} , which allows more space for geodesics to form. This force dominates for small $r_{xy} \leq 8$ with respect to the parameters in Fig. 5.6. The destructive force is caused by the increasingly difficult but necessary alignment of vertices in the various lens’ which must be achieved for optimal geodesics to form. This force is dominating for $r_{xy} \geq 8$, since more than eight lenses must accommodate aligning vertices for optimal paths to form.

Fig. 5.4 shows how the number of geodesic paths is asymptotic to the number of $\lceil r_{xy} \rceil$ hop paths as $\rho \rightarrow \infty$. This approximation breaks down as $r_{xy} \rightarrow \lceil r_{xy} \rceil$, because the lens areas are expected to contain fewer and fewer

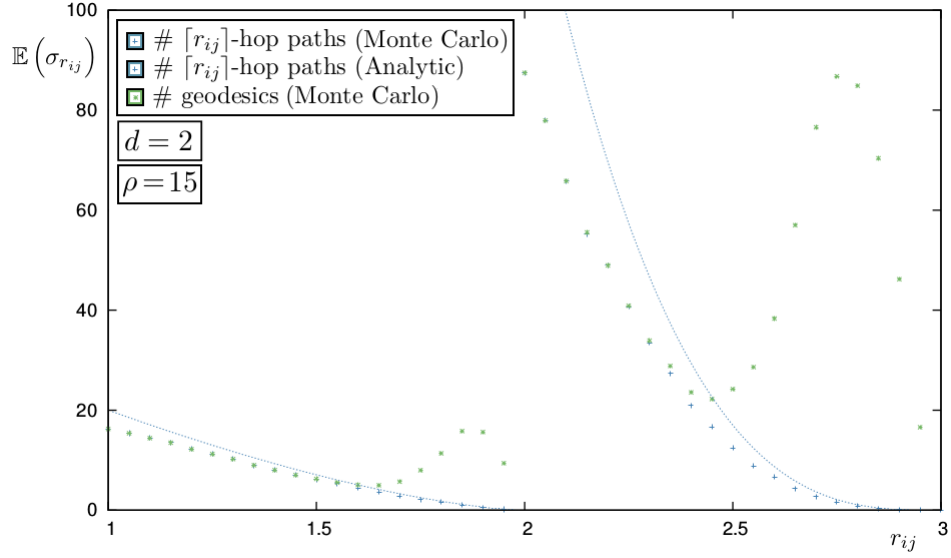


Figure 5.4: The smooth decaying blue lines are Monte Carlo data for *optimal geodesic cardinality*, with our approximation Eq. 5.3.20 with $d = 2$. The green stars are the actual shortest path counts. The blue pluses and green stars are numerical results, while the smooth curves are our analytic results.

vertices, and so the geodesic can become longer than $\lceil r_{xy} \rceil$ hops.

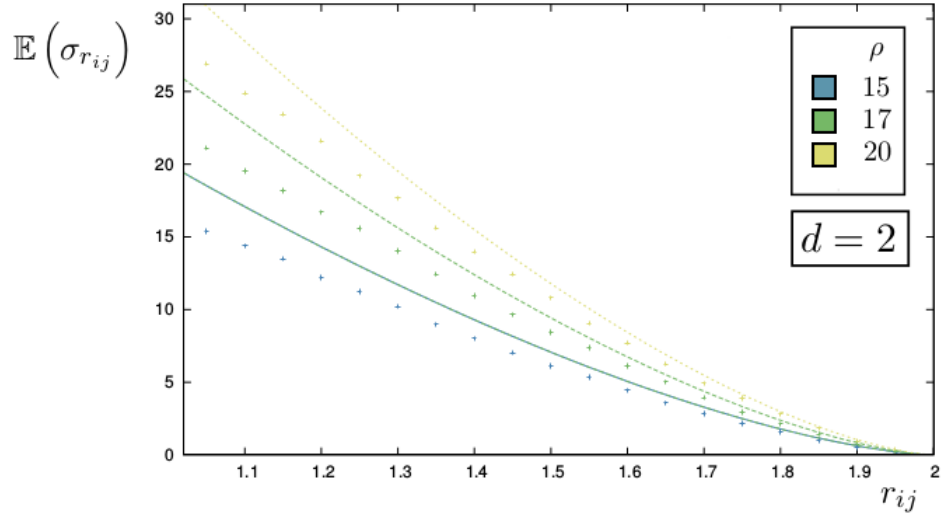


Figure 5.5: The expected number of two-hop paths and our approximation Eq. 5.3.20, for $\rho = 15, 17, 20$ and $d = 2$.

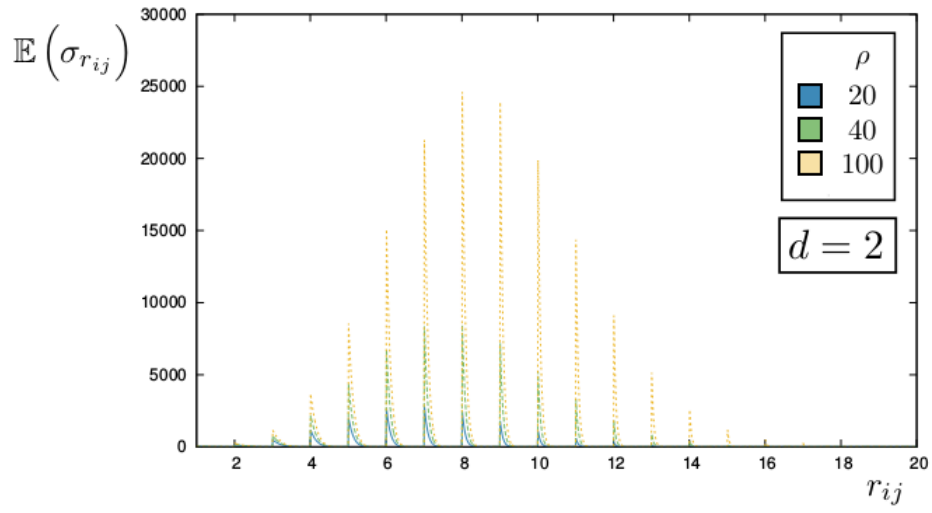


Figure 5.6: Eq. 5.3.20 plotted for three increasing densities $\rho = 20, 40, 100$ over a long range of displacements. The expected number of paths rises and falls as r_{xy} increases.

Chapter 6

Discussion

In this chapter, we discuss the relationship between our mathematical results, and communications practice. We also discuss possible future developments of this research, and how it may have a lasting impact on future multi-hop communication.

6.1 Applications in communication networks

We focus in this section on detailing the nature of our contributions to the field of wireless networks.

6.1.1 Understanding skeletons

In Fig 3.5, two example *skeletons* have been extracted from random geometric graphs bound inside obstructed domains [58]. In Chapter 4, we defined a skeleton from its use in e.g. Ercsey-Ravasz et al. [57], who demonstrated how betweenness centrality can be used to describe and analyse a network’s *skeleton* or *vulnerability backbone*. This is a percolating cluster of the most structurally important vertices. See also [58] for more recent work. These appear to be quasi-one-dimensional sub-systems, which are subgraphs embedded in a d -dimensional space which extend in only a single dimension such as around the perimeter of a disk or along a corridor region. They may have a restricted

extension into the remaining $d - 1$ dimensions, hence the use of the phrase *quasi*. Thin systems, such as thin films, have been important in physics more generally [72]. In our case, these systems appear to have control over the high performance functionality of the network when contained within bounding geometries with non-convex features. Questions therefore emerge, such as:

1. How does the connectivity of this sub-graph effect the overall network performance?
2. How can this extra connectivity be balanced with minimisation of inter-skeleton interference?
3. Do multiple small obstructions create multiple one-dimensional sub-systems which all need to be managed?
4. Overall, what is the best way skeleton vertices can be used to optimise communication?

6.1.2 Topology-based geolocalisation

There is greater sensitivity in the *number* of paths than in the *length* of paths to small changes in location in random spatial networks. As an enhancement of topological-based localisation, where hop counts to location-aware anchor vertices are converted, preferably analytically, into likely Euclidean distances, the number of paths can be used as an accuracy enabler [29, 39, 40].

This is particularly useful in dense networks, since here the number of hops from x to y is determined by the ceiling of Euclidean separation, and so does not change over potentially an entire connection interval. The number of paths, however, does scale, and moreover, with an increasing resolution at high density. A combination of path length, and path counts, could provide a key solution to localisation in dense networks beyond GPS. See e.g. the landmark paper on DV-hop [73], which approximates distances via the average distance of a hop multiplied by the number of hops between a pair of nodes.

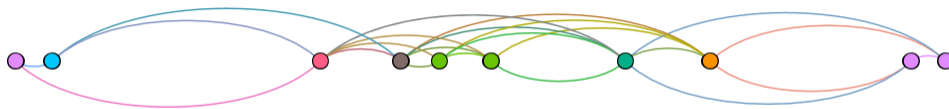


Figure 6.1: A one-dimensional unit disk graph. The colours are used to help distinguish paths. The geodesic length between the end points is three hops. This can be used to model an ad hoc communication network of vehicles queuing in traffic.

6.1.3 Future vehicular ad hoc networks

Betweenness centrality can be more easily evaluated if the domain is a one dimensional strip, such as the interval $[0, L)$. The combinatorial enumeration of paths, and evaluation of the lengths of paths, is significantly less involved. Yet the applications are perhaps more direct, as ad hoc vehicle networks are among the most promising applications of multi-hop routing, and key development area of future wireless networks [74].

Possible future research topics include:

1. Can current flow betweenness centrality be expressed as a one-dimensional field of random variables, which is a random field [75], in a one-dimensional random geometric graph on a finite interval of the real line?
2. What is the distribution of geodesic paths between two arbitrarily separated vertices in a one-dimensional random geometric graph? Can this be used to evaluate expected location-specific betweenness in closed form in one dimension?

Distributed algorithms run on a network in such a way that the resources required for their operation are shared equally between all cooperating devices. This distribution of resource consumption can prove important for battery limited sensor networks, even if they have access to the resources of a central server such as a sink or cluster head [76].

Analysis of expected centrality as a scalar field (defined on the d -dimensional domain positions), as discussed in this thesis, works towards understanding the

best way to distribute the necessary computational load of such algorithms. Continued work on this topic, such as working to see how centrality scales near obstacles in the domain, will also highlight the effect that non-convex features can have on the long term performance of these distributed network processes, such as in sensing scenarios.

6.2 Mathematical directions

Below we highlight some research directions which are more directly related to mathematical directions in random networks.

6.2.1 The distribution of the number of geodesics

What is the distribution of shortest paths between two vertices, now considering $d = 2$? The first moment of $\sigma_{r_{xy}}$ is expected number of $\lceil \|x - y\| \rceil$ -hop paths. It is interesting to ask if we can get the other moments. Note that *if* the distribution of paths is Poisson, the second moment is related to the first in a trivial way

$$\mathbb{E}(\sigma_{r_{xy}}^2) = \mathbb{E}(\sigma_{r_{xy}}) (\mathbb{E}(\sigma_{r_{xy}}) + 1) \quad (6.2.1)$$

and $\sigma_{r_{xy}}$ is distributed as

$$P(\sigma_{r_{xy}} = k) = \frac{1}{k!} \exp(-\mathbb{E}(\sigma_{r_{xy}})) (\mathbb{E}(\sigma_{r_{xy}}))^k \quad (6.2.2)$$

This actually *does* hold when $r_{xy} \in [1, 2)$, as demonstrated in the top panel of Fig. 6.2, but not for larger displacements, as demonstrated in the bottom panel of Fig 6.2. For these larger displacements, the variance

$$\text{Var}(\sigma_{r_{xy}}) = \mathbb{E}(\sigma_{r_{xy}}^2) - \mathbb{E}^2(\sigma_{r_{xy}}) \quad (6.2.3)$$

exceeds the mean by an amount proportional to both density ρ and displacement r_{xy} , and so $\sigma_{r_{xy}}$ is no longer Poisson, but conjectured *negative binomial*.

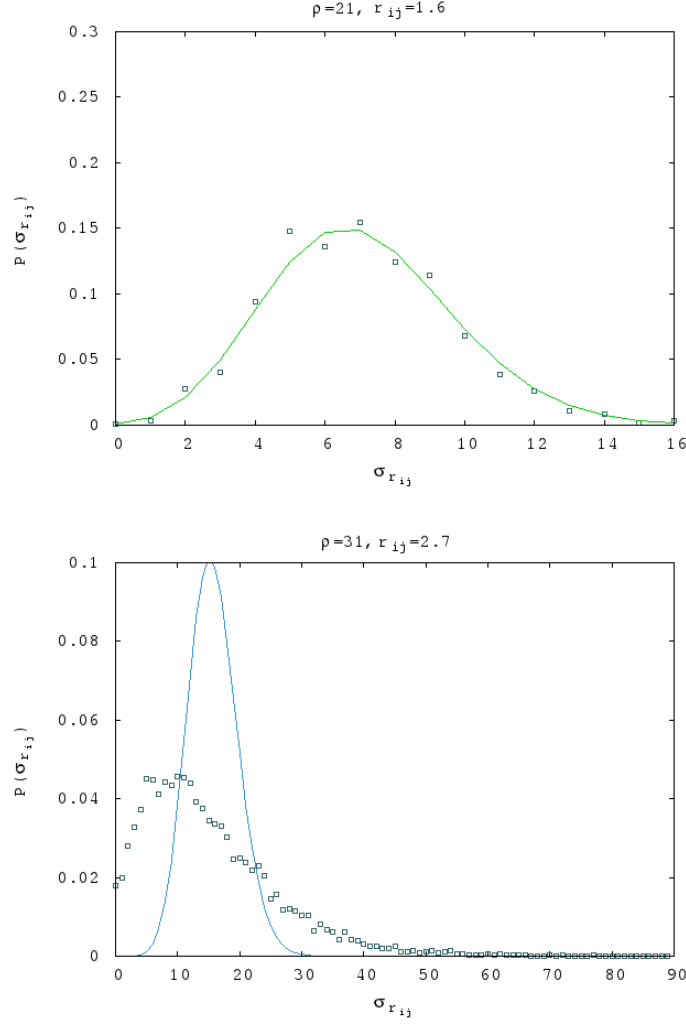


Figure 6.2: Top: The small boxes are Monte Carlo approximations to the probability $P(\sigma_{r_{xy}} = k)$ with $r_{xy} = 1.6$. In this distance interval the distribution of geodesic paths is Poisson, as described by the green line Eq. 6.2.2. Bottom: The blue line is the curve $\text{Po}(\mathbb{E}(\sigma_{r_{xy}=2.7}))$, and the boxes Monte Carlo data for this larger displacement. The number of geodesic paths is therefore not Poisson.

Conjecture 6.2.1 (Distribution of the number of geodesic paths). *Given two vertices displaced by r_{xy} in the unit disk graph $G(n, \pi)$, the random variable $\sigma_{r_{xy}}$ is distributed as*

$$P(\sigma_{r_{xy}} = k) = \binom{k+r-1}{k} p^r (1-p)^k \quad (6.2.4)$$

with p, r the solution to the simultaneous equations

$$\mathbb{E}(\sigma_{r_{xy}}) = \frac{(1-p)r}{p} \quad (6.2.5)$$

$$\mathbb{E}(\sigma_{r_{xy}}^2) = \mathbb{E}(\sigma_{r_{xy}}) \left(\frac{1}{p} + \mathbb{E}(\sigma_{r_{xy}}) \right) \quad (6.2.6)$$

An analytic expression for $\mathbb{E}(\sigma_{r_{xy}}^2)$ would allow one to numerically verify this. The basis of the conjecture is mainly the similarity in form of the probability mass functions, and also the apparent over-dispersion (i.e. the variance of $\sigma_{r_{xy}}$ is larger than its mean). One would need to investigate this further as it is not understood.

6.2.2 Non-optimal geodesics

Some paths are geodesics of length $k > \lceil r_{xy} \rceil$ hops. These occur when there are no paths of the optimal length. The shortest path is then found to be one hop longer. We call geodesics of length $\lceil r_{xy} \rceil + 1$ hops β -optimal paths, and those of length $\lceil r_{xy} \rceil + 2$ hops γ -optimal, and so on. The expected number of geodesics with $r_{xy} \in [1, 2)$ is therefore an approximation to

$$\mathbb{E}(\sigma_{r_{xy} \in [1, 2)}) = \rho A_{r_{xy}} (1 - e^{-\rho A_{r_{xy}}}) + e^{-\rho A_{r_{xy}}} \left(\rho^2 \int_1^2 l_\lambda A_\lambda d\lambda \right) \quad (6.2.7)$$

with the number of γ -optimal paths a second order correction. Investigating this decomposition of geodesic paths into contributions from paths of all lengths is a topic of further research.

In particular,

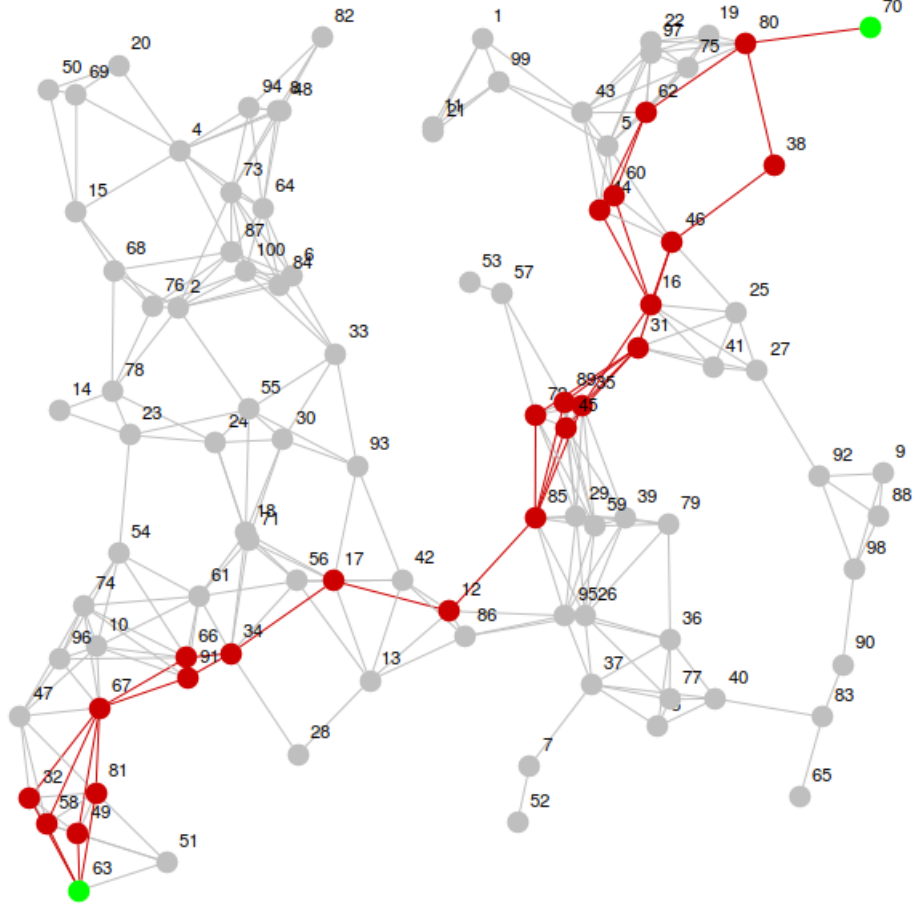


Figure 6.3: The graph shows 96 geodesics, each of 13-hops, from vertex 63 to vertex 70. Since the Euclidean distance between the endpoints is 9.8, these geodesics are not optimal. As r_{xy} increases, the probability there existing at least one 'optimal' alignment of vertices, which is an alignment of points of \mathcal{Y} that induces a path of $\lceil r_{xy} \rceil$ hops from x to y , vanishes. The chain of links is more likely to break as it grows longer. This explains the rising and falling effect in Fig. 5.6.

1. If each edge in a path is likened to a sequence of unit resistors in series (in an electronic circuit), and all paths of the same length in hops are considered to be like strings of resistors running in parallel, what is the resistance of the single resistor which can replace the set of paths which join x and y ? There will be a distribution on the possible resistances, but interestingly, this will be determined in the limit of high density by only the distribution of geodesics.
2. How successful is the modelling of data flows as a flow of current? What are the key differences?

We hope to develop the first of these goals as part of a project on *random geometric electrical networks*.

6.3 Final words

The potential ultra-dense base station deployments of 5G have been investigated from the point of view of random geometric graphs, and specifically betweenness centrality, as well as part of the theory of ad hoc wireless networks in general. It has been shown how spatial probabilistic combinatorics can play a key role in effective, common sense wireless interference management techniques, as well as various optimisation methods, such as dynamically tuning the betweenness of vertices, and bounding the length of geodesic paths. This enables delay tolerant networking, involving sociological ideas such as betweenness centrality, and current flow betweenness centrality. The future tractability of intelligent vehicles is also supported by the greater ease of analysis in one-dimensional and quasi-one dimensional random geometric graphs, compared with their higher-dimensional counterparts.

In the future, the issue of spatial dependence needs to be addressed in order to provide a greater depth to the applied mathematics of these fascinating graphs. The potential limiting performance of ad hoc communication networks is not yet understood, but with this sort of graph theoretic analysis, it may yet be harnessed.

Appendices

Appendix A

Percolation

Percolation will now be more rigorously defined. Take the hypercubic lattice $\mathcal{D} = \mathbb{L}^d$. Look at all the edges of the lattice, and designate them either *open* or *closed* with probability p . This is called *bond percolation*¹. The question is, what proportion of the lattices display a path of open links from the origin \mathcal{O} to the boundary of the lattice $\partial\mathcal{D}$, or to infinity if we consider an infinite lattice? There is a very well studied singularity at $p = p_c$ in both

$$\theta(p) = \mathbb{P}(|C| = \infty), \quad \chi(p) = \mathbb{E}_p|C| \quad (\text{A.0.1})$$

where C is the set of all vertices connected to the origin via open paths, and $\chi(p)$ is the mean cluster size. This singularity is due to either an undefined derivative at $\theta(p_c)$, or an undefined magnitude at $\chi(p_c)$, and is due to conjectured fractional power-law behaviour.

Theorem A.0.1 (There exists a non-trivial critical point for $d \geq 2$). *We have that*

$$0 < p_c < 1 \quad \text{if} \quad d \geq 2 \quad (\text{A.0.2})$$

Notice that $\theta(0) = 0$, since there are no links. Also $\theta(1) = 1$, since all vertices are linked. This theorem is the existence of a non-trivial critical

¹Site percolation, as an alternative, turns the lattice squares themselves on or off with probability p .

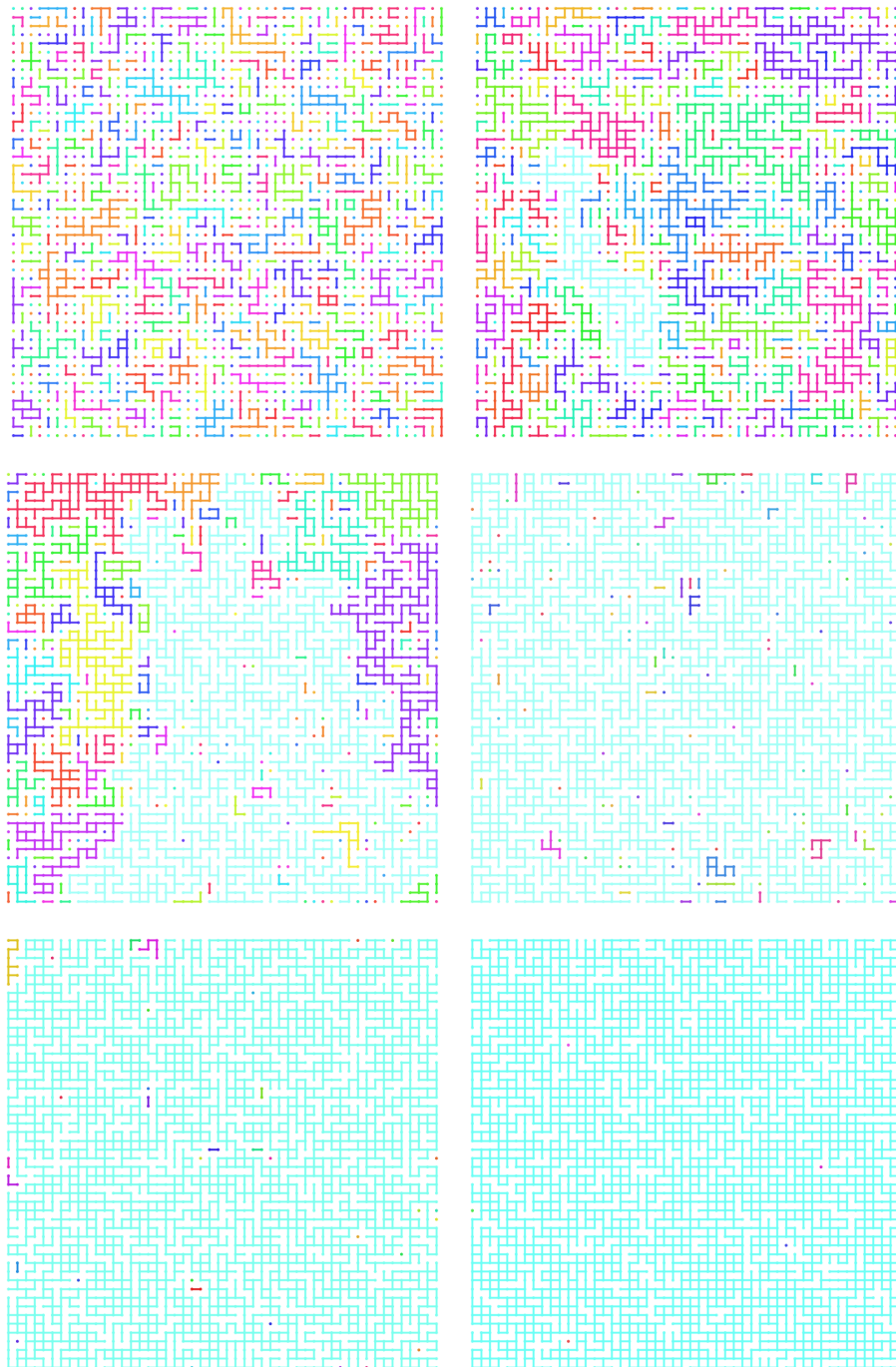


Figure A.1: 50×50 bond percolation with p increasing from 0.3 to 0.8 in steps of 0.1. Criticality occurs at $p = 0.5$. The largest connected component is highlighted in sky blue throughout.

parameter $p_c \in (0, 1)$, and immediately introduces the idea of a self-avoiding random walk (SAW).

SAW is necessarily a sequence of adjacent vertices which does not repeat². It is thus a path through the lattice, of length ν . Call Σ_n the number of SAWs of length n which leave from the origin (or, equivalently, finish at the origin). Let Σ_n^* be the number of these walks which only consist of open links. This is related to the percolation probability

$$\theta(p) = \lim_{n \rightarrow \infty} P_p(\Sigma_n^* \geq 1) \quad (\text{A.0.3})$$

Considering first Σ_n , we have that (at worst)

$$\Sigma_n \leq 2d(2d-1)^{n-1} \quad (\text{A.0.4})$$

given a symmetric random walk [11] from the origin which takes no steps back along its current path. Also

$$P_p(\Sigma_n^* \geq 1) \leq \mathbb{E}(\Sigma_n^*) = p^n \Sigma_n \quad (\text{A.0.5})$$

where we note that the expected number of SAWs along open links is not a trivial object, but can be written in terms of the total number of SAWs of length n . Thus

$$\theta(p) \leq \lim_{n \rightarrow \infty} 2d(2d-1)^{n-1} p^n \quad (\text{A.0.6})$$

implying $\theta(p)$ can only be non-zero when

$$p_c \geq \frac{1}{2d-1} \quad (\text{A.0.7})$$

demonstrating the lower bound for p_c , since $\theta(p)$ is non-decreasing in p , and equals unity when $p = 1$.

For the upper bound, the idea is to create a dual lattice identical to the main lattice (in both geometry and open edge configuration), but spatially translated half a link-length south, and half a link-length to the east. Any finite cluster of open links will induce the dual lattice to display a finite loop

²Though this is not the exact definition, it is suitable here.

of *closed* links which encloses this open cluster.

Event M_n is a completed loop of length n . We have

$$P_p \left(\sum_n M_n \geq 1 \right) \leq \mathbb{E}_p \left(\sum_n M_n \geq 1 \right) \quad (\text{A.0.8})$$

after considering the usual power series representation of the expectation. Also

$$\mathbb{E}_p \left(\sum_n M_n \geq 1 \right) = \sum_{n=4}^{\infty} \mathbb{E}_p(M_n) \leq \sum_{n=4}^{\infty} (n4^n) (1-p)^n \quad (\text{A.0.9})$$

after bounding the number of complete loops of length n , each of which is completely closed with probability $(1-p)^n$. This implies that

$$1 - \theta(p) = P_p \left(\sum_n M_n \geq 1 \right) \leq \sum_{n=4}^{\infty} (n4^n) (1-p)^n \quad (\text{A.0.10})$$

with the sum on the r.h.s strictly smaller than unity for some non-zero ϵ in $p = 1 - \epsilon$. Whatever this value of ϵ , we have $\theta(p) > 0$, and thus $0 < p_c < 1$ given $d = 2$. Also, since we can embed a lower dimensional space in a higher one

$$1 \geq p_c(\mathbb{L}^2) \geq p_c(\mathbb{L}^3) \geq p_c(\mathbb{L}^4) \geq \dots \geq 0 \quad (\text{A.0.11})$$

so $0 < p_c < 1$ for $d \geq 2$ as required.

Appendix B

Proof of the isolated vertices theorem

In this appendix we prove the following important theorem from Section 2.1:

Theorem B.0.1 (Connectivity is the same as isolated vertices). *For almost all sets \mathcal{Y}*

$$\mathbb{P}\left(G\left(n, \pi r_0^2\right) \text{ is connected}\right) = \mathbb{P}\left(\text{no isolated nodes}\right) \quad (\text{B.0.1})$$

This was first proved by Penrose [34]. We follow some parts of [35]. We first show that no two components in the graph are ‘large’.

Lemma B.0.2 (No two components in the graph are large). *Assuming $c > 0$, there exists a C such that w.h.p the random graph $G(n, c \log n)$ does not consist of two or more connected components each with Euclidean diameter¹ at least $C\sqrt{\log n}$.*

First, tile S_n with tiles (i.e. like on a household wall) of side $r_0/\sqrt{20}$, which insists that any two vertices in $G(n, c \log n)$ found in any two adjacent squares are no more than $r_0/2$ apart. Then argue that

1. A component U of Euclidean diameter at least $C\sqrt{\log n}$ covers many tiles as $n \rightarrow \infty$.

¹This is the largest Euclidean distance which can be found between any two vertices in a connected component.

2. Since the tiles have side $r_0/\sqrt{20}$, all tiles adjacent to U are empty.
3. There are many empty boundary tiles, given the size of U .
4. They cannot all be empty, and so any two large components will merge asymptotically.

We do not explicitly prove parts 1-3, but refer directly to Walter's review [35] (or Penrose's 1997 paper [34]). Hopefully these arguments are clear. The crux is to prove that boundary tiles in the limit are so numerous that at least one of them houses at least one vertex (almost surely).

How many boundary tiles surround U ? At least as many as the square root of the number of tiles underlying U . Say $|U^T|$ tiles underly U . The edge isoperimetric inequality for the grid states² that the number of boundary tiles $|\partial U^T|$ is given by

$$\min \left\{ 2\sqrt{|U^T|}, 2\sqrt{|U^{T^c}|} \right\} \quad (\text{B.0.2})$$

where U^{T^c} is the complement of the set of tiles underlying the component U . Since each component is of a diameter greater than $C\sqrt{\log n}$, it meets at least³ $(C\sqrt{\log n}) / (r/\sqrt{20})$ tiles, so

$$|\partial U^T| \geq 2\sqrt{\frac{C}{r}\sqrt{20\log n}} \quad (\text{B.0.3})$$

Now we know the size $|\partial U^T|$ of the boundary, we show that at least one of its tiles is non-empty. Notice lemma 2.14 in [35]:

Lemma B.0.3. *Suppose that G is a graph with maximum degree Δ , and that v is some vertex in G . The number of connected subgraphs of G with n vertices that contain v is at most $(e\Delta)^n$.*

This is not particularly difficult to demonstrate, and we refer to [78] for an

²This is according to Bollobás and Leader [77].

³It could be a diagonal strip-like component over S_n , which is as small as its Euclidean diameter allows.

in depth proof (Problem 45 “Connected Subgraphs” in the book of problems by Bollobás).

To highlight the main concern, consider the rooted⁴ graph G^\star , and the number $N(G^\star, n)$ of subtrees of that graph consisting of n vertices *as well as* the root vertex. Then

$$N(G^\star, n) \leq \binom{\Delta n - n + 1}{n} \quad (\text{B.0.4})$$

which requires some work which we exclude. Given

$$\begin{aligned} n! \binom{\Delta n - n + 1}{n} &= (\Delta - 1)n \left((\Delta - 1)^2 n^2 - 1 \right) (n - 3)! \binom{(\Delta - 1)n - 2}{n - 3} \\ &\leq e^n (\Delta - 1)^n \end{aligned} \quad (\text{B.0.5})$$

our bound in B.0.3 follows. The probability that almost all of set of u tiles is empty is

$$\left(e^{-r^2/20} \right)^u \quad (\text{B.0.6})$$

and (given $\Delta = 8$ for the lattice over S_n taking $d = 2$), we have

$$\mathbb{P}(\text{two components do not merge}) \leq n (8e)^u e^{-ur^2/20} \quad (\text{B.0.7})$$

after enumerating all possible boundary tile combinations. We consider the graph $G(n, c \log n)$, so $r = \sqrt{c \log n / \pi}$ and thus if C satisfies

$$2\sqrt{\frac{C}{r}} \sqrt{20 \log n} > 20\pi/c \quad (\text{B.0.8})$$

then any two components of Euclidean diameter at least $C\sqrt{\log n}$ merge

⁴A rooted graph is a graph with one marked vertex, called the root. If the graph G has a root vertex we denote it G^\star .

asymptotically. This occurs when

$$C \geq \frac{100\pi^2}{c^2 \left(\sqrt{20\pi/c} \right)} \quad (\text{B.0.9})$$

and we have an idea of how large a component can get before it merges.

Now, all disconnected components must have a Euclidean diameter strictly less than $C\sqrt{\log n}$. Notice that if all of these small disconnected components are a single vertex, then only isolated vertices can disconnect the graph $G(n, c \log n)$ as $n \rightarrow \infty$.

Lemma B.0.4 (All small components consist of a single vertex.). *Suppose C is as in B.0.2, and take the case $c = 9/10$. Then the graph $G(n, \log n - \frac{1}{2} \log \log n)$ contains no components H of 1) more than one vertex and 2) Euclidean diameter strictly less than $C\sqrt{\log n}$.*

The component H has small Euclidean diameter, and no more than one vertex. Is this diameter smaller than $\eta = (\log \log n)^2 / \sqrt{\log n}$? Centre a ball of radius η at some point x in H . Call this ball $B(x, \eta)$. Consider another ball $B(x, r_0)$ with similar center. Then if $\text{diam}(H) < \eta$ is empty then there is at least one more point in $B(x, \eta)$, and $B(x, r_0) \setminus B(x, \eta)$ is empty. The probability of this dies away with n , since

$$\left(1 - \exp(-\pi\eta^2)\right) \exp\left(-\left(A - \pi\eta^2\right)\right) = \mathcal{O}\left(\frac{\sqrt{\log n} (\log \log n)^4}{n \log n}\right) \quad (\text{B.0.10})$$

which is bounded by the growth of $1/n$, so even with a chance at every vertex $\mathbb{P}(\text{diam}(H) < \eta) \rightarrow 0$ asymptotically with n . Is $\text{diam}(H) > \eta$? Start by drawing the convex hull⁵ $\Phi(H)$ of H . Encase $\Phi(H)$ in an upright rectangle R . The diagonal length of R must be at least η . Fig. B.1 indicates in grey an area around R . R cannot contain less than four points, given it is a rectangle (though H could potentially contain fewer points). So the best situation has points on the north-east and south-west corners defining an area $A_{\text{exclusion}}$ at

⁵This is the smallest convex set which encloses all points in H .

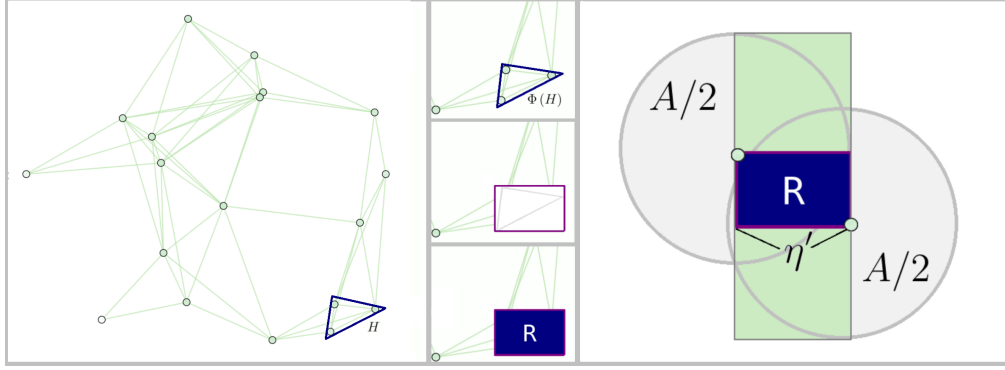


Figure B.1: The component H is bounded by its convex hull $\Phi(H)$, itself encased in the upright rectangle R . In this case, the exclusion area is non-empty, and the vertex combination fails to satisfy the conditions of the component H in Lemma B.0.4.

least

$$A_{\text{exclusion}} \geq A + (1 + o(1)) 2\eta' r_0 \quad (\text{B.0.11})$$

with η' the length of the longest side (which must be at least $\eta/\sqrt{2}$, at which point R is a square). Our green rectangle in the right panel of Fig. B.1 is slightly larger than required, hence the $o(1)$ term. Since we have

$$A + (1 + o(1)) 2r_0\eta' \geq A + (1 + o(1)) \sqrt{2}r_0\eta > A + \eta\sqrt{\log n} = A + (\log \log n)^2$$

and thus

$$\mathbb{P}(A_{\text{exclusion}} \text{ is empty}) \leq \exp(-A - r_0\eta) = o\left(\frac{1}{n(\log n)^3}\right) \quad (\text{B.0.12})$$

Given there are n vertices available for isolation in $G(n, \log n - \frac{1}{2} \log \log n)$, the number of four-vertex combinations embedded in S_n which satisfy the geometric constriction imposed⁶ by R is order $\mathcal{O}(n(\log n)^3)$. Thus the number

⁶Note that we can pick any of the n vertices in G to be surrounded by R , but the other three must be located strictly within a distance $C\sqrt{\log n}$. There are $\mathcal{O}(\log n)$ choices per vertex, so there are $\mathcal{O}(n \times \log n \times \log n \times \log n)$ combinations to try.

of combinations cannot grow fast enough for the decaying exclusion probability (Eq. [B.0.12](#)), and therefore no such rectangle R exists w.h.p.

Finally, notice the disk scaling is $\log n - \frac{1}{2} \log \log n$, so the graph disconnects w.h.p.

$$\mathbb{P}\left(G\left(n, \log n - \frac{1}{2} \log \log n\right) \text{ is connected}\right) = e^{-e^{\log \sqrt{\log n}}} \rightarrow 0 \quad (\text{B.0.13})$$

and theorem [B.0.1](#) follows.

†

Bibliography

- [1] X. Ge, S. Tu, G. Mao, C. X. Wang, and T. Han, “5G Ultra-Dense Cellular Networks,” *IEEE Wireless Communications*, vol. 23, no. 1, pp. 72–79, 2016.
- [2] T. L. Marzetta, “Noncooperative Cellular Wireless with Unlimited Numbers of Base Station Antennas,” *IEEE Transactions on Wireless Communications*, vol. 9, no. 11, pp. 3590–3600, 2010.
- [3] T. S. Rappaport, S. Sun, R. Mayzus, H. Zhao, Y. Azar, K. Wang, G. N. Wong, J. K. Schulz, M. Samimi, and F. Gutierrez, “Millimeter Wave Mobile Communications for 5G Cellular: It Will Work!,” *IEEE Access*, vol. 1, pp. 335–349, 2013.
- [4] A. Gupta and R. K. Jha, “A Survey of 5G Network: Architecture and Emerging Technologies,” *IEEE Access*, vol. 3, pp. 1206–1232, 2015.
- [5] M. D. Penrose, “Connectivity of Soft Random Geometric Graphs,” *The Annals of Applied Probability*, vol. 26, no. 2, pp. 986–1028, 2016.
- [6] M. D. Penrose, *Random Geometric Graphs*. Oxford University Press, 2003.
- [7] A. Faragó, “Network Topology Models for Multihop Wireless Networks,” *ISRN Communications and Networking*, vol. 2012, no. 362603, 2012.
- [8] J. Li, L. Andrew, C. Foh, M. Zukerman, and H. Chen, “Connectivity, Coverage and Placement in Wireless Sensor Networks,” *Sensors*, vol. 9, pp. 7664–7693, September 2009.

-
- [9] S. Broadbent and J. Hammersley, “Percolation Processes,” *Proceedings of the Cambridge Philosophical Society*, vol. 63, pp. 629–641, 1957.
 - [10] G. Grimmett, *Percolation*. Springer, 1999.
 - [11] G. Grimmett, *Probability on Graphs*. Cambridge University Press, 2010.
 - [12] G. Mao and B. D. Anderson, “On the Asymptotic Connectivity of Random Networks under the Random Connection Model,” *INFOCOM, Shanghai, China*, p. 631, 2011.
 - [13] G. Gilbert, “Random Plane Networks,” *Journal of the Society of Industrial and Applied Mathematics*, vol. 9, no. 4, 1961.
 - [14] J. Coon, C. Dettmann, and O. Georgiou, “Full Connectivity: Corners, Edges and Faces,” *The Journal of Statistical Physics*, vol. 147, no. 4, pp. 758–778, 2012.
 - [15] A. D. Flaxman, A. M. Frieze, and J. Vera, “A Geometric Preferential Attachment Model of Networks,” *Internet Mathematics*, vol. 3, pp. 187–205, 2006.
 - [16] B. Bollobás and O. M. Riordan, “Mathematical Results on Scale-Free Random Graphs,” in *Handbook of Graphs and Networks: From the Genome to the Internet*, pp. 1–34.
 - [17] J. Diaz, D. Mitsche, and X. Perez-Gimenez, “Large Connectivity for Dynamic Random Geometric Graphs,” *IEEE Transactions on Mobile Computing*, vol. 8, pp. 821–835, 2009.
 - [18] N. Magaia, A. P. Francisco, P. Pereira, and M. Correia, “Betweenness Centrality in Delay Tolerant Networks,” *Ad Hoc Networks*, vol. 33, pp. 284–305, Oct. 2015.
 - [19] I. Rhee, M. Shin, S. Hong, K. Lee, S. J. Kim, and S. Chong, “On the Levy-Walk Nature of Human Mobility,” *IEEE/ACM Transactions on Networking*, vol. 19, no. 3, pp. 630–643, 2011.

- [20] K. Lee, S. Hong, S. J. Kim, I. Rhee, and S. Chong, “SLAW: Self-Similar Least-Action Human Walk,” *IEEE/ACM Transactions on Networking*, vol. 20, no. 2, pp. 515–529, 2012.
- [21] L. C. Freeman, “A Set of Measures of Centrality Based on Betweenness,” *Sociometry*, vol. 40, pp. 35–41, 1977.
- [22] B. D. MacArthur and R. J. Sánchez-García, “Spectral Characteristics of Network Redundancy,” *Physical Review E*, vol. 80, no. 026117, 2009.
- [23] A. Nyberg, T. Gross, and K. E. Bassler, “Mesoscopic Structures and the Laplacian Spectra of Random Geometric Graphs,” *Journal of Complex Networks*, vol. 3, no. 4, p. 543–541, 2015.
- [24] P. Erdős and A. Rényi, “On Random Graphs,” in *Publicationes Mathematicae (Debrecen)*, vol. 6, pp. 290–297, 1959.
- [25] A. Bonato and J. Janssen, “Infinite Random Graphs and Properties of Metrics,” in *Recent Trends in Combinatorics* (A. Beveridge, J. R. Griggs, L. Hogben, G. Musiker, and P. Tetali, eds.), pp. 257–273, Springer International Publishing, 2016.
- [26] A. P. Giles, O. Georgiou, and C. P. Dettmann, “Betweenness Centrality in Dense Random Geometric Networks,” *Proceedings of the IEEE ICC, London, UK*, 2015.
- [27] A. Lulli, L. Ricci, E. Carlini, and P. Dazzi, “Distributed Current Flow Betweenness Centrality,” in *IEEE 9th International Conference on Self-Adaptive and Self-Organizing Systems*, pp. 71–80, 2015.
- [28] M. Mozaffari, W. Saad, M. Bennis, and M. Debbah, “Drone Small Cells in the Clouds: Design, Deployment and Performance Analysis,” in *IEEE GLOBECOM, San Diego, California, USA*, pp. 1–6, 2015.
- [29] C. Nguyen, O. Georgiou, and Y. Doi, “Maximum Likelihood Based Multihop Localization in Wireless Sensor Networks,” in *Proceedings. IEEE ICC, London, UK*, 2015.

-
- [30] P. C. Pinto, J. Barros, and M. Z. Win, "Secure Communication in Stochastic Wireless Networks - Part I: Connectivity," *IEEE Transactions on Information Forensics and Security*, vol. 7, no. 1, pp. 125–138, 2012.
 - [31] O. Georgiou, C. Dettmann, and J. Coon, "Network Connectivity Through Small Openings," in *Proceedings of ISWCS 2013, Ilmenau, Germany*, pp. 1–5, 2013.
 - [32] M. G. Almiron, O. Goussevskaya, A. A. Loureiro, and J. Rolim, "Connectivity in Obstructed Wireless Networks: From Geometry to Percolation," in *Proceedings of the Fourteenth ACM International Symposium on Mobile Ad Hoc Networking and Computing, Bangalore, India*, pp. 157–166, 2013.
 - [33] P. Gupta and P. R. Kumar, "Critical Power for Asymptotic Connectivity," in *Proceedings of the 37th IEEE Conference on Decision and Control*, pp. 1106–1110, 1998.
 - [34] M. D. Penrose, "The Longest Edge of the Random Minimal Spanning Tree," *The Annals of Applied Probability*, vol. 7, no. 2, pp. 340–361, 1997.
 - [35] M. Walters, "Random Geometric Graphs," in *Surveys in Combinatorics 2011* (Robin Chapman, ed.), Cambridge University Press, 2011.
 - [36] J. F. C. Kingman, *Poisson Processes*. Oxford University Press, 1993.
 - [37] U. Brandes, "A Faster Algorithm for Betweenness Centrality," *Journal of Mathematical Sociology*, vol. 25, pp. 163–177, 2001.
 - [38] U. Brandes and C. Pich, "Centrality Estimation in Large Networks," *International Journal of Bifurcation and Chaos*, vol. 17, no. 7, pp. 2303–2318, 2007.
 - [39] Z. Zhang, G. Mao, and B. D. Anderson, "On the Hop Count Statistics in Wireless Multihop Networks Subject to Fading," *IEEE Transactions on Parallel and Distributed Systems*, vol. 23, no. 7, pp. 1275–1287, 2012.

- [40] G. Mao, Z. Zhang, and B. Anderson, “Probability of k-Hop Connection under Random Connection Model,” *Communications Letters, IEEE*, vol. 14, no. 11, pp. 1023–1025, 2010.
- [41] X. Ta, G. Mao, and B. Anderson, “On the Probability of K-hop Connection in Wireless Sensor Networks,” *IEEE Communications Letters*, vol. 11, no. 9, 2007.
- [42] S. Mukherjee and D. Avidor, “Connectivity and transmit-energy considerations between any pair of nodes in a wireless ad hoc network subject to fading,” *Vehicular Technology, IEEE Transactions on*, vol. 57, no. 2, pp. 1226–1242, 2008.
- [43] S. Srinivasa and M. Haenggi, “Distance Distributions in Finite Uniformly Random Networks: Theory and Applications,” *IEEE Transactions on Vehicular Technology*, vol. 59, no. 2, pp. 940–949, 2010.
- [44] D. Irons and J. Jordan, “Geometric Networks Based on Markov Point Processes,” *Unpublished, currently available at the personal website of J. Jordan, which is presently www.jonathanjordan.staff.shef.ac.uk/preprints.htm*, 2011.
- [45] M. D. Penrose and A. R. Wade, “Limit theory for the Random On-Line Nearest-Neighbor Graph,” *Random Structures & Algorithms*, vol. 32, no. 2, pp. 125–156, 2008.
- [46] N. Berger, B. Bollobás, C. Borgs, J. Chayes, and O. Riordan, “Degree distribution of the FKP network model,” *Theoretical Computer Science*, vol. 379, no. 3, pp. 306 – 316, 2007.
- [47] D. Krioukov, F. Papadopoulos, M. Kitsak, A. Vahdat, and M. Boguñá, “Hyperbolic Geometry of Complex Networks,” *Physical Review E*, vol. 82, 2010.
- [48] M. E. J. Newman, *Networks: An Introduction*. Oxford University Press, 2010.

-
- [49] J. Ladyman, J. Lambert, and K. Wiesner, “What is a complex system?,” *European Journal for Philosophy of Science*, vol. 3, p. 33–67, 2013.
 - [50] L. Freeman, S. Borgatti, and D. White, “Centrality in valued graphs: A measure of betweenness based on network flow,” *Social Networks*, vol. 13, pp. 141–154, 1991.
 - [51] M. Newman, “A measure of Betweenness Centrality Based on Random Walks,” *Social Networks*, vol. 27, pp. 39–54, 2003.
 - [52] P. G. Doyle and J. L. Snell, *Random Walks and Electric Networks*, vol. 22. Mathematical Association of America, 1984.
 - [53] C. P. Dettmann, O. Georgiou, and J. P. Coon, “More is Less: Connectivity in Fractal Regions,” *Proceedings of IEEE ICC, London, UK*, 2015.
 - [54] A. P. Giles, O. Georgiou, and C. P. Dettmann, “Connectivity of Soft Random Geometric Graphs over Annuli,” *The Journal of Statistical Physics*, vol. 162, no. 4, p. 1068–1083, 2016.
 - [55] D. Tse and P. Viswanath, *Fundamentals of Wireless Communication*. Cambridge University Press, 2005.
 - [56] I. Gupta, D. Riordan, and S. Sampalli, “Cluster-Head Election Using Fuzzy Logic for Wireless Sensor Networks,” in *Communication Networks and Services Research Conference, 2005. Proceedings of the 3rd Annual*, pp. 255–260, 2005.
 - [57] M. Ercsey-Ravasz and Z. Toroczkai, “Centrality Scaling in Large Networks,” *Physical Review Letters*, vol. 105, no. 038701, 2010.
 - [58] W. Liu, Y. Yang, k. peng, H. Jiang, X. Liao, W. Wei, B. Li, and X. Jing, “A General Framework of Skeleton Extraction in Sensor Networks,” *IEEE Sensors Journal*, vol. PP, no. 99, pp. 1–1, 2015.
 - [59] Y. Wang, J. Gao, and J. S. Mitchell, “Boundary Recognition in Sensor Networks by Topological Methods,” in *Proceedings of MobiCom 2006, Los Angeles, CA, USA*, pp. 122–133, 2006.

- [60] S. Adlaj, “An Eloquent Formula for the Perimeter of an Ellipse,” *Notices of the AMS*, vol. 59, pp. 1094–1099, 2012.
- [61] W. R. Heinzelman, A. Chandrakasan, and H. Balakrishnan, “Energy-Efficient Communication Protocol for Wireless Microsensor Networks,” *Proceedings of the 33rd International Conference on System Sciences, Hawaii, USA*, 2000.
- [62] X. Liu, “A Survey on Clustering Routing Protocols in Wireless Sensor Networks,” *Sensors*, vol. 12, pp. 11113–11153, 2012.
- [63] D. Dong, Y. Liu, and X. Liao, “Fine-Grained Boundary Recognition in Wireless Ad Hoc and Sensor Networks By Topological Methods,” *Proceedings of MobiHoc '09, New Orleans, Louisiana USA*, 2009.
- [64] Y.-H. Chen, W.-H. Chung, G.-K. Ni, H. Zhang, and S.-Y. Kuo¹, “Optimal self boundary recognition with two-hop information for ad hoc networks,” *Proceedings of the IEEE Wireless Communications and Networking Conference: Mobile and Wireless Networks, Paris, France*, 2012.
- [65] W. Wang and C. Y. Tang, “Distributed Computation of Node and Edge Betweenness on Tree Graphs,” in *52nd IEEE Conference on Decision and Control*, pp. 43–48, 2013.
- [66] W. Wang and C. Y. Tang, “Distributed Estimation of Closeness Centrality,” in *2015 54th IEEE Conference on Decision and Control (CDC)*, pp. 4860–4865, 2015.
- [67] L. Page, S. Brin, R. Motwani, and T. Winograd, “The PageRank Citation Ranking: Bringing Order to the Web,” Tech. Rep. 1999-66, 1999.
- [68] A. Saxena, V. Malik, and S. R. S. Iyengar, “Estimating the Degree Centrality Ranking,” in *2016 8th International Conference on Communication Systems and Networks (COMSNETS)*, pp. 1–2, 2016.
- [69] E. E. Santos, J. Korah, V. Murugappan, and S. Subramanian, “Efficient Anytime Anywhere Algorithms for Closeness Centrality in Large and

-
- Dynamic Graphs,” in *2016 IEEE International Parallel and Distributed Processing Symposium Workshops (IPDPSW)*, pp. 1821–1830, 2016.
- [70] S. Chandler, “Calculation of Number of Relay Hops Required in Randomly Located Radio Network,” *Electronics Letters*, vol. 25, no. 24, pp. 1669–1671, 1989.
- [71] S. Li, “Concise Formulas for the Area and Volume of a Hyperspherical Cap,” *Asian Journal of Mathematical Statistics*, vol. 4, no. 1, pp. 66–70, 2011.
- [72] M. Ohring, *Materials Science of Thin Films*. Boston: Academic Press, 2001.
- [73] D. Niculescu and B. Nath, “Ad Hoc Positioning System (APS) Using AOA,” in *Proceedings of IEEE INFOCOM 2003 (San Francisco, CA, USA)*, pp. 1734–1743.
- [74] M. Gerla, E. K. Lee, G. Pau, and U. Lee, “Internet of Vehicles: From Intelligent Grid to Autonomous Cars and Vehicular Clouds,” in *2014 IEEE World Forum on Internet of Things (WF-IoT)*, pp. 241–246, 2014.
- [75] P. Clifford, “Markov Random Fields in Statistics,” in *Disorder in Physical Systems: A Volume in Honour of John M. Hammersley* (Geoffrey Grimmett and Dominic Welsh, ed.), Cambridge University Press, 1990.
- [76] Q. S. Hua, H. Fan, M. Ai, L. Qian, Y. Li, X. Shi, and H. Jin, “Nearly Optimal Distributed Algorithm for Computing Betweenness Centrality,” in *IEEE 36th International Conference on Distributed Computing Systems*, pp. 271–280, June 2016.
- [77] B. Bollobás and I. Leader, “Edge Isoperimetric Inequalities in the Grid,” *Combinatorica*, vol. 11, no. 4, 1991.
- [78] B. Bollobás, *The Art of Mathematics: Coffee Time in Memphis*. Cambridge University Press, 2006.

†